Novel quantum interactions between light and dense atomic media

Stefano Grava

Ph.D. Thesis

Thesis supervisor: Prof. Darrick E. Chang

ICFO - The Institute of Photonic Sciences
Universitat Politècnica de Catalunya

August 2022 - Barcelona

Ai miei genitori

Abstract

The interface between light and cold atomic ensembles is a fundamental platform to unravel the quantum world and develop quantum technological applications. Its success relies on the simple idea that the efficiency of such an interface can be collectively enhanced by the use of many atoms. While the interaction between its building blocks, a single photon, and a single atom, is theoretically and experimentally understood, instead, the interaction between light and a macroscopic ensemble of motionless atoms is generically a complex system featuring multiple scattering and many-body dipole interactions. To avoid the complexity, typical theories of atom-light interactions treat the atomic medium as smooth. However, it is well-known that microscopic optical effects driven by atomic granularity can lead to important effects, especially in dense media. These phenomena and their consequences on the performance of applications are not completely understood. To take them into account exactly, Chapter 1 introduces a "spin model" for light-matter interaction. The rest of the thesis is then divided into three chapters, which push forward our understanding of the interaction of light with dense atomic media.

In Chapter 2 it is argued that because of the overwhelming collective macroscopic response an ensemble can exhibit (well captured by the standard theory), many microscopically-driven effects that have been predicted, have also been challenging to observe so far. An essential step is thus to suppress the macroscopic light propagation, so as to allow the microscopic correlations to build up and to be analyzed in a background-free fashion. To solve this issue, a technique to suppress the macroscopic optical dynamics in free space, which allows to precisely investigate many-body aspects of light-matter interaction, will be presented and demonstrated. In particular, we unravel and precisely characterize a microscopic, density-dependent dipolar dephasing effect that generally limits the lifetime of the optical spin-wave order in ensemble-based atom-light interfaces.

In Chapter 3 we will go beyond the short-time and dilute limits consid-

ered previously, to develop a comprehensive theory of dephasing dynamics for arbitrary times and atomic densities. In particular, our non-perturbative approach is based on the strong-disorder renormalization group (RG), in order to quantitatively predict the dominant role that near-field optical interactions between nearby neighbors have in driving the dephasing process. This theory also enables one to capture the key features of the many-atom dephasing dynamics in terms of an effective single-atom model. These results should shed light on the limits imposed by near-field interactions on quantum optical phenomena in dense atomic media, and illustrate the promise of strong disorder RG as a method of dealing with complex microscopic optical phenomena in such systems.

Chapter 4 tries to answer the question of why ordinary materials exhibit a refractive index of order unity and if the answer can come from an electrodynamical argument. While textbook theories predict nonphysical values when extrapolated to densities of solids, here, we will evaluate the exact linear optical response of a three-dimensional lattice of two-level atoms, first from the band structure and then from a direct numerical simulation. Interestingly, when multiple scattering of light is exactly taken into account, as a result of perfect interference, it is found that an ideal unity-filled array of atoms can have a refractive index that grows with the density and is furthermore real. This implies that a saturation mechanism for the index should come from the quantum chemistry interactions that arise in real materials. Whether saturation could be circumvented, could lead to novel optical materials with transformative technological potential.

Sumario

La interfaz entre la luz y conjuntos de átomos fríos es una plataforma fundamental para explorar el mundo cuántico y para el desarrollo de las tecnologías cuánticas. Sus logros están basados en la sencilla idea de que la eficiencia de esta interfaz puede mejorar al utilizar muchos átomos. A pesar de que la interfaz entre sus constituyentes, un único átomo y un único fotón, está experimentalmente y teóricamente entendida, en cambio, la interacción entre la luz y un conjunto macroscópico de átomos inmóviles es un sistema complejo que incluye dispersiones múltiples e interacciones dipolo-dipolo entre muchos cuerpos. Para reducir esta complejidad, las teorías tradicionales tratan el medio atómico como continuo. Sin embargo, es conocido que los efectos ópticos microscópicos, causados por la granularidad de los átomos, pueden dar lugar a consecuencias importantes, sobre todo en el caso de medios densos. Estos fenómenos y sus consecuencias en la eficiencia de las aplicaciones siguen sin entenderse por completo. Para tenerlos en cuenta exactamente, el Capítulo 1 introduce un "modelo de espines" para la interaccíón luz-materia. El resto de la tesis se divide luego en tres capítulos, que impulsan nuestra comprensión de la interacción de la luz con medios atómicos densos.

En el Capítulo 2 se argumenta que debido a la enorme respuesta macroscópica colectiva de un conjunto (captada correctamente por la teoría estándar), muchos de los efectos microscópicos que se han predicho también han sido difíciles de observar hasta ahora. El reto, por lo tanto, es suprimir la propagación de la luz macroscópica, para permitir que las correlaciones microscópicas se acumulen y se analicen sin ese fondo. Para resolver este problema, se presentará y demostrará una técnica para suprimir la dinámica óptica macroscópica en el espacio libre, que permite investigar con precisión los aspectos de muchos cuerpos de la interacción luz-materia. En particular, caracterizamos con precisión un efecto de desfase dipolar microscópico, que depende de la densidad, y limita la vida útil del orden de onda de espín óptico en las interfaces átomo-luz basadas en conjuntos.

En el Capítulo 3 iremos más allá de los límites diluidos y de tiempo corto considerados anteriormente, para desarrollar una teoría completa de la dinámica de desfase para tiempos y densidades atómicas arbitrarias. En particular, nuestro método no-perturbativo se basa en el grupo de renormalización (RG) del desorden fuerte, para predecir cuantitativamente el papel dominante que tienen las interacciones ópticas de campo cercano entre átomos vecinos en el proceso de desfase. Estos resultados deberían aclarar los límites impuestos por las interacciones de campo cercano en los fenómenos ópticos cuánticos en medios atómicos densos e ilustrar la promesa del RG como método para tratar los fenómenos ópticos microscópicos complejos en estos sistemas.

El Capítulo 4 trata de responder a la pregunta de por qué los materiales ordinarios exhiben un índice de refracción de orden uno y si la respuesta puede proceder de un argumento electrodinámico. Si bien las teorías de los libros de texto predicen valores no físicos cuando se extrapolan a densidades de sólidos, aquí evaluaremos la respuesta óptica lineal exacta de una red tridimensional de átomos de dos niveles, primero a partir de la estructura de bandas y luego a partir de una simulación numérica directa. Curiosamente, cuando se tiene en cuenta de manera exacta la dispersión múltiple de la luz, como resultado de la interferencia perfecta, se encuentra que una matriz de átomos ideal tiene un índice de refracción que crece con la densidad y, además, es real. Esto implica que un mecanismo de saturación para el índice debería provenir de las interacciones de la química cuántica que surgen en los materiales reales. La posibilidad de evitar la saturación podría dar lugar a nuevos materiales ópticos con un potencial tecnológico transformador.

Publications

1) Y. He, Q. Cai, L. Ji, Z. Fang, Y. Wang, L. Qiu, L. Zhou, S. Wu, S. Grava and D. E. Chang, “Unraveling disorder-induced optical dephasing in an atomic ensemble”, 2021, preprint at arXiv:2101.10779v1

2) S. Grava, Y. He, S. Wu and D. E. Chang, “Renormalization group analysis of near-field induced dephasing of optical spin waves in an atomic medium”, 2022, *New J. Phys.* **24** 013031

3) F. Andreoli, G. M. Andolina, S. Grava, B. Windt, D. E. Chang *et al.*, "The maximum refractive index of an atomic crystal: from quantum optics to quantum chemistry". To be submitted.

The results of the first publication (under review) are included in Chapter 2 while the second publication has been adapted into Chapter 3. Chapter 4 instead contains unpublished work to be submitted soon.

Ackowledgments

First and foremost, I want to thank Darrick. You saw potential in me, guided me through these challenging and exciting years, and thought me how science should be done. I will always be grateful for all those things. I would also like to extend my sincere thanks to members of the defense committee, who generously provided knowledge and expertise. Additionally, this endeavor would not have been possible without the generous support from the ICFOstepstone program, by which ICFO and the European Union financed part of my research. During these years I also had the pleasure of collaborating with Prof. Dr. Saijun Wu and his group. Despite Covid-19 making it impossible for me to visit, we maintained an intense collaboration from which I learned and professionally grew a lot. Finally, I also want to thank my colleagues, Marco, Marcos, Mariona, Andreas, Loïc, David, Lukas, James, Francesco, Javier, Roberto, Giuseppe, Daniel, Teresa, Daniel, Bennet, Marcello, and Charlie. You all thought me something and showed me that a group is more than the sum of its components. Special thanks also to all the other friends I made at ICFO for the beautiful moments spent together.

Ringrazio soprattutto i miei genitori. Se questo è possibile è principalmente grazie a voi, al supporto datomi durante tutti questi anni e all'amore incondizionato nonostante la distanza. Per questo la tesi è dedicata a voi.

Per ultima vorrei ringraziare Martina. Sei la persona più importante al mondo. Il tuo abraccio mi completa, mi trasforma e mi rende felice. Grazie per essere la migliore compagna di viaggio ♥

Contents

Part I

Introduction

CHAPTER 1

Introduction

The quantum interface between atomic ensembles and light is considered to be one of the most important routes to widespread quantum technologies. The field started with the realization that optically thick free space ensembles can be efficiently interfaced with quantum optical fields and during the past decades it provided many demonstrations of fundamental phenomena and applications [1]. Atomic ensembles are being actively pursued, for example, to realize quantum memories for light [2–5], for quantum-enhanced metrology [6–12], for entanglement generation between light and atomic spins [13], to realize nonlinear optical devices operating at the single-photon level [14–18] and for quantum simulation [19–22].

In order to understand the physics governing the efficiency of an atom-light interface, it makes sense to first consider the probability of interaction between its simplest representatives, a single two-level atom and a single resonant photon, pictorially represented in Fig. 1.1a. In free space, this can be given in terms of the ratio between the atomic absorption cross-section $\sigma_0 = 3\lambda_0^2/2\pi$, the effective area seen by a photon, and the transverse area A_b of an incoming laser beam. For an atom shined by resonant light, the cross-section scales as the square of the wavelength of the beam, such that the probability that a single point-like atom scatters a photon scales like $P \approx \lambda_0^2/A_b$ [23]. As the typical wavelength of optical transitions is of the order of $\lambda_0 \sim 1\mu$m while the physical size of an atom is of the order of the Bohr radius $a_0 \sim 0.05$ nm, the atomic response to light can be considered huge. Practically, however, due to the diffraction limit, which prevents the focusing of light below the wavelength scale, $A_b > \lambda_0^2$, this interaction is generally weak, $P \ll 1$. The current record for P, achieved by focusing light to a small area around a single ^{87}Rb atom, is around $P \sim 20\%$ [24]. Nevertheless, the possibility to trap and address a single atom revitalized

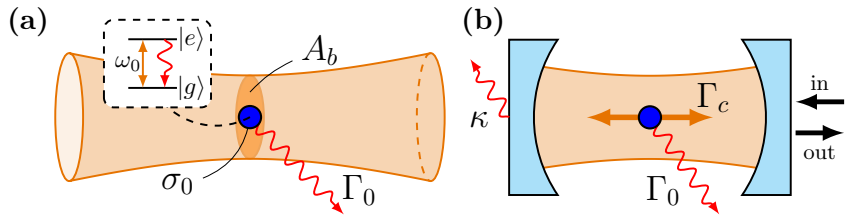

Figure 1.1: (a) Schematic representation of the free-space interaction between a single photon, focused to a focal spot of area A_b and a single atom. The atom is minimally modeled as a point-like object with two internal energy states, a ground $|g\rangle$ and an excited one $|e\rangle$, separated by a frequency ω_0 and connected by an optical dipole transition. The excited state can decay, emitting a photon, with a decay rate Γ_0. (b) Representation of a cavity QED system. The same two-level atom is coupled to a cavity mode and can decay into free space modes at a rate Γ_0 or into a cavity mode with an cooperativity-enhanced rate Γ_c. The cavity can also leak at a rate κ, due to material absorption.

the study of the the atom-light interaction at the fundamental level [25–31]. Historically, however, many other practical methods for overcoming the problem and enhancing the atom-photon interaction probability were proposed.

One paradigm consists in confining the atom in a single-mode cavity, constituting the field of cavity quantum electrodynamics (CQED) [32–34], schematically represented in Fig. 1.1b. Effectively, this increases the absorption cross-section by the number of bounces that the photon makes before escaping from the system (at a rate κ); this number is determined by the quality of the resonator and quantified by its finesse $\mathcal{F}$. The product, $C = \mathcal{F}\lambda_0^2/A_b$, known as the "cooperativity", is the relevant figure of merit of the system and more precisely quantifies how well the atom and the photons in the cavity mode interact. Indeed, since C can be larger than one, rather than a probability, the cooperativity should be interpreted as a branching ratio, $C = \Gamma_c/\Gamma_0$. As illustrated in Fig. 1.1b an initially excited atom can either emit into a cavity mode, at a rate Γ_c, or into free space at a spontaneous emission rate Γ_0. Intuitively, the ratio between coherent and useful transfer and undesired losses constitutes a key parameter in the performance of a CQED system. Entering the high cooperativity regime ($C \gg 1$) opened up the possibility to coherently control both internal degrees of freedom, the atomic excitation, and the cavity field, to realize, for example, reversible state transfer between them [35], to generate non-classical states of light such as single photons [36, 37] or entangled pairs [38], or to implement a photon-photon phase gate [39, 40]. Besides being a

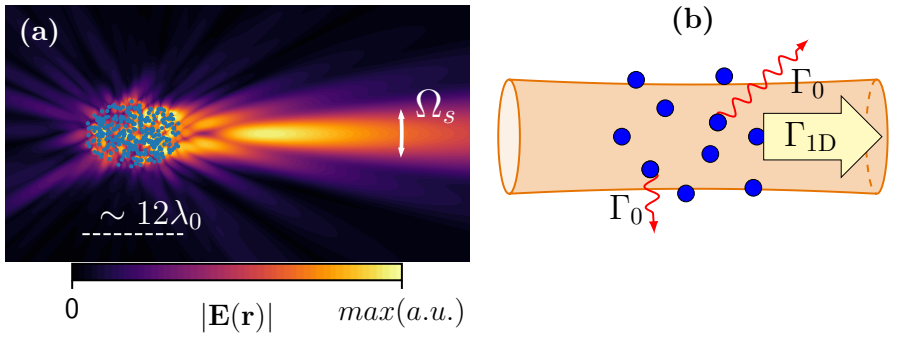

Figure 1.2: (a) Directional emission of a system of $N = 300$ atoms/dipoles in a uniform distribution of density $\eta = 1$ and a average optical depth $\overline{\mathrm{D}} = 10$, excited in a matched spin wave ($|\mathbf{k}| = k_0$). The amplitude of the emitted field is reconstructed as discussed in the main text or in more details in Appendix A. Each emitter has a fixed dipole orientation along $\hat{x}$ and a fixed phase $e^{i\mathbf{k}\cdot\mathbf{r}_i}$ where $\mathbf{r}_i$ are the atoms position and the $|\mathbf{k}| = k_0$ (b) An atomic excitation can either be effectively "lost" in 4π or being emitted into a well defined mode.

beautiful demonstration of fundamental ideas in the quantum realm, these results constitute the first technological demonstrations of the individual nodes required to operate a future quantum network [34, 41]. Importantly, these results were facilitated by the theoretical development of the necessary tools to treat open systems. Indeed, the physics of the interplay between the cavity mode and the atom is captured by the well-known Jaynes-Cummings model [42], while through an elegant input-output formalism [43], the properties of the field exiting the system (the output) can be determined based upon knowledge of the input field and the dynamics of the atom-cavity system alone. Despite the remarkable achievements of CQED, however, a robust and scalable implementation that can be easily integrated with photonics remains elusive.

Another way to enhance atom-light interactions is represented in 1.2b and consists in using a large disordered ensemble of identical atoms [1, 2], such that if a photon fails to interact there will always be another atom to interact with. In such a system, the relevant figure of merit is $\mathrm{D} = N\sigma_0/A_b$, known as the optical depth; intuitively it is just the single-atom scattering probability introduced above times the total number of atoms. With a sufficiently high optical depth, one might therefore reach the limit in which a single photon has a $\sim 100\%$ probability of being absorbed and converted into an atomic excitation. Another way to understand the efficient coupling between light and atomic ensembles is to consider the

emitted field from a cloud of N classical dipoles characterized by a resonant frequency ω_0, as in Fig. 1.2a. In particular, when their phases match the one of an incoming resonant field at each atom's position $\mathbf{r}$, i.e. $e^{i\mathbf{k}\cdot\mathbf{r}}$, where $|\mathbf{k}| = k_0 = \omega_0/c$, just as it happens for phased dipole antennas [44], the atoms emit constructively at a rate $N\Gamma_{1D}$ into a well-defined quasi-1D direction of emission [45], around the wave vector $\mathbf{k}$ with a solid angle $\Omega_s \sim (k_0 R)^{-2}$, where R is the characteristic size of the cloud. Remarkably, similarly to the CQED case, the emerging picture (Fig. 1.2b) is that one can effectively define "good" emissions in a well-defined mode and "bad" ones, which are photons emitted in 4π that cannot be recollected. The branching ratio, which quantifies the performance of such a light-matter interface, is the optical depth, such that $\mathrm{D} = N\Gamma_{1D}/\Gamma_0$.

The possibility to enhance interactions by atom number, thus making an efficient light-matter interface, has led to the many experimental demonstrations listed in the first paragraph. In order to understand all these phenomena, which are going to be of central importance in this thesis, here, the standard theoretical approach to treating atom-light propagation in large ensembles, the so-called Maxwell-Bloch equations, will be reviewed. In particular, it will emerge how, in the linear regime, the optical depth D emerges as the figure of merit of the system in concrete applications like quantum memories.

1.1 The Maxwell-Bloch equations

Already at the classical level, light propagation through a disordered ensemble is known to be a complex problem. Multiple scattering of light and interference distorts the incident wavefront strongly; moreover, light diffusing through the medium forms a volume speckle field that has no correlations on a distance larger than the wavelength of light, for example, limiting imaging resolution [46, 47]. The quantum mechanical problem is even more complex, as a two-level system is a nonlinear frequency mixer, capable of generating a continuum of new frequencies from an initial pulse. A priori, keeping track of this continuum as it propagates and re-scatters from other emitters appears to be a difficult task. To reduce the complexity, the standard theoretical approach to treat such a system is based upon the semi-phenomenological one dimensional Maxwell-Bloch equations, first introduced in [48, 49] and reviewed in more detail in [1, 2, 50–55]. In most cases of interest, a quasi-1D propagating field (e.g., a Gaussian beam), $\hat{\varepsilon}(z,t)$ illuminates an ensemble, and its interaction with the atoms

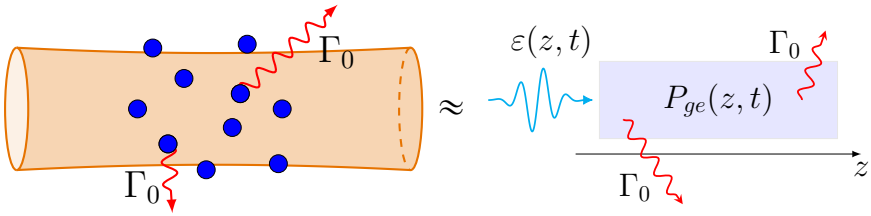

Figure 1.3: MBE approach to light propagation in atomic media. The granular nature of the atomic distribution (left) is smoothed out in favour of a continuous medium (right) of the same optical depth. An external field $\varepsilon(z,t)$ can drive the smooth polarization field $P_{ge}(z,t)$. In turn the polarization field can either act back as a source for the electromagnetical field and spontaneously lose the excitation at a rate Γ_0, as prescribed by Eq. (1.1). Here we show the reduction to a quasi-1D problem but also more sophisticated 3D have been developed, as discussed in Appendix A.

is directly treated; any possible scattering into the remaining 4π solid angle is not explicitly calculated but is treated by an approximate prescription. Furthermore, the granularity of the atoms is ignored, and it is assumed that their properties can be described by smooth quantum polarization fields, $\hat{P}_{ge}(z,t)$ as in Fig. 1.3. In terms of these new quantum fields, in the rotating frame of the incoming light, the equations of motion become the well-known Maxwell-Bloch equations:

$$\begin{aligned} \left(\partial_t + c\partial_z\right)\hat{\varepsilon} &= ig\sqrt{N}\hat{P}_{ge} \\ \partial_t\hat{P}_{ge} &= -i\left(\Delta - i\Gamma_0/2\right)\hat{P}_{ge} - ig\sqrt{N}\hat{\varepsilon}\left(\hat{P}_{ee} - \hat{P}_{gg}\right) \end{aligned} \tag{1.1}$$

Here, g is the usual light-matter coupling in free-space $g = d_{ge}\sqrt{\frac{2\omega_0}{\hbar\varepsilon_0 V}}$ where $V = A_b L$ is the interaction volume, given by the product of the cross-section of the mode A_b and the length of the system L, which contains N atoms. The quantity d_{eg} is the dipole matrix element associated with the two-level transition. Moreover, Δ is the detuning of the probe field with respect to the resonant frequency ω_0. This coupled set of equations simply describes that the electrical field is governed by a one-dimensional wave equation in which the polarization field acts as a source. In turn, the field linearly drives the polarization of the medium. The effect of the remaining continuum of electromagnetic modes is assumed to result in a local, independent decay rate $\Gamma_0 = \frac{\omega_0^3 d_{ge}^2}{3\pi\hbar\varepsilon_0 c^3}$ for atomic excitations, identical to the spontaneous emission rate of a single, isolated atom in vacuum. Despite the simplifications, effectively reducing the problem to

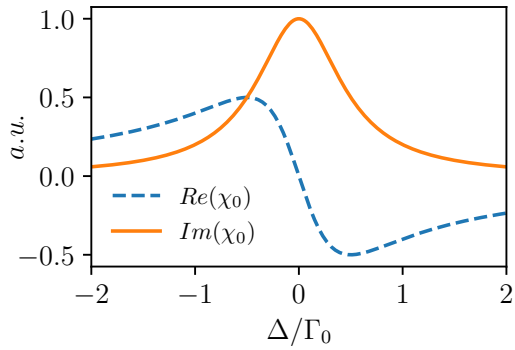

Figure 1.4: The single-atom susceptibilities χ_0 for a two-level atom (Eq. (1.2)), as functions of the dimensionless detuning Δ/Γ_0 of the probe field. The dashed and solid curves give the real and imaginary parts of χ_0, respectively, with the former related to propagation phase and the latter to atom absorption.

a quasi-1D quantum field theory, for this set of two coupled, nonlinear partial differential equations on operators, no general solution is known. One particularly simple limit of Eq. (1.1) is to investigate its linear optical response, in which D concretely emerges as the key parameter of the system.

1.1.1 Linear response

A further simplification comes from noticing that the level of nonlinearities in atomic ensembles is typically weak since the number of atoms is typically larger than the number of absorbed photons, $P_{gg} - P_{ee} \approx 1$, where now, for example, $P_{ee} = \langle \hat{P}_{ee} \rangle$ represents the expectation value. In other words, in an ensemble with many atoms, it is unlikely for two consecutive photons to hit the same atom which can now be treated as a harmonic oscillator that never gets excited twice, neglecting its nonlinear nature. This leaves us with a set of linear equations for classical fields, which can be studied, for example, in the stationary regime. The equation for the electric field thus simply reads:

$$\begin{aligned} &\partial_z \varepsilon = i\chi k_0 \varepsilon \\ &\chi = \frac{N}{V}\chi_0 \qquad \chi_0 = -\frac{3\pi\Gamma_0}{2k_0^3}\frac{1}{\Delta + i\Gamma_0/2}. \end{aligned} \tag{1.2}$$

Within this approach, therefore, the optical response, or how the field propagates through the medium, is simply characterized by the linear susceptibility χ, which is found to have several important properties. First, it is

simply proportional to the linear response, χ_0, of a single, isolated atom in free space and to the density of the ensemble, which makes it more explicit that the underlying assumption is that every atom responds to light independently of the surrounding emitters. Second, as represented in Fig. 1.4, importantly, the susceptibility is a complex quantity, whose imaginary part (orange curve) describes absorption and takes a maximum value at resonance, as $\chi(\Delta=0) = i\frac{3\pi}{k_0^3}\frac{N}{V}$. As expected for two-level atoms, because the response to a probe field is around resonance is primarily absorptive, solving for the field in Eq, (1.1), one finds that the intensity decays exponentially, following the well-known Beer's law, $I(z)=I_0e^{-2\mathrm{Im}\chi k_0 z}=I_0e^{-\mathrm{D}}$, which depends only on the optical depth of the system [1, 2, 54], defined as:

$$\mathrm{D} = 2\mathrm{Im}\chi(0)k_0L = \frac{3}{2\pi}N\frac{\lambda_0^2}{A_b} = N\frac{\sigma_0}{A_b}. \tag{1.3}$$

The susceptibility enters also, for example, in the complex refractive index of the medium, as $n=\sqrt{1+\frac{N}{V}\chi_0}$, whose real part instead describes dispersion. This topic will be discussed more in-depth during the thesis, in particular in Chapter 4. Here, it is sufficient and interesting to notice that within the MBE treatment, the resonant absorption of the atomic medium is found to linearly scale with the density (and thus to the number of emitters), $\mathrm{Im}(\chi) \sim N/V$. The same unbounded increase is also found in the refractive index where $n \sim \sqrt{N/V}$, a prediction that is going to be discussed in more detail in Chapter 4. While linearization (or more precisely, a Gaussian approximation) severely limits the range of Hilbert space that can be accessed, the resulting dynamics (combined with a more complex atomic-level structure) does already allow for some useful applications, such as quantum memory for light and spin squeezing.

1.1.2 Electromagnetically induced transparency

The efficient absorption of a resonant beam provided by an optically thick two-level ensemble is not particularly useful; however, the system can be functionalized by adding a second ground (or metastable) state $|s\rangle$, in a Λ-type scheme (as in Fig. 1.5a). The additional transition $|s\rangle - |e\rangle$ is driven by a copropagating (classical) control field with a Rabi frequency of Ω_c with the same detuning Δ of the probe beam $\mathbf{E}$, ideally to facilitate the light–atom state mapping. This configuration allows for the linear optics phenomenon of electromagnetically induced transparency (EIT) [2, 56]. The linear response and propagation of the probe field can readily be solved in a manner similar

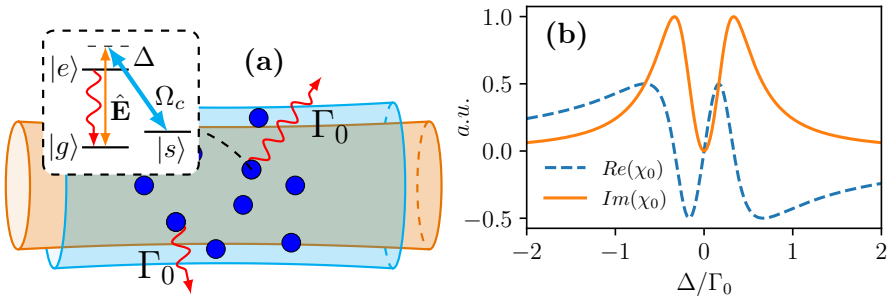

Figure 1.5: (a) EIT three-level scheme. The ground state $|g\rangle$ and the excited state $|e\rangle$ interact with the quantum probe field ε (orange), detuned from the resonance by Δ. The transition $|e\rangle - |s\rangle$ is driven instead by a strong classical control field with Rabi frequency Ω_c (cyan), detuned from the two-photon resonance by Δ. (b) Single-atom susceptibilities χ_0 for a three-level scheme, as functions of the dimensionless detuning Δ/Γ_0 of the probe field and for $\Omega_c/\Gamma_0 = 1/3$.

to Part a) for two-level systems, after generalizing Eq. (1.1) to three levels. The main physical results can be summarized as follows. The population in the state $|e\rangle$ (and the corresponding spontaneous emission) can be completely suppressed when the two-photon resonance condition ($\Delta = 0$) is satisfied, because of destructive interference between the two excitation pathways. This leads to the medium becoming transparent to the probe field ($\mathrm{Im}\chi = 0$, Fig. 1.5b) within a characteristic bandwidth $\Delta_{\mathrm{EIT}} = \frac{\Omega_c^2}{\Gamma_0\sqrt{\mathrm{D}}}$ around the two-photon resonance condition, realizing EIT. In the process, the incoming photon state strongly hybridizes with collective atomic spin-wave excitations S to create "dark-state polaritons" that propagate through the medium at a reduced group velocity, $v_g = \frac{\Omega_c^2}{\Gamma_0}\frac{2L}{\mathrm{D}}$. The light-matter excitation can be therefore slowed down reducing the strength of the control field. Since photons in free space, travel at the speed of light, intuitively the more the polariton is slowed down ($\Omega_c \to 0$), the more its spin-wave component should be dominant. Indeed the ratio v_g/c actually determines also the mixing angle between light and matter excitation. For realistic values of slow light, such as $v_g = 17\ m/s$ [57], this roughly corresponds to a population ratio of 10^{-7} and therefore, in such a condition, a dark-state polariton is almost entirely a spin-wave excitation.

1.1.3 Quantum memories for light

A quantum memory is a device that allows on-demand storage and retrieval of an arbitrary quantum state, a fundamental building block in quantum

communication [41, 58] and linear optical quantum computation [59]. Intuitively the described setup is already a memory, which can store a pulse for a delay time $\tau_d = L/v_g$, provided the width of the incoming light $\Delta\omega_p$ to satisfy $\Delta\omega_p < \Delta_{\text{EIT}}$. Its performance is quantified by the ratio of the achievable time delay to the initial pulse length $\tau_p > 1/\Delta_{\text{EIT}}$ and is limited by the so called bandwidth-delay product, $\tau_d/\tau_p \leqslant \Delta_{\text{EIT}}\tau_d = \sqrt{\text{D}}$, which in turn depends on the square root of the optical depth. The bandwidth-delay product is important as it also dictates how many spatially separated photons can be stored simultaneously in the quantum memory, $n_{ph} \approx 0.2\sqrt{\text{D}}$, which, for realistic setups ($\text{D} \approx 50 \div 300$ respectively in Ref. [18] and Ref. [3]) is $n_{ph} \sim 1 \div 4$.

Within EIT, a protocol to achieve storage involves typically involves three steps [3–5, 56, 60–66]. First, a resonant ($\Delta = 0$) control field is used to open a spectral transparency window ($n = 1$) in the medium, where the quantum light can enter freely. The control field can then be adiabatically reduced to zero. As we have seen, this process realizes a coherent transfer within the polaritonic excitation, from its photonic component to the matter one. At the same time the excitation slows down and can be stopped, as $v_g \to 0$ as $\Omega_c \to 0$. After a certain storage time, a second pulse in the control field can then make the medium transparent again, realizing on-demand retrieval of the states of light.

Interestingly, the EIT scheme is not the only way to store a photon in an atomic ensemble. With the very same Λ-scheme atoms of Fig. 1.5, several different approaches to photon storage can be taken. In the Raman configuration [67, 68], the fields have a large detuning ($|\Delta| \gg \Gamma_0\text{D}$) and the photons are absorbed into the stable ground state $|s\rangle$ by stimulated Raman transitions. Moreover, in the photon-echo approach [69–78] (the name reminds of spin-echoes experiments in nuclear magnetic resonance [79]), a controlled and reversible inhomogenous broadening is be used to dephase/rephase an atomic excitation for storage and recollection in an ensemble of two-level atoms. Ideally, when a short pulse is absorbed by an atomic ensemble, each atom will be in phase with the incoming field. This is the phase-matched state that has been discussed at the beginning of this chapter. Now, if an inhomogeneous broadening can be turned on, each emitter will acquire new frequencies. A notable example here is given by gradient-echo memories (GEM), where a spatially dependent frequency shift can be controlled with an external field [71–73, 75]. As a result, the atoms will quickly evolve to be out of phase, suppressing the strong collective emission. If, after a certain storage time, the atoms can later be brought back into phase with each other, the individual dipole moments will again

create an electric field that matches the originally absorbed light, and a photon echo will be emitted. Provided that the engineered inhomogeneous broadening can be reversed and that the spontaneous emission is slow compared to the storage time, the echo can approach the amplitude of the input light and act as an efficient memory.

To conclude, a remarkable result that has been obtained within the MBE treatment is that for all these different methods, when optimized, the storage and retrieval of an arbitrary photon shape has a maximum efficiency that only depends on the optical depth of the medium $\eta \sim 1 - 5.8/\mathrm{D}$ [54]. As a consequence, in recent experiments in EIT storage [3–5] a lot of efforts were made to push the optical depth of the atomic clouds to unprecedented values of $\mathrm{D} \approx 1000$ [4], reaching a storage efficiency of 92.0(1.5)%.

1.2 The flaw

Our theoretical understanding of atom-light interactions in such systems is largely based upon the MBE, where the atoms are treated as a smooth, polarizable medium that interacts with optical fields and where the optical depth emerges as the figure of merit of the performance of such a light-matter interface.

Despite having fundamentally improved our understanding of the interface between light and large ensembles of atoms and allowing for the above-mentioned applications, however, this macroscopic picture cannot be strictly correct. Indeed, in order to capture emission into 4π, the polarization field is assumed to spontaneously decay at the same rate Γ_0 of a single, isolated atom, which, as seen, implies that an atomic medium exhibits absorption, as characterized by an imaginary part of the optical susceptibility ($\mathrm{Im}\chi \neq 0$). However, since an atom has no internal decay channels, the atomic excitation is 100% converted into a photon."Losses" are therefore simply photons re-scattered into unwanted directions/modes (as in Fig. 1.1). Now, if another atom happens to be sufficiently close to the first one, the scattered photon has the chance to interact with it and re-scatter again, mediating the interaction between the emitters and building up correlations. Ultimately, scattering is a wave phenomenon and the intensity emitted must depend on interference between the light emitted by different atoms. Because of these reasons, in order to satisfy energy conservation and to fully take into account the wave nature of light, the correct loss description must therefore have atomic correlations and positions built-in. The assumption of independent emission (and the

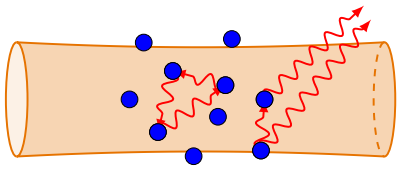

Figure 1.6: Examples of multiple scattering of light and collective spontaneous emission effects in light propagation through atomic ensembles.

resulting "absorption", despite the atom being purely dispersive), therefore, should be considered a historical attempt to avoid keeping track of all the spatio-temporal emission and interference, often considered intractable and/or unimportant.

To further build up our intuition we present here two simple examples in which light scattering could never be captured by MBE, as a consequence of its assumptions: two close-by atoms and a 2D dense array of atoms. Conveniently, these simple examples will constitute the building blocks for the ideas that will be discussed during the thesis.

1.2.1 Two strongly interacting atoms

Consider the simple scenario represented in Fig. 1.7a, where two close-by atoms are illuminated by a single photon. If the light is scattered by an atom, intuitively, the closer a second nearby atom happens to be, the higher will be the chance for the photon to scatter again. Importantly, contrary to the MBE approach, here, the atom's discrete positions are explicitly taken into account. In concrete, an excited atom at position $\mathbf{r}_1$ can de-excite, as represented by the spin operator σ^1_{ge}, emitting a photon, while a second atom at $\mathbf{r}_2$ can be excited, as described by σ^2_{eg}. The strength of such process (and its vice-versa $\sigma^1_{eg}\sigma^2_{ge}$) is really dictated by how light can propagate the distance $\mathbf{r}_{12} = \mathbf{r}_1 - \mathbf{r}_2$ from one point-like atom to the other, which is given in terms of the Green's function $G_0(\mathbf{r}_{12})$, the solution to the wave equation in free space [80]. Putting these ideas together, we anticipate here the basic form of such dipole-dipole interaction which captures the above-mentioned effect:

$$H_{2b} \sim G_0(\mathbf{r}_{12}, \omega_0)\ \sigma^1_{eg}\sigma^2_{ge} + h.c. \tag{1.4}$$

While the above Hamiltonian will be discussed in much more detail in Sec. 1.3, that is, light can mediate an effective interaction between atoms, which is naturally expected to modify its propagation as well as the atomic

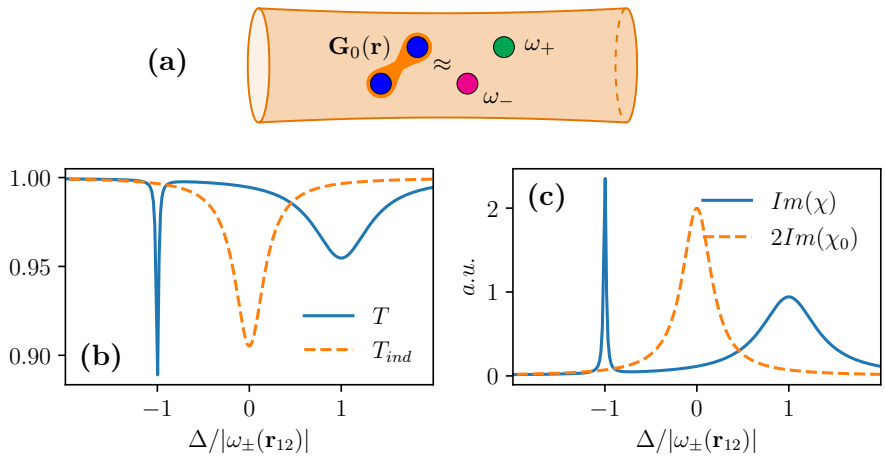

Figure 1.7: (a) Two atoms, interacting via dipole-dipole photon exchange are equivalent to two non-interacting new atoms, with new frequencies $\omega_\pm$ and new linewidths. (b) Transmission spectra of a realistic focused beam (beam waist $w_0/\lambda_0 = 2.5$) illuminating two identical atoms placed at a distance $|\mathbf{r}|/\lambda_0 = 0.1$. The orange dashed line represent the transmission of that can be calculated for the same beam and the same atomic positions, but turning off the interaction of Eq. (1.4).

state.

Interestingly, the real part of the Green's function contains a short-range component, $G_0(\mathbf{r}, \omega_0) \sim_0 1/r^3$, which dominates at small inter-atomic distances ($k_0 r < 1$) and describes near-field coherent interactions. As a consequence, the bare resonance frequency ω_0 of two close-by atoms is expected to symmetrically shift by the interaction, $\omega_\pm \sim 1/r^3$, and to be associated to new dressed states. The process can be called renormalization since the effect of such strong and local near-field interaction can be approximately captured by redefining the frequency. While the description in terms of the new frequencies and new normal modes of the system might seem abstract, it has important consequences. For example, if the interaction is sufficiently strong (high shifts), when light is recollected in transmission as in Fig. 1.7b (the formalism to rigorously evaluate such quantities will be discussed in Section 1.3), the spectrum (solid blue line) shows two dips at the new resonant frequencies $\omega_\pm$ and new linewidths, naturally associated to the imaginary part of the Green function, $\mathrm{I}m(G_0)$, which dictates dissipation. Thus, as in Fig. 1.7a, the system should be rather thought of as made of two *new effective* atoms that are characterized

by two new frequencies $\omega_{\pm}$ (represented by different colors), rather than two copies of a single isolated atom. This is in contrast with the transmission that can be obtained just considering two identical copies of independent atoms (dashed orange line in Fig. 1.7b), which would predict just twice as the resonant absorption, also signaled by the imaginary part of the susceptibility in Fig. 1.7c.

We introduced the idea that by simply adding a second close-by atom, because of the fundamental dipole-dipole interaction, the optical response (transmission and susceptibility) and the dynamics are fundamentally different from what MBE would predict, i.e. the sum of the response of two independent emitters. A full theory for describing light-matter interaction with atomic ensembles must therefore have photon-mediated dipole-dipole interaction built in. We will introduce such a theory in Sec. 1.3.

1.2.2 2D array of atoms

In this kind of system, one naturally expects interference effects to be particularly prominent, where constructive or destructive interference might be maximal. Indeed, to give a concrete example, in Fig. 1.8a we show an exact calculation of linear light scattering from a sub-wavelength ($d < \lambda_0$) square array of atoms (technique described later), revealing that the a sub-wavelength array can function as a perfect reflector for light [81–85]. In Fig. 1.8b we further plot the transmission and the reflection spectrum of a finite array. High reflection can be maintained over a bandwidth $\Gamma_c \gg \Gamma_0$, much larger than the one of a single isolated atom, as plotted in Fig. 1.8b. Another striking feature is that generically the light response is found to be dispersive, i.e. thanks to the strong interference in emission, light can either be transmitted or reflected, but only within the same input mode ($T + R = 1$). Finally, relevant to Ch. 4, where the refractive index of a 3D array of atoms will be discussed, it is important to notice that the 2D array can also imprint a $\sim \pi/2$ shift to transmitted light, as plotted in Fig. 1.8c. Such phenomena could never have been predicted from Eq. (1.1), where the optical response is independent of the precise atomic positions, and where excitation of the atoms is necessarily accompanied by dissipation (Γ_0).

This simple example is important because it shows that given the same resources, the same number of atoms N, but now reorganized regular fashion, can already provide a better light-matter interface by suppressing the "bad" emissions into unwanted modes that necessarily arise in disordered ensembles (as in Fig. 1.2). Since the effect explicitly relies on the precise

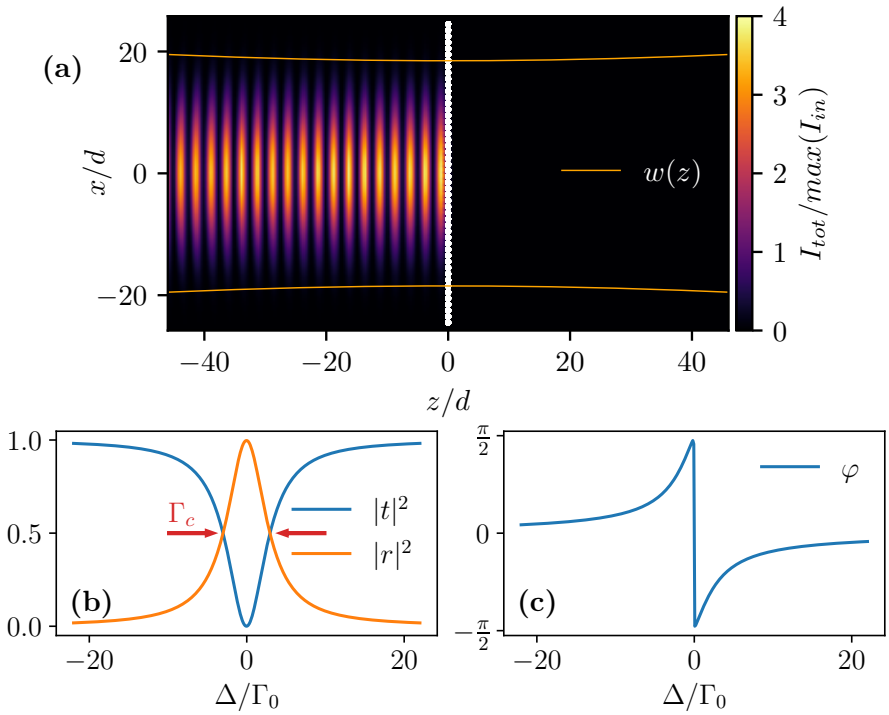

Figure 1.8: (a) Perfect reflection from a sub-wavelength 2D array of $N = 50^2$ atoms (white dots) placed in a square lattice of constant $d/\lambda_0 = 0.2$, with λ_0 the resonant wavelength. The incoming field from the left is a Gaussian beam with beam waist $w_0 = 0.3L \sim 3\lambda_0$ where L is the size of the lattice. The intensity of the total field $I_{\text{tot}} = |\mathbf{E}_{\text{tot}}|^2$, composed by the input field the rescattered one by the atoms, exhibits constructive (left) and destructive (right) interference. For the same parameters (b) shows typical transmittance (blue line) and reflectance (orange line) as a function of the detuning. The mirror is highly reflective over a linewidth Γ_c. (c) Phase shift acquired by the transmitted field, as appears in the complex transmission coefficient $t = |t|e^{i\varphi}$. All the above mentioned quantities and the formalism to calculate them are discussed in detail in Ch. 4.

discrete position of the atoms, our theory must therefore have them built-in in the first place.

Motivated by fully taking into account the granularity of atomic position, the wave nature of light, and the striking collective effect of Fig. 1.8, we seek to challenge the standard assumption of independent emission in the thesis. To correctly evaluate the optical response of an ensemble of atoms we will make use of a well-established theoretical formalism that is able to take account of the collective behavior in spontaneous emission/re-absorption in

the ensemble, which is presented in the next section.

1.3 A spin model approach to light-matter interaction

The possibility that an atomic ensemble can experience a significantly enhanced radiation rate via interference ("superradiance") was already pointed out in the seminal work of Dicke [86]. Since then a lot of effort has gone into developing and refining a quantum formalism to describe atoms coupled to radiation that includes collective effects. One such formalism was developed by Welsch and co-workers [87, 88], and is based on the classical electromagnetic Green's tensor. It can be shown [89–91] that the full dynamics of light emission and re-scattering of an arbitrary collection of atoms in free space, specified only by their discrete fixed positions, can be related to an effective open model containing only the atomic degrees of freedom and the incident field. Here we will motivate the main results, which can be understood in terms of a classical analogy [91] and review the latest results in this direction.

Indeed the problem that we want to solve is similar to the classical one of finding the total field $\mathbf{E}(\mathbf{r};\omega)$, given a known input field $\mathbf{E}_{\text{in}}(\mathbf{r};\omega)$, scattered by collection of N polarizable dipoles $\mathbf{p}_j(\omega)$ located at $\mathbf{r}_j$ (see Fig. 1.9). It is well known that the field at any given point in space, can always be written, in the frequency domain, as the sum of the external or driving field and the field re-scattered by the dipoles

$$\mathbf{E}(\mathbf{r};\omega) = \mathbf{E}_{\text{in}}(\mathbf{r};\omega) + \mu_0\omega^2 \sum_j \mathbf{G}_0(\mathbf{r},\mathbf{r}_j;\omega)\cdot\mathbf{p}_j(\omega) \tag{1.5}$$

where μ_0 is the vacuum permeability and $\mathbf{G}_0(\mathbf{r},\mathbf{r}';\omega)$ is the Green's function, the fundamental solution of the electromagnetic wave equation in free space [80]:

$$\left[(\boldsymbol{\nabla}\times\boldsymbol{\nabla}\times) - \frac{\omega^2}{c^2}\right]\mathbf{G}_0(\mathbf{r},\mathbf{r}';\omega) = \delta(\mathbf{r}-\mathbf{r}')\mathbf{I} \tag{1.6}$$

that, defining the associated wavenumber $k = 2\pi/\lambda = \omega/c$ and the distance $r = |\mathbf{r}|$, explicitly takes the form of the 3×3 tensor:

$$\mathbf{G}_0(\mathbf{r}_i,\mathbf{r}_j;\omega) = \frac{e^{ikr}}{4\pi r}\left[\left(1+\frac{i}{kr}-\frac{1}{(kr)^2}\right)\mathbb{1} + \right. \\ \left. + \left(-1-\frac{3i}{kr}+\frac{3}{(kr)^2}\right)\frac{\mathbf{r}_i\otimes\mathbf{r}_j}{r^2}\right] \tag{1.7}$$

Since Eq. (1.5) just describes the field propagation, which is equivalent for both a classical and a quantum field (Maxwell's equations are valid both classically and quantum mechanically), after promoting the dipoles and the field to quantum operators, it is also expected to be valid in the quantum realm. In concrete, it is sufficient replacing the classical dipole moment $\mathbf{p}_j$ by the operator $\hat{\mathbf{p}}_j^+$, and $\mathbf{E}(\mathbf{r})$ by the field operator $\hat{\mathbf{E}}^+(\mathbf{r})$, respectively their positive-frequency component. Moreover, an atom only have a significant optical response in a narrow bandwidth around its resonance frequency ω_0, therefore, it is possible to approximate $\mathbf{G}_0(\mathbf{r}_i - \mathbf{r}_j, \omega) \approx \mathbf{G}_0(\mathbf{r}_i - \mathbf{r}_j, \omega_0)$, which allows the Fourier transform of Eq. (1.5) to become local in time. Intuitively, retardation effects are expected to be negligible (Markovian approximation), when $\Delta\omega L/c \ll 1$, where L is the characteristic length of the system and $\Delta\omega$ is the bandwidth of the atomic dynamics. The latter is roughly given by the spontaneous emission decay rate, Γ_0, which is typically around a few MHz, resulting in a significant phase difference only over a length of $L \geqslant 1m$, much longer than typical atomic setups. As a result the total field at a given time only depends on the instantaneous atomic state, which results in an input-output equation for the positive rotating field [87, 91]:

$$\mathbf{E}^+_{\text{tot}}(\mathbf{r}, t) = \mathbf{E}^+_{\text{in}}(\mathbf{r}, t) + \mu_0 d_{ge}\omega_0^2 \sum_j \mathbf{G}_0(\mathbf{r}, \mathbf{r}_j, \omega_0) \cdot \boldsymbol{\wp}\, \sigma^j_{ge}(t). \tag{1.8}$$

In parallel, to reach (1.8), as ubiquitous in quantum optics, we expressed the dipole operator $\hat{\mathbf{p}} = \boldsymbol{\wp}^* d_{ge}\hat{\sigma}_{eg} + \boldsymbol{\wp} d_{ge}\hat{\sigma}_{ge}$ in terms of an orientation vector $\boldsymbol{\wp}$, the coherence operators σ associated to the dipole transition between a ground state $|g\rangle$ and an excited one $|e\rangle$, and the dipole matrix element such that $d_{ge} = \langle g|\hat{\mathbf{p}} \cdot \boldsymbol{\wp}|e\rangle$. The hat, to explicitly indicate a quantum operator, is further dropped for the sake of simplicity. Now that the field has been expressed solely in terms of the input field and the atomic operators, one needs to solve for the latter, deriving the Heisenberg equation of motion from the full atom-field Hamiltonian. Intuitively, since the field itself depends only on other atoms via the input-output equation, the atomic dynamics can be fully derived from an equivalent master equation for the atomic density operator $\hat{\rho}(t)$ that describes the atomic dynamics:

$$\dot{\hat{\rho}} = -\frac{i}{\hbar}\,[H, \hat{\rho}] + \mathcal{L}[\hat{\rho}] \tag{1.9}$$

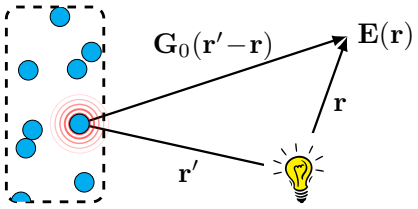

Figure 1.9: A light source (light bulb) shines an ensemble of classical dipoles (blue dots). The total field at the point $\mathbf{r}$ is the sum of the field coming from the source (input) plus the scattered one by the dipoles, $\mathbf{E}_{\rm tot}(\mathbf{r}) = \mathbf{E}_{\rm in}(\mathbf{r}) + \mathbf{E}_{\rm sc}(\mathbf{r})$. The Green's function $\mathbf{G}_0(\mathbf{r}', \mathbf{r})$ renders the electric field at the field point $\mathbf{r}$ due to a single point source at $\mathbf{r}'$.

The Hamiltonian and the Lindblad operator take the form:

$$\begin{aligned} H =& H_{\rm at} + \hbar \sum_{i \neq j}^{N} J^{ij} \sigma_{eg}^{i} \sigma_{ge}^{j} \\ J^{ij} =& \frac{3\pi\Gamma_0}{k_0} \wp^* \cdot \mathrm{Re}\mathbf{G}(\mathbf{r}_i, \mathbf{r}_j, \omega_{eg}) \cdot \wp \end{aligned} \tag{1.10}$$

$$\begin{aligned} \mathcal{L}[\hat{\rho}] =& \sum_{i,j}^{N} \frac{\hbar\Gamma^{ij}}{2} \left(2\sigma_{ge}^{i} \hat{\rho} \sigma_{eg}^{j} - \left\{ \sigma_{eg}^{i} \sigma_{ge}^{j}, \hat{\rho} \right\} \right) \\ \Gamma^{ij} =& -\frac{6\pi\Gamma_0}{k_0} \wp^* \cdot \mathrm{Im}\mathbf{G}_0(\mathbf{r}_i, \mathbf{r}_j, \omega_{eg}) \cdot \wp. \end{aligned} \tag{1.11}$$

Although the equations above look quite different compared to the standard Maxwell-Bloch equations, they of course reduce to well-known results. For a single atom in free space, for example, the theory recovers exactly the usual spontaneous emission rate of the Weisskopf-Wigner theory $\Gamma^{ii} = \Gamma_0 = \frac{\omega_{eg}^3 d_{ge}^2}{3\pi\hbar\varepsilon_0 c^3}$. The dynamics of the wavefunction under the master equation can be equivalently described in the quantum jump formalism of open systems [92–95]. Within this formalism, the evolution is deterministic under an effective non-Hermitian Hamiltonian for spins

$$H = H_{\rm at} - \frac{3\pi\Gamma_0}{k_0} \sum_{i,j}^{N} \boldsymbol{\wp}^* \cdot \mathbf{G}_0(\mathbf{r}_i, \mathbf{r}_j, \omega_{eg}) \cdot \boldsymbol{\wp}\, \sigma_{eg}^{i} \sigma_{ge}^{j}, \tag{1.12}$$

but must be accompanied by stochastic application of the recycling "quantum jump" $\sigma_{ge}\rho\sigma_{eg}$ operator in Eq. (1.11). The model can be intuitively understood as the term $\sigma_{eg}^{i}\sigma_{ge}^{j}$ enables an exchange of excitations between

atoms, as one should expect from a photon-mediated emission and re-absorption. Moreover, its strength naturally depends on how a photon propagates from atom j to atom i, as encoded in the Green's function in free space.

We thus propose that Eqs. (1.8) and (1.12) constitute a novel, but exact, formulation of atom-light interactions, which properly accounts for atomic positions, multiple scattering, and wave interference. Generally, these equations state that the true degrees of freedom are the atomic spins themselves. If their dynamics or correlations can be solved through Eq. (1.12), then all of the quantum field properties and correlations can be constructed "for free" using Eq. (1.8), based upon knowledge of the atoms and the input field. Once the dynamics of the atoms is solved, the electric field at every point can be recovered through the input-output equation (1.8) that relates the field to the atomic operators.

These equations present a number of interesting and attractive features. For example, up to now the single-particle Hamiltonian (H_{at}) nor which distribution of the emitters that we are considering have been specified. Moreover, in the spirit of its early theoretical development [87], the formalism can be also generalized in the presence of arbitrary dielectric structures, specified by $\epsilon(\mathbf{r})$, the position-dependent and possibly frequency-dependent relative permittivity of the medium, allowing the model to equally well capture a whole range of actively investigated atom-light interfaces (cavities, nanophotonic structures, etc.) simply by replacing the Green's function, solution of (1.6).

Due to its universality and flexibility, the spin model is, therefore, the ideal candidate to study the problem of light-matter interaction with ensembles of atoms.

It is also interesting to note that the case of one excitation is special, as the Hamiltonian is an $N \times N$ matrix (see later) and the system is formally equivalent to a linear optics problem. Beyond that, however, Eq. (1.12) represents an out-of-equilibrium, open, (generally) long-range interacting many-body spin system. These are all contemporary themes in condensed matter physics or quantum information [19, 96], which opens up the possibility to find novel and unexpected links between quantum optics and other fields.

Having elucidated the formalism to self-consistently treat light-matter interaction with atomic media that will be used during the thesis it is important to review some important results that have already been obtained. Even more importantly, this will allow us to discuss the general directions and long-term goals of the field, which can be nicely summed up into two

fundamental questions:

- Is there some new and exciting physics beyond MBE?
- Are the performance of quantum technology simply limited by the optical depth as MBE would predict? Can we do better?

Regarding the first point, for example, the macroscopic picture that MBE offers has been challenged by theoretical considerations based on refined treatments of microscopic details, such as atomic granularity, dipole-dipole interactions, and multiple scattering. Already within the linear optics regime, highly nontrivial effects are predicted in disordered ensembles, such as superradiance and subradiance [97–103], modifications of refractive indices and scattering rates [82, 104–110], coherent back-scattering [111–113], and 3D Anderson localization of light [114–117]. The disorder can be also exploited to achieve perfect focusing in complex media [47, 118]. Remarkably, one of the latest results was to show that in contrast to what MBE would predict (see Sec. 1.1), the maximum index does not indefinitely grow with increasing density but rather saturates to a real-life value ($n \sim 1$) [119]. Starting from the simple idea introduced in Sec. 1.2.1, the authors develop a strong-disorder renormalization group approach that is able to treat the near-field interaction between all the strongly interacting pairs in a disordered ensemble and results in an inhomogeneous broadening of atomic resonance frequencies. This ensures that, regardless of the physical atomic density, light at any given frequency only interacts with at most a few near-resonant atoms per cubic wavelength, thus limiting the optical response and thus the maximum index.

At the same time, the possibility of identifying new phenomena or more powerful protocols for applications involving arrays, such as by suppressing light emission into unwanted modes, as anticipated in Sec. 1.2, has gained significant interest recently. Despite the current limitations of each platform, arrays of atoms are already available in laboratories. Notable examples include the experimental realization of a Mott phase with ultracold atomic gases [120] and optical tweezer arrays [121], which naturally leads to the necessity of understanding how light propagates through regular atomic structures.

For one-dimensional arrays of atoms, for example, when coupled to a 1D photonic continuum realized by a waveguide such as an optical fiber [122–124] or a microwave waveguide [125, 126], an elegant input-output formalism has been developed [43, 89, 127]. Potential applications includes new realization of CQED-like physics with atomic mirrors instead of

conventional optical cavities [128, 129], create exotic many-excitation dark states with fermionic spatial correlations [130] or multipartite entangled steady states [131, 132], and use classical light sources to generate entangled quantum many-body states of light [133–138] and quantum computation [139]. Moreover, a one-dimensional chain of atoms has been shown to display subradiant states [90, 91, 130, 140–144]. These modes are guided, can propagate freely through the structure at a reduced (subradiant) decay rate, but can also efficiently be interfaced to 1D waveguides for write/read-out operations and exponentially reducing the error of photon storage [90] with respect to previously known bounds (MBE). Moreover, periodic modulation of the properties of the dielectric waveguide can fundamentally alter the otherwise linear dispersion relation of light, to realize a photonic crystal waveguide (PCW) [145]. In these structured systems, propagation is well described by a band structure $\omega(k)$ and can be engineered to create band-gaps, i.e. range of frequencies in which light cannot propagate, or flat bands, which corresponds to a strong reduction in the group velocity of light $v_g(k) = \partial\omega/\partial k \sim 0$, to further boost light-atom interaction simply increasing their interaction time [146]. As a result, not only strong light-matter interaction without the need for a conventional optical cavity can be realized in such systems [129, 147–151], but for example, an excited atom whose transition frequency resides in the gap would not be able to spontaneously emit and the atom-photon system can form a bound state [135, 152–155]. While reaching the regime in which coherent interactions dominate dissipative and decoherence effects paves the way to design interesting many-body states of light [137] or to explore fundamental physics [156] in a similar fashion to what has been done in the CQED setup. Moreover, the richness of a structured 1D photonic bath effectively provides ways to engineer atom-atom interactions to realize interesting new many-body models when arrays are coupled to PCW [155, 157], beyond what is possible and fundamentally fixed in free space, the dipole-dipole interaction, as we have seen in this chapter.

Additionally, as discussed, the formalism allows also the study of light-matter interfaces beyond the single excitation regime. In a recent study [158], for example, it was shown that the appropriate combination between the spin model and Matrix Product State (MPS) numerical techniques provides the first general numerical technique to solve the MBE beyond linearized or Gaussian regimes.

As anticipated, the strong collective response of a 2D array of atoms has also attracted notable interest [159–162]. Importantly, the key aspects of this approach such as an enhanced light-matter coupling strength and

the directional mirror reflection of the incoming light using a 2D array [81–85] atoms has been recently experimentally demonstrated [163]. Leveraging such a powerful interface, for example, single-photon storage with polynomial improvement in error scaling [164] has been proposed. When the nature of the atoms is taken into account, intriguing nonlinear optical phenomena can arise [165–167]. Specifically, the Rydberg blockade can be used to induce a conditional response to light in order to produce interesting quantum optical states [168, 169] or to realize a photon-photon gate [170]. Moreover, atomic arrays in 2D can also exhibit intriguing topological properties such as the existence of long-lived topological edge states [171–173].

1.4 Overview of the thesis results

In the first part of this chapter, the standard approach to describing light-matter interaction with atomic media has been reviewed. It has been further discussed that such a formalism is necessarily flawed since it does not take into account the multiple scattering and wave interference that necessarily builds up when light propagates in a complex and granular atomic medium. Furthermore, we provided two concrete examples in which the MBE formalism cannot predict the correct behavior: two strongly interacting atoms, and a 2D atomic array. We then reviewed a theoretical description, a spin-model for light-matter interaction, which can capture such phenomena in a many-body open interacting theory. Again, it is important to understand these and similar microscopically-driven anomalous optical effects, both within and beyond the linear optics regime, so as to refine our knowledge of quantum light-matter interactions and practically improve ensemble-based quantum optical technologies. Following these lines, we present our contribution of the thesis to the answer to those questions, introducing its main results.

1.4.1 Unraveling dephasing in atomic media

In reviewing different approaches to realizing an efficient light-matter interface, cold atoms ensembles emerged as a realistic platform for various quantum technologies. Our theoretical understanding of atom-light interactions in such systems, and consequently the performance of the above-mentioned applications, is largely based upon the Maxwell-Bloch equations (MBE), where the atoms are treated as a smooth, polarizable medium that interacts with optical fields. This macroscopic picture has

been challenged by theoretical considerations based on refined treatments of microscopic details, such as atomic granularity, dipole-dipole interactions, and multiple scattering. Within the linear optics regime, highly nontrivial effects are predicted such as modifications of refractive indices and scattering rates [104–108, 110], coherent back-scattering [111–113], and 3D Anderson localization of light [114, 116, 117]. It is important to understand these and similar microscopically-driven anomalous optical effects, both within and beyond the linear optics regime, so as to refine our knowledge of quantum light-matter interactions and practically improve ensemble-based quantum optical technologies.

To experimentally quantify such microscopic effects, the measurements need to be carefully designed to isolate any effects being well-described by the standard MBE. This is challenging since, as shown before in Fig. 1.2a, most of the light is collectively emitted in a highly directional fashion and at enhanced rate $\Gamma_{\mathbf{k}} \sim D\Gamma_0$. As a consequence, measurements have so far been restricted to either recollect the emitted light, and useful intensity correlations, from a different direction [117], probing the 4π speckle pattern in Fig. 1.2a, or to explore emission at late times when most of the collective excitation has already left the system [106–108]. The verification of subtle microscopic effects also relies on a side-by-side comparison with numerical approaches but is computationally limited to moderate sample sizes L and atom numbers N, even if the modeling is classical [174]. In addition, despite efforts in the field of nonlinear optics [175–181], techniques to precisely quantify microscopic near-field correlations of optical excitations, similar to those regularly achieved in nuclear magnetic resonance (NMR) studies [182–186], are still missing. In Chapter 2, a background-free, precise measurement of microscopically-driven anomalous optical effects, made possible by actively suppressing the macroscopic dynamics, is demonstrated. This technique unveils a previously unidentified density-dependent dephasing mechanism of dipole spin waves on an optical transition which is attributed to microscopic fluctuations of resonant dipole interactions in an otherwise ideal ensemble of laser-cooled atoms. The excellent agreement between the experimental data and a simple theory based on the statistical chance to find strongly interacting pairs in a disordered ensemble is the main result discussed in this chapter.

The first part of the chapter is thus dedicated to introducing the measurement scheme, which relies on being able to shift the wavevector $\mathbf{k} \to \mathbf{k}'$ of collective spin-wave excitations in the atomic medium [45, 187–189]. As we will see, the combination of an additional auxiliary transition and sub-nanosecond control pulses can deterministically and coherently

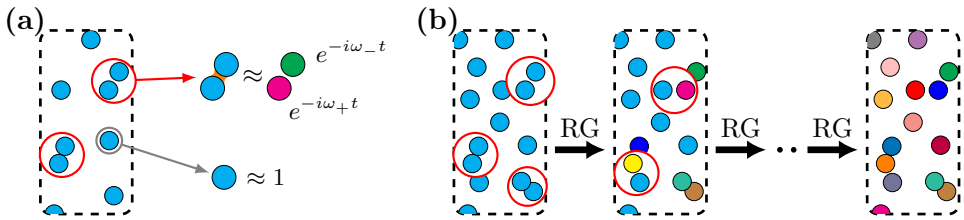

Figure 1.10: (a) A pair-wise approach to the many-atom optical dynamics. In a dilute atomic medium, a small fraction of pairs of atoms (red circles) are separated by a distance much smaller than a wavelength, and thus interact strongly via their near fields. These atoms can be replaced with a non-interacting, dynamically equivalent pair with new effective resonance frequencies (indicated by different colors), which evolve with the phase $e^{-i\omega_\pm t}$. Single isolated atoms instead will not significantly contribute to time evolution. (b) Representation of the RG scheme [119]. Each step is characterized by identifying the most strongly interacting pairs and replacing them with two new atoms with different frequencies, which do not interact anymore through the near field. Unlike in (a), one can continue this process (including the renormalization of atoms previously renormalized) until all near-field interactions have been eliminated. The overall system at the end is then equivalent to an inhomogeneously broadened ensemble of spectral distribution $P(\omega)$.

write a position-dependent phase on each atom. With this robust geometric phase imprinting technique, general control over the atomic excitation wavevector can be achieved. In particular, one can create highly mismatched spin waves $|\mathbf{k}'| \neq \omega_0/c$ [189]. As their name suggests, being out of phase with respect to free-space radiation, these atomic excitations cannot efficiently radiate, but rather constitute states in which all the atoms on average emit as if they were independent, with no preferred direction of emission and at the rate Γ_0. In other words, they are essentially free of collective evolution under MBE. While phase-matched spin waves with $|\mathbf{k}| = \omega_0/c$ are most naturally created in the lab, the shift to a phase mismatched state can then be applied on-demand. This gives sufficient time to the atoms to build up microscopic correlation due to the dipole-dipole interaction. Importantly, by shifting back the spin wavevector to match the dispersion relation of light, the atomic state can be mapped back to light for efficient optical measurements. By studying the time-dependent decay of the mismatched spin waves, we unveil and precisely characterize a dephasing effect that should generally exist in *any* ensemble-based light-matter interface, and which can be significant even at moderate density $\rho < |\mathbf{k}|^3$.

Theoretically, the dephasing mechanism is shown to arise from the

combination of random atomic positions and the near-field interactions between the optically excited pairs of close-by atoms. In particular, as already anticipated in Sec. 1.2.1, the optical response of a pair of strongly interacting atoms is equivalent to a similar pair, but in which the effect of the strong near field has been renormalized into new effective frequencies. Within the same line of reasoning, also the dynamics is expected to be captured. The standard approach (MBE) would predict that the phase of a single excitation shared between the two atoms would not evolve in the rotating frame $e^{i\omega_0 t}$ of the single atom, and thus the phase coherence to be preserved. Indeed, this is true for single isolated atoms, far apart from all the other emitters, which, as represented in Fig. 1.10a, display no dynamics. Close-by pairs instead (highlighted by red circles), because of the strong and coherent interaction and the consequent spitting, will cause the phase of the two renormalized atoms to evolve differently, i.e. with $e^{i\omega_\pm t}$.

In a many-body system now, with the atoms being initialized in a well-defined phase relation, close-by pairs, locally disrupting the phase order, will cause the spin wave to *dephase*. To capture such an effect we develop a simple theory that, based on the presented replacing strongly of interacting pairs that statistically occur in a randomly distributed ensemble (as in Fig. 1.10a) in favor of new atoms with new effective frequencies, is able to analytically construct a frequency probability distribution $P(\omega)$ for an atom to have a close neighbor and thus a new effective frequency ω. The net effect of the near-field interaction is thus captured as an inhomogeneous broadening of the two-level transition. Because of this, spin waves are shown to experience a short-time exponential dephasing rate $\gamma = C\Gamma_0\eta$ on top of their natural collective spontaneous emission decay. The dephasing is found to linearly depend on the density η. Importantly, since our approximate solution of the many-body dynamics just relies on the understanding of the two-body problem, it can be easily generalized to describe more realistic hyperfine atomic transitions (as the $D1$ line in ^{87}Rb in the experiment), which results in a different prefactor C. The theory, valid in the short time regime and at the moderate densities that can be experimentally achieved ($\eta < 10$) and where nearest-neighbor pairs of atoms are expected to give the biggest contribution, displays excellent agreement with the experimental data.

These results should have implications for quantum technologies based on atom-light interfaces, for example, imposing bounds on atomic densities in order to achieve desired fidelities. More importantly, this work represents one first step toward precisely measuring interacting spin dynamics in the optical domain in a way similar to microwave NMR research [182–184, 186],

but involving the much stronger electric dipole interaction, and for radiation at a much shorter wavelength. While we specifically investigate dephasing here, we believe that our powerful method to suppress macroscopic dynamics will generally facilitate investigations of diverse other anomalous effects [109, 114, 116, 117] in the optical domain, where microscopic correlations are likely overshadowed by collective radiation.

Contribution of the authors

This work, reported in [190] and under peer review, involved close collaboration with the experimental group of Prof. Saijun Wu at Fudan University (Shanghai). Together with Dr. Yizun He and the other authors, they conceived and realized the experiment to measure the microscopic dynamics in cold atomic ensembles and performed the numerical simulations of the MBE. The contribution of the author of this thesis, supervised by Prof. Dr. Darrick E. Chang, was to understand the inadequacy of the MBE approach and to develop the theory to explain the experimentally found additional dephasing in terms of strongly interacting pairs and extend it to realistic hyperfine transitions used in the experiment.

1.4.2 Dephasing in dense media: A renormalization group approach

In the previous project, we argued that there should exist an additional dephasing on top of spontaneous emission decay for optical spin waves, with a rate that is exponential at early times and is directly proportional to atomic density. It was argued that this initial dephasing arises from the strong near-field interaction of a small fraction of particularly close nearest neighbors, quantitatively reproducing the experimental results. Separately, though, one might wonder what governs the dephasing behavior at later times, or what occurs at very high densities, when many atoms sit within a wavelength of each other and experience strong near-field interactions. We also note that near-field interactions have been recognized to play key roles in other collective behavior, ranging from the modification of superradiance in small systems [191] to late-time subradiance [102] in extended systems. Beyond exact numerics, however, the development of effective theories generally remains a challenge in many-atom disordered systems.

In Chapter 3, a comprehensive theoretical picture of the spin-wave dephasing phenomenon is provided by applying a non-perturbative technique based on strong disorder renormalization group (RG), which is a

powerful method to elucidate the physics in diverse disordered condensed matter systems [192–199] and has also recently been applied to atom-light interactions [119]. As in the short-time theory of dephasing, one key idea underlying this approach is that for highly disordered atomic media, strong near-field interactions between particularly close nearest neighbors allow such pairs to be approximately diagonalized first. The resulting dynamics is equivalent to replacing the pair with two, new *effective* atoms with renormalized frequencies, as illustrated in Fig. 1.10a. The RG theory goes significantly beyond this, however, by realizing that nearby, strongly interacting pairs (including atoms previously renormalized) can continue to be identified and diagonalized, i.e. the many-atom system interacting via the near field can be thought of and diagonalized in terms of an extended hierarchy of strongly interacting pairs (Fig. 1.10b). The final result is that the original system is dynamically equivalent to an inhomogeneously broadened medium with a well-defined distribution of resonance frequencies $P(\omega)$, and with the strong near-field interactions effectively removed. This approach was recently used to predict that a disordered atomic medium has a limiting value of the maximum refractive index, regardless of its physical density [119]. It will be shown that RG not only works to capture the stationary optical response of a dense gas but also to capture the above-mentioned time-dependent dephasing dynamics of spin waves, in a simple and non-perturbative way. The validity of the RG approach is quantitatively verified by comparison with full, microscopic coupled-dipole simulations of large ($N \sim 10^4$) atomic ensembles.

Contribution of the authors

The author of this thesis, again supervised by Prof. Dr. Darrick E. Chang, conceived the idea of applying a recently developed strong disorder renormalization group technique [119] to study the dephasing dynamics in dense ensembles of atoms. The findings are reported entirely in Chapter 3. Prof. Saijun Wu and Dr. Yizun He provided expertise and contributed through an intense exchange of ideas which ultimately shaped this project into its final published form [200].

1.4.3 Refractive index of a 3D atomic array

The refractive index is the most important defining property of a material in photonics, setting the practical limitations to waveguiding, lensing, imaging, optical lithography, etc. Despite the technological importance

that an ultrahigh index material would have, all known optical materials have an index of order $O(n) \sim 1$. Starting from this basic observation, recently pointed out by several authors [119, 201–203], Chapter 4 presents recent efforts to understand what are the fundamental physical mechanism that prevents reaching a high index and if an answer can come from a simple electrodynamical model.

The starting point is realizing that textbook theories do not provide a satisfactory answer. Indeed, as described in the introduction the standard approach (MBE) treats an ensemble of atoms as a smooth medium, characterized by a linear susceptibility, which is simply proportional to the linear response of a single, isolated atom, and the density. This scaling comes from the assumption that atoms interact with the optical field independently, neglecting the possible complex behavior associated with wave interference and multiple scattering of light, and implies that the refractive index should also grow with the density. When evaluated at the typical densities of everyday materials, where the atoms sit a few Bohr radii from each other, the predicted index reaches huge nonphysical values.

In Sec. 1.2.2 it was already anticipated that multiple scattering and photon-mediated interactions between emitters are expected to play a major role in systems that exhibit a discrete translational invariance. In concrete, a 2D array of atoms can function as a perfect mirror, and imprint up to a $\pi/2$ shift to the phase of the transmitted field. Intuitively, stacking multiple two-dimensional arrays, should provide the maximal optical response per unit of length and thus the maximal index. For these reasons, the optical response of a unity-filled, three-dimensional optical lattice of atoms, will be investigated, making use of the previously introduced spin model formalism in combination with generalized input-output equations.

The paradigmatic case of an infinite array is discussed first. In such a system the natural basis to describe the propagation of excitations inside the system is the one of spin waves, characterized by a well-defined wavevector. For each of these modes, we describe how to calculate its energy and its decay rate, i.e. the band structure, which is found to possess several interesting properties, the most important being completely real, describing lossless propagation. It is further argued that a sub-wavelength array, as in Sec. 1.2.2, necessarily scatters light into a single mode, i.e. light can either be reflected or transmitted, as the lattice prevents coherent scattering of light into any diffraction orders. In this dispersive single-mode environment, we then predict that the propagation of light in the medium, as seen from the outside of a sufficiently big array, should be completely determined by the calculated unidirectional band structure. In particular, as the phase

index can be seen as the ratio between the effective momentum of light inside the medium and the free space one, $n = k_{\text{eff}}/k_0$, the maximum index is given by those modes that live at the end of the Brillouin zone. In concrete, n can be as big as $n_{\max} = \pi/dk_0 = \lambda_0/2d$ and then display an unbounded increase with the atomic density.

We then discuss how to calculate the exact linear optical response for a finite system, through the previously introduced spin model formalism in combination with generalized input-output equations. It is shown that by illuminating the array from outside, light can only be either reflected or transmitted into the same input mode, constituting, as predicted, a dispersive light-matter interface. Finally, the refractive index directly from the phase acquired by the transmission coefficient and the one that can be predicted by the band structure are shown to perfectly agree.

The central result of the chapter is therefore that in a dense, ordered configuration of point-like atoms, where multiple scattering and photon-mediated interactions are not only fully taken into account, quantum optics allows for the phase refractive index to be as big as $n_{\max} \sim \eta^{1/3}$ and to be furthermore completely real.

In the last part of the chapter instead, we speculate that even higher densities, once the lattice constant is comparable with the Bohr radius, where the electronic orbitals start to overlap, new quantum chemical interactions necessarily appear. Their possible effect on the refractive index problem is discussed, leaving a more quantitative analysis for the future. Overall, understanding the fundamental limitations of the refractive index in real-life materials might open new paths to realizing ultra-high index materials exploiting the perfect interference mechanism.

Contribution of the authors

The author of this Ph.D. thesis and its supervisor, first studied the refractive index of a perfect 3D array of well-separated atoms and this contribution is reported entirely in Chapter 4. The quantum chemistry part, here introduced to provide an overview of the whole refractive index project, is being currently investigated by F. Andreoli, G. M. Andolina, and B. Windt, members of the Theoretical Quantum Nano-Photonics group at ICFO, led by Prof. Dr. Darrick E. Chang.

Part II

Results

CHAPTER 2

Unraveling microscopic dipolar interactions in quantum atom-light interfaces

2.1 Introduction

In the introduction to the thesis, we discussed how interactions between light and atomic ensembles are generically complex phenomena. Even in the weak optical excitation limit, microscopic correlations can build up through resonant dipole interactions and multiple scattering, leading to highly nontrivial anomalous optical response [104–110] or even wave localization [111–117]. For stronger excitations [142, 165, 167, 204–206], the many-body dynamics may start to span the exponentially large Hilbert space and become difficult to understand and to be numerically treated. Nevertheless, our prevailing theory of quantum light-atom interfaces, the Maxwell-Bloch equations (MBE) [1, 2, 50–55] that largely ignore microscopic correlations, remains highly successful. To experimentally quantify the microscopic correlations, the challenge is that measurements need to be carefully designed to isolate any effects being well-described by the standard MBE [106–109, 117]. Although methods to elucidate interactions beyond MBE have also been developed in the field of nonlinear optics [175–181], their utility clearly lags behind the level at which microscopic degrees of freedom can be investigated within nuclear magnetic resonance (NMR) research and even exploited for studying fundamental quantum dynamics [184–186] and quantum computation [207, 208].

What is causing the difference between NMR and atom-light interfaces on resolvable microscopic correlations? A key answer was provided in a seminal paper more than 70 years ago [209] where Van Vleck suggested that his treatment of many-body spin-relaxation dynamics in NMR may

not be applicable to light, due to the Doppler and radiation broadening. Indeed, in the optical domain, the atomic motion and radiation effectively smooth away and damp out the microscopic correlations. Today, while the introduction of laser-cooling techniques can freeze out the atomic motion, the collective radiation [98, 189, 210, 211] and more generally the propagation of light itself remain an effective damping mechanism to suppress local optical dipolar correlations from freely building up, thereby limiting the precision in the state-of-art linear [106–109] and nonlinear [177–181] spectroscopy for probing microscopic correlations with macroscopic atomic samples. At the same time, despite the emergence of a theoretical approach that in principle can capture all the above-mentioned phenomena (the spin-model for light-matter interaction discussed in Sec. 1.3), their investigation has been generally limited to numerical simulations, which already in the linear regime is restricted to small cloud sizes and small atoms number compared to experiments. A simpler approach that can capture the main physical consequences of dipole-dipole interaction for comparison with the experiments is therefore desirable.

A general method to probe microscopic correlation dynamics at quantum atom-light interfaces is presented in this chapter. Besides using a motionless gas of laser-cooled atoms, the key novelty of this approach is to completely suppress collective radiation and macroscopic light propagation, by shifting the collective optical excitation in $\mathbf{k}-$space beyond the light cone [189]. The reversible suppression of collective dynamics allows the interaction associated with microscopic dynamics to accumulate over a long time, before a backward $\mathbf{k}$-shift to map the effects onto collective radiation for efficient measurement. By applying the method to an atomic ensemble, a fundamental density-dependent dipolar dephasing that limits the lifetime of atomic excitations is discovered. A simple analytical theory that captures the additional dephasing rate is provided. This is based on the dominant role of strong near-field optical interactions and the consequent strong frequency shifts between close-by pairs of atoms in a disordered ensemble, which in turn affects the short-time dynamics. The general method in this demonstration is important for discovering and exploring many-body aspects of quantum atom-light interfaces and optical anomalous effects beyond MBE and should be considered as an optical counterpart to the historical NMR spin-relaxation measurement [182].

This chapter closely follows the efforts presented in Ref. [190], as a result of a collaboration with the experimental group of Prof. Saijun Wu at Fudan University (Shanghai) and is organized as follows. In Sec. 2.2 both the existing formal theory (MBE) and our spin model approach in

the context of the relaxation dynamics of optical spin waves are reviewed. This will allow us to anticipate the main result of this work, a previously unidentified additional source of decay of spin-wave order. In Sec. 2.3, the experimental setup will be presented together with a discussion on the coherent technique to suppress macroscopic dynamics. Measurements will reveal a local-density-dependent dipolar dephasing of phase-mismatched spin waves. Sec. 2.4 will provide a simple theoretical model of the dephasing effect that is based on the role of strongly interacting pairs in the disordered atomic media. Importantly, the theory can be easily generalized to treat the realistic hyperfine atomic level structure of the atomic species. By doing so, the predicted dephasing rate agrees well with the experimental data. To conclude the chapter, Sec. 2.5 presents an expanded discussion and prospects on both the measurement method and the microscopic dipolar dephasing effect in the optical domain.

2.2 Optical spin wave relaxation

We begin by briefly reminding the previously introduced formalism for light-matter interactions, which in principle fully accounts for the granularity of atoms and multiple scattering. For concreteness, let's consider an ensemble of N two-level atoms with the ground and excited states $|g_j\rangle, |e_j\rangle$, leaving the important discussion of more realistic hyperfine level structures for later. The atoms are randomly distributed at location $\mathbf{r}_j$, $j = 1, \cdots, N$ according to a smooth density profile $\rho(\mathbf{r})$ with a spatial width σ. The atoms can interact via the emission and re-absorption of a single photon, whose resultant dynamics can be described by the effective Hamiltonian:

$$H = -\frac{3\pi\Gamma_0}{k_0}\sum_{i,j}^{N} \boldsymbol{\wp}^* \cdot \mathbf{G}_0(\mathbf{r}_i, \mathbf{r}_j, \omega_{eg}) \cdot \boldsymbol{\wp}\ \sigma_{eg}^i \sigma_{ge}^j \tag{2.1}$$

We remind that here, $\sigma_j^{ge} = |g_j\rangle\langle e_j|$ and $\sigma_j^{eg} = (\sigma_j^{ge})^\dagger$ are the single atom spin-lowering and raising operators respectively, and $\boldsymbol{\wp} = \hat{\mathbf{x}}$ is orientation of the dipole, assumed to be fixed along with $\hat{\mathbf{x}}$. The free-space electromagnetic Green's tensor $\mathbf{G}_0(\mathbf{r}_{ij}, \omega_0)$ with $\mathbf{r}_{ij} \equiv \mathbf{r}_i - \mathbf{r}_j$ physically describes how light propagates from a point source at $\mathbf{r}_j$ to another point $\mathbf{r}_i$, thus encoding the photon-mediated interaction. As mentioned in the previous chapter and important to later considerations, $\mathbf{G}_0$ contains both a far-field, radiating component $\mathbf{G}_0^{\text{far}}(\mathbf{r}_{ij}) \sim_\infty 1/r_{ij}$ and a $\mathbf{G}_0^{\text{near}}(\mathbf{r}_{ij}) \sim_0 1/r_{ij}^3$ near-field component.

The Hamiltonian of Eq. (2.1) is non-Hermitian and includes both coherent interactions and dissipative collective emission. In the case of an isolated, excited atom, this Hamiltonian predicts a spontaneous emission rate of $\Gamma_0 = \omega_0^3 d_{ge}^2/3\pi\hbar\varepsilon_0 c^3$. Generally, as mentioned in the introduction, a complete quantum description of dissipation would require a master equation, but the non-Hermitian Hamiltonian is sufficient in the single-excitation regime of interest here. Physically, any dissipation of atomic excitations must be in the form of emitted photons. The specific properties of the emitted light are encoded in the quantum electric field operator [87, 91],

$$\hat{\mathbf{E}}_s(\mathbf{r}) = \mu_0 d_{ge}\omega_0^2 \sum_i^N \mathbf{G}(\mathbf{r}-\mathbf{r}_i,\omega_0)\cdot\boldsymbol{\wp}\,\sigma_{ge}^i, \tag{2.2}$$

which can be always reconstructed with the knowledge of the atomic state. This formalism can thus be applied to investigate the emission and dynamical properties of single-excitation spin waves. Formally these take the form $|\mathbf{k}\rangle = S^+(\mathbf{k})|g_1,g_2,\cdots,g_N\rangle$ with $S^+(\mathbf{k}) = (1/\sqrt{N})\sum_j e^{i\mathbf{k}\cdot\mathbf{r}_j}\sigma_j^+$ [45, 187]. Such states are the fundamental basis to study collective light-matter interaction.

Of particular interest here will be the survival ratio between such a state prepared initially, $|\mathbf{k}(0)\rangle = |\mathbf{k}\rangle$, and the evolved state under Eq. (2.1) at later times,

$$O_{\mathbf{k}}(t) = |\langle\mathbf{k}|\mathbf{k}(t)\rangle|^2. \tag{2.3}$$

One expects that the dominant contribution to the initial decay of $O_{\mathbf{k}}(t)$ will be due to collective emission.

Specifically, in typical situations, the spin wave is excited by a traveling optical pulse, with the wavevector $|\mathbf{k}| = k_0 = \omega_0/c$ matching the dispersion relation of light and whose phase pattern in a macroscopic cloud of atoms is represented in Fig. 2.1(a). As anticipated in the introductory chapter of this thesis, the spin wave emits in analogous fashion as a phased array antenna. The emission of light by different atoms in the forward $\mathbf{k}$ direction, within a narrow superradiant emission solid angle $\Omega_s \sim (k_0\sigma)^{-2}$ (see Appendix A), adds constructively, while interference of the randomly positioned atoms in other directions washes out when averaged over microscopic configurations. This enhancement can be seen by directly calculating the single-photon spatial wave function, $\boldsymbol{\varepsilon}_{\mathbf{k}}(\mathbf{r}) = \langle g_1,g_2,\cdots,g_N|\mathbf{E}_s(\mathbf{r})|\mathbf{k}\rangle$ via Eq. (2.2) as illustrated in Fig. 2.1(c). Correspondingly, the initial decay rate of spin-wave population is given by $\Gamma_{\mathbf{k}} = -2im\langle\mathbf{k}|H|\mathbf{k}\rangle$, and can readily be evaluated to be $\Gamma_{\mathbf{k}} = \Gamma_0 + \overline{\mathrm{D}}(\hat{\mathbf{k}})\Gamma_0/4$ after smoothing out the position granularity

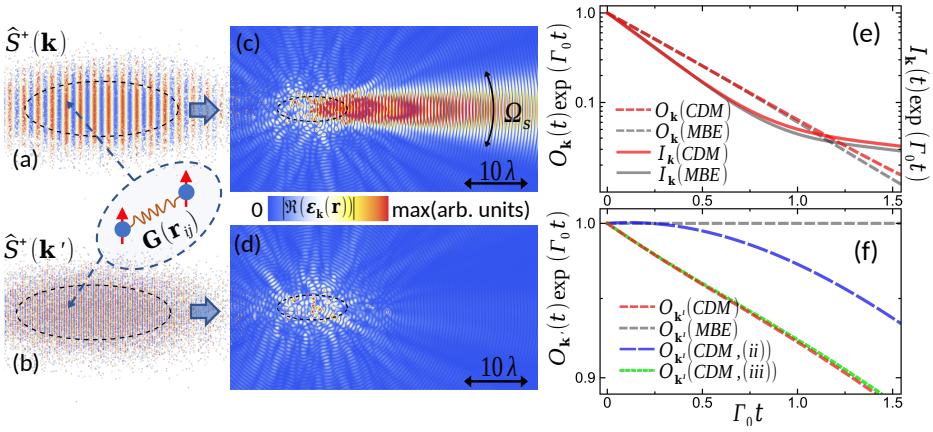

Figure 2.1: Decay of singly excited optical spin waves in a randomly distributed cloud of atoms with dipole interactions, as prescribed by Eq.(2.1). (a) and (b) illustrate the spin-wave order initiated in a Gaussian distributed random 2-level gas for $|\mathbf{k}| = \omega_0/c$ and $|\mathbf{k}'| = 2.9\omega_0/c$, respectively. The corresponding electric fields $|re(\boldsymbol{\varepsilon}_\mathbf{k}(\mathbf{r}))|$, emitted at time $t = 0$ and calculated over a two-dimensional cut at the sample center, as discussed in the main text and in Appendix A, are simulated with the coupled dipole model (CDM) and plotted in (c) and (d). In (e) and (f), the time evolution of the spin-wave survival ratio for the phase-matched and mismatched cases, respectively, is plotted. Here, the survival ratios are normalized by $O_\mathbf{k}(t)e^{\Gamma_0 t}$ and $O_{\mathbf{k}'}(t)e^{\Gamma_0 t}$, to compensate for any trivial decay that can be attributed to the single-atom, independent spontaneous emission rate. The survival ratio is calculated using both CDM (dashed red) and the Maxwell-Bloch equations (MBE, dashed gray), as presented in Appendix A. In (e), the simulated emission intensity $I_\mathbf{k}(t)$ within the superradiant solid angle Ω_s, as described in the main text and normalized to $I_\mathbf{k}(t) = 1$ at $t = 0$, is plotted. The simulations above contain $N = 532$ atoms with a peak density at the center of the Gaussian distribution being $\eta_0 = \rho_0\lambda_0^3 \approx 5$. (f) shows the survival ratio as predicted by MBE with a gray dashed line and in dashed red the distinct faster decay under CDM dynamics. Finally, also in (f), the survival ratio of a mismatched spin wave is calculated selectively removing close-by pairs of atoms with an interatomic distance of $rk_0 < 1$ (iii), plotted in dashed blue, which roughly accounts for the 3% of the number of emitters. This is compared with the green solid curve (ii), where the same quantity is considered, but now removing the same amount of atoms in a random fashion, to highlight the important role of strongly interacting pairs on the dynamics.

$\{\mathbf{r}_j\}$, as prescribed by the MBE approach [45, 189, 212]. The first and second terms reflect the random emission into most of 4π (which occurs at the single-atom rate), and the collectively enhanced emission in the forward direction, respectively. Here, $\overline{\mathrm{D}}(\mathbf{k}) = \int \mathrm{D}(\mathbf{r}_\perp)^2 d^2\mathbf{r}_\perp / \int \mathrm{D}(\mathbf{r}_\perp) d^2\mathbf{r}_\perp$ is the resonant optical depth of the atomic gas $\mathrm{D}(\mathbf{r}_\perp)$ averaged over the $\mathbf{r}_\perp$ plane perpendicular to the $\mathbf{k}$-direction [189, 212].

The simulated dynamics of the survival ratio $O_\mathbf{k}(t)$ and the superradiant intensity $I_\mathbf{k}(t)$ is plotted in Fig. 2.1(e), both of which are subject to spatio-temporal evolution of the spin wave as it propagates through the ensemble. Here $I_\mathbf{k}(t) = \int_{\Omega_s} |\boldsymbol{\varepsilon}_\mathbf{k}(\mathbf{r}, t)|^2 d\Omega$ is the emission integrated over the full superradiant angle Ω_s, which is more experimentally accessible than $O_\mathbf{k}(t)$. One sees that in contrast to an expected nearly exponential decay of $O_\mathbf{k}(t)$, the decay of intensity $I_\mathbf{k}(t)$ deviates from being exponential at long times, which is due to an angular redistribution of the forward emission associated with the collective spin-wave dynamics (similar effects were found in Ref. [213]). These quantities can be obtained by directly evolving the spin wave under Eq. (2.1) via the Schrodinger equation, which is possible as the single-excitation Hilbert space is of size $\sim N$. More specifically, the amplitudes β_j for $|\psi(t)\rangle = 1/\sqrt{N} \sum_j \beta_j(t) \sigma_j^+ |g_1, g_2, \cdots, g_N\rangle$ obey the same set of N equations as a classical resonantly coupled dipole model (CDM, see Appendix A) [119, 212]. Importantly, although these conclusions have been reached using Eq. (2.1) where granularity is accounted for, they can also be derived within the conventional MBE for smooth and classical fields $\langle \hat{\mathbf{E}}_s \rangle$ and $\langle \hat{\mathbf{P}} \rangle = \langle \sum_j \wp \, \sigma_j^{ge} \delta(\mathbf{r} - \mathbf{r}_j) \rangle$ while treating atoms as a continuous medium [106, 213] (see Appendix A). Indeed, the deviation from the MBE results due to the extra microscopic physics contained in the CDM simulations seems quite subtle in Fig. 2.1(e), the fundamental reason being the difficulty to extract information on the microscopic dynamics on top of a huge collective dissipative response of the medium.

Separately, however, let's consider a similar scenario, but starting from a spin wave with wavevector $|\mathbf{k}'| > \omega_0/c$ strongly mismatched from radiation (Figs. 2.1(b)(d)(f)). While such a spin wave is not naturally generated optically, it is possible to efficiently excite them as described in the following section. Because of the phase mismatch, now there is no direction along which emission will constructively interfere, after averaging over microscopic configurations of a random gas, and similar calculations based on energy emission predict an initial decay rate of $\Gamma_{\mathbf{k}'} = \Gamma_0$ [214], *i.e.*, an exponential decay with a *precisely known* rate according to spontaneous emission from single, isolated atoms.

The main discovery in this work is that the above conclusion is *incom-*

plete. In the following sections instead, it will be experimentally shown and theoretically argued that the initial decay of optical spin waves generally behaves as $O_{\mathbf{k}}(t) = e^{-\Gamma_{\mathbf{k}} t}$, with $\Gamma_{\mathbf{k}} = \Gamma_{\mathbf{k}}^{\text{coll}} + \gamma$ deviating from the standard MBE prediction by a local density-dependent rate $\gamma \propto \rho\lambda_0^3\Gamma_0$ with $\lambda_0 = 2\pi/k_0$. This additional term arises due to dephasing, and only appears by accounting for the effect of granularity in the dynamics of the dipole-dipole interactions, in particular, between close pairs of atoms. The rate γ can be significant even for a dilute gas with $\rho < k_0^3$. While a complete theoretical picture will be presented in Sec. 2.4, an initial glimpse into the effect is provided by comparing CDM and MBE simulations of the spin-wave dynamics. In particular, while the survival ratio $O_{\mathbf{k}}(t)$ is seen to be trivial within the MBE (dashed gray curve of Fig. 2.1(f)), the CDM predictions (dashed red curve) strongly deviate and decay faster. The important role of close-by pairs (having a distance less than $\lambda_0/2\pi$, about 3% percent of all atoms in the simulation) is illustrated by removing such pairs from the ensemble, which results in a survival ratio (dashed blue curve) that goes back to the MBE results at short times. In contrast, removing the same percentage of atoms randomly (dashed green) results in almost no difference, compared to CDM simulations of the original ensemble. Together, these simulations clearly show the dramatic effect that "freezing" macroscopic dynamics can have in order to observe microscopic optical phenomena, now displaying a strong deviation from MBE predictions as long as teasing the important role of strongly interacting pairs that has been anticipated in the introductory chapter.

2.3 Setup and measurements

From the previous section, mismatched spin waves emerged as an interesting class of states to study the microscopic correlation build-up as a consequence of dipole-dipole interaction, the fundamental reason being wavevector mismatch which prevents them from efficiently radiating. The small coupling with free-space radiation, however, intuitively also makes them difficult to excite them in the first place with resonant light. In this section, we summarize a recently developed spin-wave **k**-control technique [189] which is used to investigate the decay dynamics of phase-matched and mismatched spin-wave order in a laser-cooled gas. This tool constitutes a novel approach to suppressing the strong collective macroscopic atomic response shown in Fig. 2.1, opening up the possibility of precisely measuring microscopic correlation build-up. The experiments and the resulting measurements were

performed at Fudan University, in the group of Prof. Saijun Wu. Here, we first provide the essential ideas underlying the experimental technique. We then discuss their concrete implementation and give the main experimental results, in order that they may be compared with theory.

Schematically represented first in Fig. 2.2, the protocol composes a key ingredient of the measurement protocol and allows to isolate the macroscopic superradiant dynamics in order to perform a background-free measurement of the dephasing rate, as it going to be discussed step-by-step. In the introduction, $\mathbf{k}$ and $\mathbf{k}'$ were used to indicate respectively matched and mismatched wavevectors, for the sake of simplicity. Here, to fully appreciate the control that can be achieved both in the spin-wave directionality and degree of matching, and to fully understand the experimental setup, we will carefully specify each laser-induced momentum kick needed to geometrically impart the desired spin-wave phase order. The experimental technique relies on sending a series of very short (sub-ns) pulses to deterministically shift the spin wavevector, before the collective emission has a significant effect. These short pulses act on an additional transition $|g\rangle - |a\rangle$, as represented in Fig. 2.2(a). To understand the basic mechanism it is sufficient to consider a single atom, at position $\mathbf{r}$, initially prepared in the state $|g\rangle + e^{i\mathbf{k}_p\cdot\mathbf{r}}|e\rangle$, where $|\mathbf{k}_p| = k_0$ is the matched wavevector of a probe field used to initially excite the $|g\rangle - |e\rangle$ transition. Then, a pair of short pulses, conveniently delayed (see Refs. [189, 190]) and with opposite wave vector $\mathbf{k}_c$ will drive consecutive ($|g\rangle \rightarrow |a\rangle$ and $|a\rangle \rightarrow |g\rangle$) π rotations. Meanwhile, the state $|e\rangle$ is affected negligibly by the control pulses due to the chosen large frequency difference between $|e\rangle$ and $|a\rangle$. Although an atom in the $|g\rangle$ state returns to $|g\rangle$ following the two control pulses, these pulses have non-trivial local phases $e^{\pm i\mathbf{k_c}\cdot\mathbf{r}}$ that depend on the atomic position (with the sign $\pm$ depending on the order of the pulses), which can also be equivalently visualized as the solid angle enclosed by a loop in the Bloch sphere (see Fig. 2.2(b1-3)).

The procedure can also be performed multiple times n, as long as the steps are well within the coherence time $1/\Gamma_0$. Although the phase imprinting is a single atom effect, when applied to an ensemble it is equivalent to shifting the initial wavevector of the spin wave to $\mathbf{k}_p \rightarrow \mathbf{k}_p \pm 2n\mathbf{k}_c$, as illustrated in Fig. 2.2(c). Importantly, the process can also be reversed by exchanging the order of the control pulses, which gives generic coherent control over the direction and the degree of mismatch of the wavevector of a spin wave. Once a phase-matched excitation is conveniently excited, this innovative control technique can be therefore used to map it to a mismatched one to explore its dynamics, and then to map it back

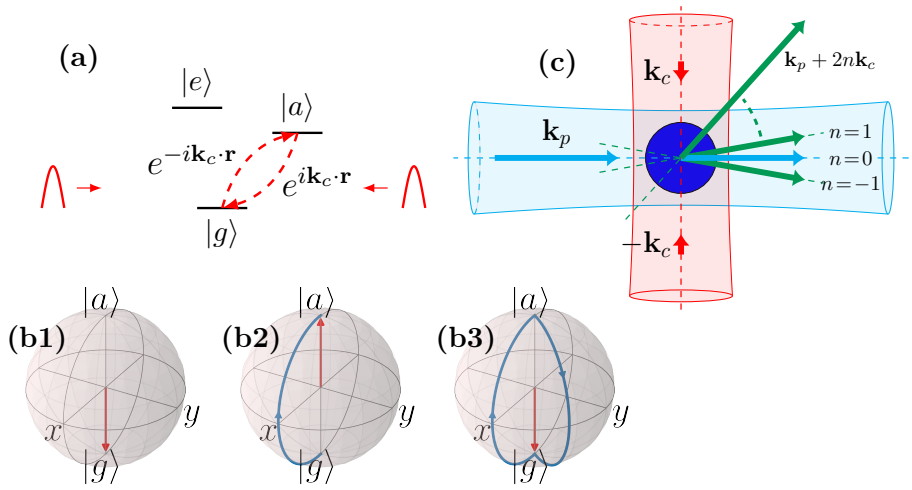

Figure 2.2: (a) Phase imprinting on a single atom with two counter-propagating pulses. (c) The phase imprinting technique is applied to an atomic ensemble, n times. Depending on the time order of the control pulses one can map the initial momentum of the matched spin wave into $\mathbf{k}_p \to \mathbf{k}_p \pm 2n\mathbf{k}_c$. (b1-3) Bloch sphere representation of the projected $|g\rangle - |a\rangle$ dynamics for an atom subjected to the phase imprinting technique. The initial ground state $|g\rangle$ of the atom is represented in (i). (ii) In the rotating frame of the control laser, a π pulse transfers the population into the auxiliary excited state $|a\rangle$. (iii) A second counter propagating pulse then transfers back the population to the ground state $|g\rangle$. The total evolution on the Bloch sphere encloses a non-trivial solid angle, leading to the imprinting of a position dependent geometric phase $\pm 2i\mathbf{k}_c \cdot \mathbf{r}$ (with the sign $\pm$ depending on the order of the pulses).

to a matched one for optical measurements. The concrete experimental realization of is illustrated in Fig. 2.3. In this setup optical spin waves are defined on the $5S_{1/2}, F = 2$ to $5P_{3/2}, F' = 3$ hyperfine transition of a cold ^{87}Rb gas, with the Zeeman sub-levels respectively labeled as $|g\rangle$ and $|e\rangle$ (see Fig. 2.3(b)). First, a short probe pulse with wavevector $\mathbf{k}_p$ and duration τ_p is applied to resonantly excite the $|g\rangle - |e\rangle$ dipole transition, to generate a matched spin-wave $|\mathbf{k}_p\rangle$ (generation step in Fig. 2.3(e)). A weak Rabi frequency Ω_p with pulse area $\theta_p = \Omega_p\tau_p \ll 1$ that allows to restrict the description to single-excitation dynamics [211, 212, 215]. As anticipated, control over the wavevector $\mathbf{k}$ associated with the resulting spin wave is achieved by cyclically driving an auxiliary $|g\rangle - |a\rangle$ D1 transition ($|a\rangle$ labels the $5P_{1/2}, F'$ sub-levels). In particular, driving population inversions from $|g\rangle \to |a\rangle$ and back $|a\rangle \to |g\rangle$ with a pair of pulses on the D1 transition, with

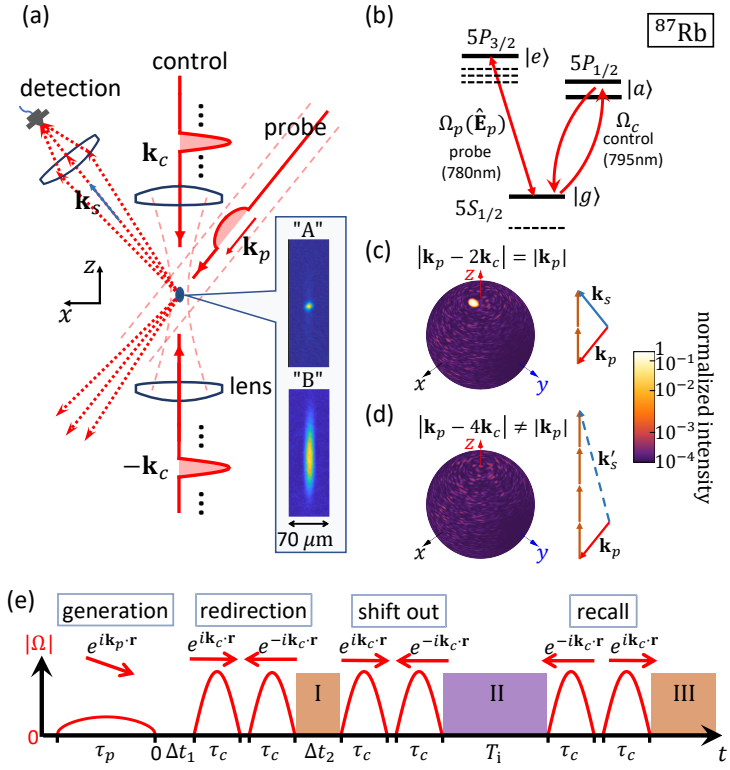

Figure 2.3: Measurement scheme of optical spin wave decay. (a) Schematic of the setup. Shapes of atomic samples labeled as "A" and "B" are illustrated with absorption images. Also illustrated are the directions and wavevectors associated with the exciting probe beam, the control pulses, and the direction for detection of emission. (b) Atomic level diagram and laser coupling scheme. The probe beam couples to the $|g\rangle$-$|e\rangle$ transition with the levels indicated for ^{87}Rb, while fast control pulses couple to an auxiliary $|g\rangle$-$|a\rangle$ transition. (c, d): Angular distribution of the light emission for the phase matched $S^+(\mathbf{k}_s = \mathbf{k}_p - 2\mathbf{k}_c)$, and mismatched $S^+(\mathbf{k}'_s = \mathbf{k}_p - 4\mathbf{k}_c)$ spin-wave, as predicted by CDM simulations. (e): Timing diagram for shifting a $S^+(\mathbf{k}_p)$ spin-wave excitation to $\mathbf{k}_s = \mathbf{k}_p - 2\mathbf{k}_c$ (interval I), $\mathbf{k}'_s = \mathbf{k}_p - 4\mathbf{k}_c$ (interval II) and back to $\mathbf{k}_s = \mathbf{k}_p - 2\mathbf{k}_c$ (interval III).

the first and second pulses having wavevectors $\pm\mathbf{k}_c$ and $\mp\mathbf{k}_c$, respectively, as represented in Fig. 2.3(a), which exactly leads to a wavevector shift $\mathbf{k}_p \rightarrow \mathbf{k}_p \mp 2\mathbf{k}_c$ of the spin-wave excitation $S^+(\mathbf{k}_p)$. The control direction $\mathbf{k}_c$ is finely aligned to ensure that the new direction $|\mathbf{k}_s| = \omega_0/c$, with $\mathbf{k}_s = \mathbf{k}_p - 2\mathbf{k}_c$, is also phase-matched, and thus the spin wave preferentially emits in the $\mathbf{k}_s$ direction (Fig. 2.3(c)). This has the advantage that the spin-wave population can be read out by the detection of superradiant emission [188], but without the strong background induced by the probe beam [98, 210, 211, 216, 217] caused by the probe pulse that now propagates in a different direction.

After generating the phase matched spin wave $S^+(\mathbf{k}_s)$, the dynamics of phase-mismatched spin waves is investigated by immediately applying a second pair of control pulses to shift to the new wavevector $\mathbf{k}'_s = \mathbf{k}_s - 4\mathbf{k}_c$, where $|\mathbf{k}'_s| = 2.9\omega_0/c$. After waiting for an interrogation time T_i for the $S^+(\mathbf{k}'_s)$ spin wave to accumulate dynamics (especially from the near-field dipole-dipole interactions of interest), a backward shift $\mathbf{k} \rightarrow \mathbf{k} + 2\mathbf{k}_c$ is applied to convert the spin wave back to $\mathbf{k}_s$, onto the light cone, to recall the superradiance (Figs. 2.3(c)(d)(e)). In general, the strength of the superradiant emission immediately following the interrogation time and recall, $I_{\mathbf{k}_s}(T_i)$, decays as a function of increasing T_i. Recording this strength for various $t = T_i$ directly reveals the survival ratio $O_{\mathbf{k}'_s}(t)$ of the phase-mismatched spin wave and allows us to infer the dephasing rate γ, as described below.

2.3.1 Decay of phase-mismatched spin waves

To unravel the microscopic dephasing dynamics predicted by CDM, the full spin-wave control sequence (Fig. 2.3(e)) is used to create and investigate the phase-mismatched $S^+(\mathbf{k}'_s)$ excitation. Typical superradiance signals during such measurements, with interrogation times $T_i = 0.5, 15.2, 30.0$ ns, are given by the different color curves in Fig. 2.4(a) and (b). For each interrogation time, the signal $I_{\mathbf{k}_s}(t)$ has two peaks. The first peak corresponds to the interval I in Fig. 2.3(e) and arises immediately following the generation of the spin wave $S^+(\mathbf{k}_p)$ by the probe pulse, and the re-direction by the first pair of control pulses to orient this spin wave $S^+(\mathbf{k}_s)$ along the phase-matched (and detected) $\mathbf{k}_s$ direction. The signal then effectively vanishes once the second pair of control pulses is applied, to shift to a phase-mismatched excitation $S^+(\mathbf{k}'_s)$, where it remains for a time $\sim T_i$ until it is recalled back to $S^+(\mathbf{k}_s)$ to produce the second peak (interval III). Not surprisingly, once recalled back to a phase-matched state, the

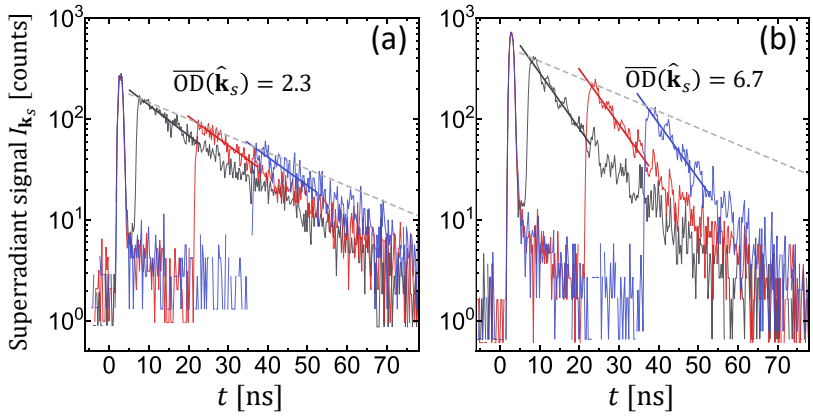

Figure 2.4: Extrapolating the survival ratio $O_{\mathbf{k}'_s}(t)$ from decay of the recalled superradiant emission. In both (a) and (b), shows the measured superradiant intensity $I_{\mathbf{k}_s}(t)$ versus time t and for different interrogation times $T_i = 0.5, 15.2, 30.0$ ns as indicated by the different colors. The dashed gray line indicates the decay $e^{-\Gamma_0 t}$ of a single, isolated atom.

superradiant intensity $I_{\mathbf{k}_s}$ decays at a superradiant rate that is enhanced by large $\overline{\mathrm{D}}(\mathbf{k}_s)$. More important for us, however, is the decay of the peak intensity $\sim I_{\mathbf{k}_s}(T_i)$ versus interrogation time T_i, which directly reveals how the phase-mismatched spin wave decays during the interval T_i, *i.e.*, the decay of the survival ratio $O_{\mathbf{k}'_s}$ (Eq. (2.3)) for the mismatched spin wave. Experimentally, the goal is to fit the initial decay rate of the peak intensity $I_{\mathbf{k}'_s}$ vs. T_i to an exponential (as indicated by the dashed gray line in Fig. 2.4), and look for density-dependent deviations from the single-atom spontaneous emission rate Γ_0.

The estimated decay rate $\Gamma_{\mathbf{k}'_s}$ with peak density ρ_0 and the associated dimensionless density parameter $\eta_0 = \rho_0 \lambda_0^3$ are plotted in Fig. 2.5. A density-dependent dephasing rate $\gamma \approx 0.013(4)\eta_0\Gamma_0$ of the survival ratio $O_{\mathbf{k}'_s}(t)$ can be extracted from the data. This deviation of $\Gamma_{\mathbf{k}'_s}$ from the MBE-predicted rate $\Gamma_{\mathbf{k}'_s} = \Gamma_0$ is the main experimental result of this work.

In the next section, we explain the physical origin of this density-dependent decay, first discussing its basic microscopic origin in terms of strongly interacting pairs of two-level atoms, and later generalizing to the realistic hyperfine level structure of the atomic species used in the experiments. Importantly, this simple theory can capture a density-dependent dephasing, as represented by the predicted decay of a spin wave in Fig. 2.5 (red line), agreeing well with the experimental data.

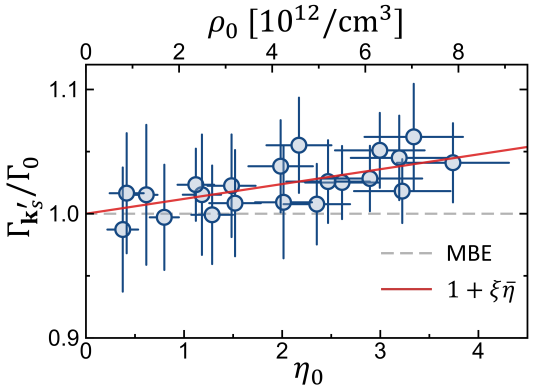

Figure 2.5: The initial decay rates of the spin wave survival ratio, plotted vs estimated dimensionless peak density parameter $\eta_0 = \rho_0\lambda_0^3$. The error bars reflects the full statistical and systematic uncertainties. The solid line gives the prediction from the dipolar dephasing theory of Eq. (2.5) with $\bar{\eta} = \eta_0/2\sqrt{2}$ as the mean density of a Gaussian distribution, as discussed in Sec 2.4. The dashed gray line, $\Gamma_{\mathbf{k}'_s} = \Gamma_0$ is instead the prediction based on MBE, which ignores microscopic effects associated with atomic granularity.

2.4 Unraveling dephasing

As anticipated, here, we introduce and discuss a simple theoretical model that not only clearly identifies strongly near-field interacting pairs of atoms as the source of microscopic dephasing mechanism but also quantitatively reproduces the observed density-dependent dephasing rate as in Fig. 2.5 of the previous chapter.

It is important to stress that while the microscopic model (Eq. (2.1)) can be numerically solved for moderate atom number at the weak excitation limit, its complexity scales directly with the number of atoms N, and with the number of disorder configurations needed to obtain disorder-averaged results, which can even become exponential if the multilevel hyperfine structure of realistic atoms is fully taken into account. Furthermore, despite the necessary simplifications (smaller systems, two-level atoms...) the numerics does not directly elucidate the underlying physics. For this reason, we develop a bottom-up approach to solve for the dynamics, that, as anticipated and schematically represented in Fig. 2.6, consider first the simpler problem involving just a pair of two-level atoms separated by a distance $r \lesssim k_0^{-1}$, with $k_0 = \omega_0/c$ to be the wavenumber of the light, that can be statistically found in a disordered gas. In that case, the dipole-dipole

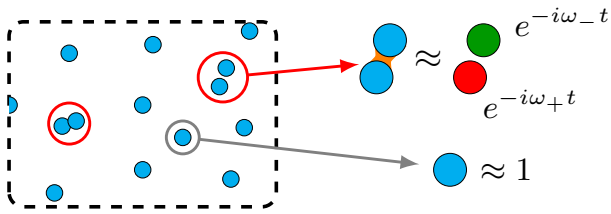

Figure 2.6: Representation of our pair-wise solution for the dephasing dynamics in a disordered ensemble at moderate densities ($\eta \lesssim 1$). Strongly interacting pairs that statistically occur are highlighted with a red circle. In the single-atom rotating frame, $e^{-i\omega_0 t}$, we replace them with two dynamically equivalent new effective atoms with frequency shifts $\omega_\pm$, induced by the strong and coherent near-field interaction. Single isolated atoms instead, approximately do not contribute to dephasing.

interaction given by the Eq. (2.1) Hamiltonian, is dominated by the $\sim 1/r^3$ near-field component. To be more specific, we can explicitly separate out the Green's function terms that are proportional to $\sim 1/r^3$, obtaining

$$\hat{\mathbf{x}} \cdot \mathbf{G}_0(\mathbf{r}) \cdot \hat{\mathbf{x}} \underset{r k_0 < 1}{\sim} G^{\text{near}}(\mathbf{r}) \equiv \frac{1}{4\pi k_0^3 r^3}(3\cos\theta^2 - 1). \tag{2.4}$$

where θ is the angle between the dipole polarization (linearly polarized along $\hat{\mathbf{x}}$) and the distance between two atoms $\mathbf{r}$. The near-field contribution is real, and thus the corresponding interaction is purely coherent and Hermitian. In the single-excitation manifold, this interaction is diagonalized by symmetric and anti-symmetric wave functions, $|\pm\rangle = (|eg\rangle \pm |ge\rangle)/\sqrt{2}$, which experience opposite frequency shifts $\omega_\pm(\mathbf{r}) = \pm 3\Gamma_0(3\cos^2\theta - 1)/4k_0^3 r^3$ relative to the bare atomic transition frequency. The important realization here is that the time evolution for the two body problem can now be studied in terms of its normal modes. Concretely, in the single atom rotating frame $e^{-i\omega_0 t}$, an initially prepared two-body mismatched spin-wave $|\psi^{2b}_{\mathbf{k}'_s}\rangle$, will evolve as $\langle\psi^{2b}_{\mathbf{k}'_s}|\psi^{2b}_{\mathbf{k}'_s}(t)\rangle = e^{-i\omega_+ t}|c^+_{\mathbf{k}'_s}|^2 + e^{-i\omega_- t}|c^-_{\mathbf{k}'_s}|^2$, having defined the projections $c^\pm_{\mathbf{k}'_s} = \langle\psi^{2b}_{\mathbf{k}'_s}|\pm\rangle$. Although the magnitude of $\mathbf{k}'_s$ might be constrained in an experiment, we can take the conceptual limit where $|\mathbf{k}'_s|/k_0 \to \infty$, or infinite mismatch, which corresponds to assigning a random phase to each atom, and implies that the actual spin wave should have on average equal overlap with the $\pm$ eigenstates, i.e. that $|c^\pm_{\mathbf{k}'_s}|^2 \to 1/2$. The dynamics of a strongly interacting pair in Fig. 2.6 can be therefore equivalently modeled by replacing with two new atoms of new resonance frequencies $\omega_\pm$, that now do not interact anymore through the near field, but still evolve with a phase $e^{i\omega_\pm t}$ while single isolated atoms will not be

affected. Thus, a pair of strongly interacting atoms effectively acts as a local coherent phase scrambler in the time evolution of a spin-wave $|\psi^{2b}_{\mathbf{k}'_s}\rangle$.

We now turn to the evolution of a spin wave in a many-atom system, due to dipole-dipole interactions. We consider the decay of spin-wave survival ratio $O_{\mathbf{k}'_s}(\delta t) = |\langle \mathbf{k}'_s|e^{-iH_{\rm eff}\delta t}|\mathbf{k}'_s\rangle|^2$ within a short interval $\delta t \ll 1/\Gamma_0$. We begin by dividing $H_{\rm eff}$ of Eq. (2.1) into Hermitian and anti-Hermitian parts, $H_{\rm r} = (H_{\rm eff} + H^\dagger_{\rm eff})/2$ and $H_{\rm a} = (H_{\rm eff} - H^\dagger_{\rm eff})/2$, which describe coherent and dissipative interactions, respectively. Examining the coherent interactions first, the $1/r^3$ scaling of the near field implies that close-by neighbors will interact with each other more strongly than with all other atoms combined [119]. Thus, we can approximately diagonalize $H_{\rm r}$ by isolating close-by nearest neighbors and simply diagonalizing these pairs exactly as we have described for the two-atom problem while treating all other interactions between atoms as a (negligible) perturbation. In other words, an approximate complete basis of single-excitation eigenstates is given by $|e_i\rangle$ with energy $\omega \approx 0$ for all atoms that do not have a close-by neighbor, and $(|e_i g_j\rangle \pm |g_i e_j\rangle)/\sqrt{2}$ with energy $\omega_\pm(\mathbf{r}_{ij})$ for all atoms i, j that form close-by pairs. The short-time dynamics can then be evaluated by decomposing the initial spin wave on this basis. Then, in the time-dependent survival ratio $O_{\mathbf{k}'_s}(\delta t) \approx |\int d\omega P(\omega) e^{-i\omega\delta t}|^2$, the spectral function $P(\omega)$ becomes the probability distribution of finding close-by pairs with energy $\omega_\pm$. While a detailed derivation of $P(\omega)$ is provided in the following subsection (see Eq. (2.8)) it is important to notice here that its two fundamental properties derive from the $\omega_\pm \sim 1/r^3$ near-field interaction, and the consequent frequency shifts, in a random gas. First, in combination with the probability of finding a nearest neighboring atom in an infinitesimal shell of radius r being $f^{(2)}(r) \sim_0 4\pi r^2$, the high-frequency tails of the distribution will generally scale (symmetrically) as $P(\omega) \propto 1/\omega^2$ [218]. This scaling guarantees that the survival ratio experiences an *initial* exponential decay due to near-field interactions of $O_{\mathbf{k}'_s}(\delta t)$ as $e^{-\gamma\delta t}$. Secondly, the peculiar cubic scaling of the near-field, also implies that if the density increases also the induced shifts have to grow by the same factor, because of the reduced average nearest neighbor distance. That is, the distribution width $\Delta \propto \eta$ has to linearly broaden with the density. As expected in a Fourier transform now, the rate $\gamma \propto \Delta\omega$ is proportional to the width of the distribution such that the newly identified rate

$$\gamma = \xi\eta\Gamma_0, \tag{2.5}$$

to linearly scales with the density and to be proportional to a coefficient ξ, which can only depend on the specific model of the atom that we are

taking into account (2-level vs hyperfine transition), as discussed in detail in 2.4.2.

Returning to the spontaneous emission arising from the anti-Hermitian term $H_{\rm a}$, mathematically, at short times its effect on evolution commutes with that of $H_{\rm r}$ (*e.g.*, by considering a Suzuki-Trotter expansion). As the initial ensemble-averaged spontaneous emission rate of a phase-mismatched spin wave is simply that of a single atom, $\Gamma^{\rm coll}_{\mathbf{k}'_s} = \Gamma_0$ [214], we can conclude that the total initial decay of the survival ratio is given by $\Gamma_{\mathbf{k}'_s} = \Gamma_0(1+\xi\eta)$. When such a prediction for the dephasing rate is compared with the experimentally measured one in Fig. 2.5, for the specific $F = 2 \rightarrow F = 3$ D_2 transition of ^{87}Rb (see Sec. 2.4.2), we observe good agreement with the data. Importantly here, the calculations assumes an infinite and homogeneous atomic cloud. In an experiment, an ensemble generally follows a position dependent distribution $\rho(\mathbf{r})$, which can be generally taken into account substituting a *mean* density $\rho \rightarrow \overline{\rho} = \int \rho^2(\mathbf{r}) d^3\mathbf{r} / \int \rho(\mathbf{r}) d^3\mathbf{r}$ in Eq. (2.6). For a Gaussian distribution it is easy to show that the mean density is related to the peak density as $\overline{\rho} = \rho_0/2\sqrt{2}$.

While we elucidated here the key physical mechanism and the main points of a predictive theory of the additional dephasing rate that arises in disordered ensembles, before discussing its implications in Sec. 2.5, we clearly specify how to derive the effective frequency distribution $P(\omega)$ in the next section, for the simpler and more intuitive case of two-level atoms. Then, as anticipated, in Sec. 2.4.2 we generalize the theory to more realistic and more complex dipole transitions and dipole-dipole interaction between hyperfine atomic levels. This will allow for a fair comparison between predictions and experiments.

2.4.1 The effective frequency distribution of strongly interacting pairs

As anticipated in the previous sections of this chapter, the near-field interaction emerged as being the dominant process that contributes to dephasing. Instead of solving the full many-body problem, one realizes that its highly local contribution can be taken into account approximately diagonalizing the near field into the following complete basis in the single-excitation manifold: $|e_i\rangle$ with energy $\omega \approx 0$ for all atoms that do not have a close-by neighbor, and $(|e_i g_j\rangle + |g_i e_j\rangle)/\sqrt{2}$ with energy $\omega_{\pm}(\mathbf{r}_{ij})$ for all atoms i, j that form nearest neighbor close-by pairs. As also stated previously, the dynamics induced by the near-field interactions can be evaluated by projecting the initial spin wave into this basis and assuming that overlap

with symmetric/anti-symmetric pair states is equal.

To be more precise, one can start from the probability distribution of nearest neighbors in a random gas of density ρ [219],

$$f^{(2)}(\mathbf{r}) = \rho e^{-\frac{4\pi}{3}r^3\rho} \tag{2.6}$$

which gives the probability of finding the closest neighbor at a position $\mathbf{r}$ (such that $\int d^3\mathbf{r} f^{(2)}(\mathbf{r}) = 1$), given one atom at the origin. Within the approximations stated above and further assigning to each atom in a close-by pair a frequency $\omega_{\pm}(\mathbf{r})$, the spin wave survival ratio is formally given by

$$O_{\mathbf{k}'_s}(t) = \left| \int d^3\mathbf{r} f^{(2)}(\mathbf{r}) \frac{1}{2} \left(e^{-i\omega_+(\mathbf{r})t} + e^{-i\omega_-(\mathbf{r})t} \right) \right|^2 \tag{2.7}$$

Here, as we are primarily interested in the short-distance and high-frequency contribution of particularly nearby pairs, we need not impose any specific distance cutoff (*e.g.*, $r < k_0^{-1}$) in the integral.

To proceed further, it is convenient to introduce the change of variables $\omega = \omega_{\pm}(\mathbf{r}) = \omega_{\pm}(r, \theta)$, to convert the integrand into the Fourier transform of the frequency probability distribution $P(\omega)$ – that of strongly interacting and symmetrically excited pairs in the ensemble. Doing so, especially paying attention to the changes sign at $|\cos\theta| = 1/\sqrt{3}$ of $\omega_{\pm}(r, \theta)$, leads to the following compact form:

$$P(\omega) = \frac{\Gamma_0}{16\pi^2} \frac{\eta}{\omega^2} \int_0^1 d(\cos\theta) |h(\theta)| e^{-\frac{\Gamma_0\eta}{8\pi^2} \left| \frac{h(\theta)}{\omega} \right|}, \tag{2.8}$$

having introduced the function $h(\theta) = 3\cos^2\theta - 1$ for simplicity and $\eta = \rho\lambda_0^3$ being the local dimensionless density parameter. Although the derived $P(\omega)$ might not be in a simple form, it is straightforward to see that the high-frequency tails are symmetric and behave asymptotically like

$$P(\omega)_{\pm\infty} \sim \xi\eta\Gamma_0 \frac{1}{2\pi\omega^2}, \tag{2.9}$$

where the defined $\xi = 1/(6\pi\sqrt{3})$ is a numerical factor that, as anticipated, depends on the details of the atomic structure, here specifically evaluated within the 2-level approximation and can be easily calculated looking at the asymptotic behavior $\omega \to \infty$ of the integral in Eq. (2.8).

2.4.2 Hyperfine atoms

The presented calculations thus far rely on the approximation of an atom as a two-level system. However, real atoms have a complex multilevel

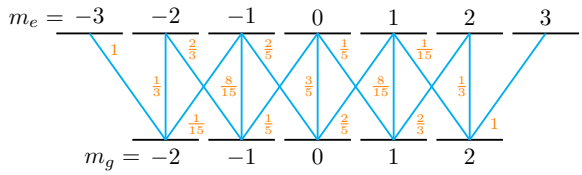

Figure 2.7: Multilevel atomic structure, corresponding to the $F_g = 2 \to F_e = 3$ transition of the $D2$ line in ^{87}Rb probed in the experiment. The states are labeled by their Zeeman quantum number $m_{g(e)}$, while in orange we indicate the strength of the allowed transitions, as characterized by the squared Clebsh-Gordan coefficients $|C_e^g|^2$.

structure. This is specifically illustrated in Fig. 2.7 for the experimental case of interest, involving the maximum angular momentum ground ($F_g = 2$) and excited ($F_e = 3$) state manifolds of the D2 transition of ^{87}Rb. Here, the set of ground (excited) states $\{g(e)\}$ consist of all possible Zeeman levels $|m_{g(e)}| \leqslant F_{g(e)}$ along some given quantization axis.

This point is generically far from being a simple technicality as already the ground states manifold grows as $(2F_g + 1)^N$, where N is the number of atoms, making the numerical problem untreatable already at the single excitation level. However, as the proposed approach to approximately capture the many-body dynamics only relies on the full understanding of the two-body problem, as before, one just needs to study the simpler case of two hyperfine atoms, strongly interacting through their near field. Also, in this case, the eigenmodes of the two-body problem will be used as an approximate basis to diagonalize the spin-wave of a many-atom system. We will show that this leads simply to a modification of the dephasing coefficient ξ. In the presence of multiple ground and excited states, the dipole-dipole interaction (Eq. (2.1) for two-level atoms) can be readily generalized to [144]

$$H = -\frac{\omega_0^2 d_{F_e F_g}^2}{\varepsilon_0 c^2} \sum_{ij} \mathbf{e}^*_{g'e'} \cdot \mathbf{G}(\mathbf{r}_{ij}, \omega_0) \cdot \mathbf{e}_{ge} C_{e'}^{g'} C_e^g \sigma^i_{e'g'} \sigma^j_{ge}. \tag{2.10}$$

The interaction describes photon emission and re-absorption between two atoms at a distance r_{ij} and the labels g, e, g', e' refer to arbitrary Zeeman levels. The strengths of these dipole transitions depend on a reduced dipole matrix element $d_{F_e F_g}$ that is independent of the Zeeman levels, Clebsch-Gordan coefficients $C_e^g = \langle F_g, m_g | F_e, m_e; 1, m_g - m_e \rangle$, and the overlap of the emitted/collected photon polarization with the spherical basis of choice,

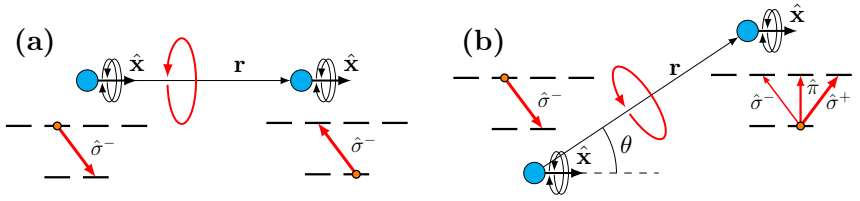

Figure 2.8: (a) Resonant dipole-dipole interactions in the molecular basis. When the molecular axis, defined by the distance between the atoms $\mathbf{r}$, aligns with the quantization axis $\hat{x}$, the interaction preserves the total angular momentum projection along $\hat{x}$. Thus if one atom emits a $\hat{\sigma}^-$ photon, the second atom can only absorb it on a $\hat{\sigma}^-$ transition. (b) In an arbitrary orientation of the molecular axis respect to the quantization axis (for example $\hat{\mathbf{x}} \cdot \hat{\mathbf{r}} = \cos\theta$) this is no longer true. In particular a photon emitted by one atom can generically drive all the possible transitions of the second atom, depending on θ.

given by

$$\mathbf{e}_{ge} = \mathbf{e}_{m_g - m_e} = \begin{cases} -(\hat{z} + i\hat{y})/\sqrt{2}, & m_g - m_e = 1 \\ \hat{x}, & m_g - m_e = 0 \\ (\hat{z} - i\hat{y})/\sqrt{2}, & m_g - m_e = -1 \end{cases} \tag{2.11}$$

Here, we conveniently choose to align π transitions ($m_g - m_e = 0$) with the beam polarization $\hat{x}$. Interestingly, the total spontaneous emission rate of any one of the excited states (equal for all states) can be related to these quantities by $\Gamma_0 = \sum_g |C_e^g|^2 \frac{\omega_0^3 d_{F_e F_g}^2}{3\pi\hbar\varepsilon_0 c^3}$. In particular, by considering the "closed transition" with $|C_e^g|^2 = 1$ we have $\Gamma_0 = \frac{\omega_0^3 d_{F_e F_g}^2}{3\pi\hbar\varepsilon_0 c^3}$.

As before, we will consider the specific case of two atoms sufficiently close to each other ($r < k_0^{-1}$) that the interaction of Eq. (2.11) is dominated by the coherent near-field component of the Green's function (compare with Eq. (2.4) for two-level atoms).

The form of Eq. (2.10) greatly simplifies when the quantization axis $\hat{x}$ aligns with the natural "molecular" axis, defined as being the vector $\mathbf{r}$ connecting the two atoms, as represented in Fig. 2.8a. In this case, the interaction is only non-zero when an excited atom emits on a transition ($\hat{\sigma}^-$ for example) that is equal to the transition of the second, ground-state atom as it absorbs the photon, thus preserving the projection of the total angular momentum along the quantization axis $\hat{x}$. In an arbitrary configuration, however, as in Fig. 2.8b where the molecular and quantization axes do not agree, this is no longer true, and the ground state atom can be excited along with any transition once absorbing the photon. As a consequence,

already the two-body problem appears to be complex since eigenstates of the Hamiltonian (2.10) necessarily involve non-trivial superpositions of multiple Zeeman states. The problem will be therefore approached numerically.

First, we diagonalize (2.10) within the single-excitation manifold for a pair of atoms at fixed distance r, obtaining $n = 2\times(2F_e+1)\times(2F_g+1)$ non-trivial eigenstates, $\{\psi_j\}_{j=1,\dots n}$, and eigenvalues, $\{\omega_j\}_{j=1,\dots n}$. The eigenvalues can only depend on the distance between the atoms r (not on the angle θ) and, just considering the near field interaction, will have the general form

$$\omega_j(r) = C_j \frac{\Gamma_0}{k_0^3 r^3} \tag{2.12}$$

where C_i is generically a non trivial combination of CG coefficients.

The angular part will appear in the projection over the eigenstates as we now discuss. As before we assume the pair to be in a $\hat{x}$ polarized two-body mismatched spin-wave ($|\mathbf{k}'_s| = 2.9\omega_0/c$)

$$\begin{aligned} |\psi^{2b}_{\mathbf{k}'_s}\rangle &= S^\dagger_{\mathbf{k}'_s}|g_1,g_2\rangle \\ S^\dagger_{\mathbf{k}'_s} &= \frac{1}{\sqrt{2}}\left(e^{i\mathbf{k}'_s\cdot\mathbf{r_1}}\sigma^1_{e1,g1} + e^{i\mathbf{k}'_s\cdot\mathbf{r_2}}\sigma^2_{e2,g2}\right) \end{aligned} \tag{2.13}$$

such that $m_{e1} = m_{g1}$, $m_{e2} = m_{g2}$. Each atom is assumed to initially be in a randomly chosen Zeeman sublevel $g_{1,2}$ and to obtain observables we will average over all the possible sublevel configurations.

While the excited state looks simple because of our convenient choice of the polarization basis, generally it will not be an eigenstate of the dipole-dipole interaction Hamiltonian but will have some overlap with them $h_j(\theta) = |\langle\psi^{2b}_{\mathbf{k}'_s}|\psi_j\rangle|^2$, such that all the modes would naturally contribute to the dephasing in the time evolution. Then, making the same assumptions as before for the evolution of a many-atom spin wave, the survival ratio of Eq. 2.7 for two-level atoms naturally generalizes to

$$O_{\mathbf{k}'_s}(t) = \left|\int d^3\mathbf{r} f^{(2)}(\mathbf{r}) \sum_j h_j(\theta) e^{-i\omega_j(r)t}\right|^2 \tag{2.14}$$

Further defining the integrals $H_j = \int_{-1}^{1} d\cos\theta\ h_j(\theta)$ and performing multiple changes of variables $\omega = \omega_j(r)$ according to the sign of the eigenvalue it is again possible to define the frequency distribution of strongly interacting, excited pairs of atoms:

$$P(\omega) = \frac{\Gamma_0}{12\pi^2}\frac{\eta}{\omega^2}\sum_j H_j|C_j| e^{-\frac{\Gamma_0\eta}{6\pi^2}|\frac{C_j}{\omega}|} \tag{2.15}$$

transition	2-level	$0 \to 1$	$\frac{1}{2} \to \frac{3}{2}$	$1 \to 2$	$\frac{3}{2} \to \frac{5}{2}$	$2 \to 3$
$6\pi\xi$	$1/\sqrt{3}$	1	0.77	0.69	0.66	0.64

Table 2.1: The coefficient ξ (multiplied by 6π in the Table) for the density-dependent dephasing rate $\gamma = \xi\eta\Gamma_0$, as calculated for different atomic structures. These include two-level atoms, and transitions $F_g \to F_e$ involving ground and excited state manifolds with angular momenta F_g and F_e, respectively.

Also here, the distribution is found to have symmetric tails, which asymptotically behave like

$$P(\omega)_{\pm\infty} \sim \xi\eta\Gamma_0 \frac{1}{2\pi\omega^2} \tag{2.16}$$

where now the dephasing coefficient ξ introduced in the main text, which depends on the details of the atomic structure generalizes to

$$\xi = \frac{1}{6\pi} \sum_j H_j |C_j|. \tag{2.17}$$

This quantity is evaluated numerically in Table 2.1 for various different hyperfine transitions. This thus generalizes the result for 2-level atoms $\xi = \frac{1}{6\pi\sqrt{3}}$ that we found in Eq. (2.17).

2.5 Discussion & Outlook

In the introduction of this thesis and more thoroughly in this chapter it was discussed how MBE are considered the standard approach both to describe light-matter interaction and excitation propagation dynamics in cold atoms ensembles in terms of smooth fields as well as the performance of quantum technological applications in terms of the optical depth. As argued, such an approach, while effectively capturing the strong collective resonant emission that characterizes an efficient light-matter interface at high D, explicitly neglects microscopic effects like multiple scattering arising from dipole-dipole interaction.

Beyond MBE, these effects are important because they have been predicted to give rise to interesting phenomenology and could potentially affect the performance of applications. Probing microscopic correlations has been difficult exactly because of the huge collective directional emission, which forced measurements to take place in low-light conditions, either looking at the emitted field from different angles with respect to the main

light propagation direction or at late times when most of the superradiant emission left the system.

Within this context, in this chapter, a general method to probe microscopic dynamics in cold atomic ensembles in a background-free fashion has been demonstrated, which is expected to be generically useful to probe microscopic spin dynamics in cold atoms. This is possible by managing the phase-matching condition in the time domain so as to transiently suppress macroscopic collective dynamics associated with optical spin-wave excitations. More broadly, the ability to reversibly generate and retrieve mismatched spin waves is anticipated to have important applications in the envisioned atomic array scenarios [84, 90, 142, 171, 204, 205, 220]. With this method, a density-dependent dipolar dephasing rate of optical spin waves has been measured. The previously overlooked dephasing effect is fundamental to a randomly positioned atomic gas and has been described by a simple quantitative theory.

Importantly, the unraveled dephasing effect on spin-wave order is expected to be of direct and widespread relevance to the performance of quantum light-matter interfaces, as we are going to discuss. As the strong near-field resonant dipole interaction between closely spaced pairs of atoms is a universal property of dense atomic ensembles [102, 104, 110, 174], the consequent observed dephasing mechanism is therefore fundamental, as opposed to other error sources such as Doppler broadening due to atomic motion and dephasing due to magnetic field inhomogeneities are generically considered "technical", as they can be reduced cooling down the atoms or better shielding the atomic cloud.

To understand why let's recall that the efficiency of the light-matter interface between a single photon and an ensemble of cold atoms is fundamentally limited by the competition between the spontaneous and collective emissions. While the first happens at the rate of a single atom in free space Γ_0 and covers the whole 4π solid angle, collective emission in a well-defined direction happens at an enhanced rate $\Gamma_{\mathbf{k}}^{\mathrm{coll}} = \Gamma_0(1 + \mathrm{D}/4)$. This gives a branching ratio, and thus an efficiency, which while simply proportional to the optical depth $\Gamma_{\mathbf{k}}^{\mathrm{coll}}/\Gamma_0 \sim \mathrm{D}$, remains fundamentally limited by spontaneous emission. In applications, the spontaneous emission leads to photon storage infidelity as $\varepsilon \sim 1/\mathrm{D}$ [54]. For example, in subradiance-based ultrafast quantum memory [214], photons are proposed to be stored as phase-mismatched dipole spin waves for a spontaneous emission limited storage time proportional to $1/\Gamma_0$.

Here, with the newly identified dephasing mechanism which enhances the decoherence rate by the $(1+\xi\eta)$ factor, this bound should be accordingly

modified as $\varepsilon \sim (1 + \xi\eta)/\mathrm{D}$. The correction can be significant if the local density of the atomic sample is high. This suggests that there could be upper bounds on the maximum atomic densities tolerable to reach a given fidelity. Furthermore, as total atom number (or optical depth) is also an important resource [1], this, in turn, would set a limit on the minimum system size, which has implications in efforts to make compact quantum devices based upon ensembles.

In parallel, again, to overcome this limitation, one might resort to atomic arrays [83] where the fluctuations of near-field interactions are controlled, as has been demonstrated recently [163].

CHAPTER 3

Dephasing in optically dense atomic media: a renormalization group approach

3.1 Introduction

In Ch. 2, it was experimentally observed that optical spin waves suffer from a dephasing that is exponential at early times and is directly proportional to atomic density. It was argued that this initial dephasing arises from the strong near-field interaction of a small fraction of particularly close nearest neighbors, quantitatively reproducing the experimental results. Separately, though, one might wonder what governs the apparently non-exponential behavior at later times, or what occurs at very high densities, when many atoms sit within a wavelength of each other and experience strong near-field interactions. We also note that near-field interactions have been recognized to play key roles in other collective behavior, ranging from the modification of superradiance in small systems [191] to late-time subradiance [102] in extended systems. Beyond exact numerics, however, the development of effective theories generally remains a challenge in many-atom disordered systems. Here, we provide a comprehensive theoretical picture of the spin-wave dephasing phenomenon by applying a non-perturbative technique based on strong disorder renormalization group (RG), which is a powerful method to elucidate the physics in diverse disordered condensed matter systems [192–199] and has also recently been applied to atom-light interactions [119]. As in the short-time theory of dephasing, one key idea underlying this approach is that for highly disordered atomic media, strong near-field interactions between particularly close nearest neighbors allow such pairs to be approximately diagonalized first. The resulting dynamics is equivalent to replacing the pair with two, new *effective* atoms with

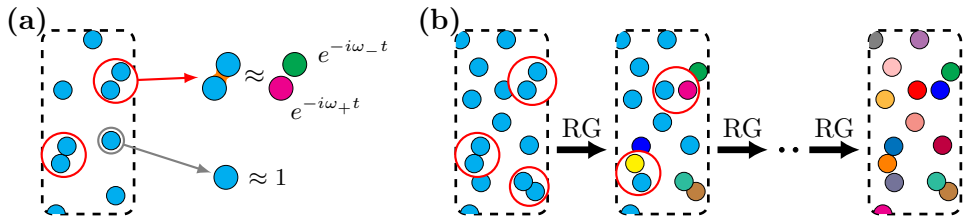

Figure 3.1: (a) A pair-wise approach to the many-atom optical dynamics. As derived in Ref. [190], in a dilute atomic medium, a small fraction of pairs of atoms (red circles) are separated by a distance much smaller than a wavelength, and thus interact strongly via their near fields. These atoms can be replaced with a non-interacting, dynamically equivalent pair with new effective resonance frequencies (indicated by different colors), which evolve with the phase $e^{-i\omega_\pm t}$. Single isolated atoms instead will not significantly contribute to time evolution. (b) Representation of the RG scheme [119]. Each step is characterized by identifying the most strongly interacting pairs and replacing them with two new atoms with different frequencies, which do not interact anymore through the near field. Unlike in (a), one can continue this process (including the renormalization of atoms previously renormalized) until all near-field interactions have been eliminated. The overall system at the end is equivalent to an inhomogeneously broadened ensemble of spectral distribution $P(\omega)$, plotted in Fig. 3.4.

renormalized frequencies, as illustrated in Fig. 3.1(a). The RG theory goes significantly beyond this, however, by realizing that nearby, strongly interacting pairs (including atoms previously renormalized) can continue to be identified and diagonalized, i.e. the many-atom system interacting via the near field can be thought of and diagonalized in terms of an extended hierarchy of strongly interacting pairs (Fig. 3.1(b)). The final result is that the original system is optically equivalent to an inhomogeneously broadened medium with a well-defined distribution of resonance frequencies $P(\omega)$, and with the strong near-field interactions effectively removed. This approach was recently used to predict that a disordered atomic medium has a limiting value of the maximum refractive index, regardless of its physical density [119]. Here, we show that RG not only works to capture the stationary optical response of a dense gas but also to capture the above-mentioned time-dependent dephasing dynamics of spin waves, in a simple and non-perturbative way. The validity of the RG approach is quantitatively verified by comparison with full, microscopic coupled-dipole simulations of large ($N \sim 10^4$) atomic ensembles. This work constitutes a step forward in understanding the consequences of the fundamental dipole-dipole interaction in disordered media when the true granular nature of the

atomic distribution is taken into account.

This chapter is an adaptation of the published work of Ref. [200], the result of again a collaboration and intense exchange of ideas with Prof. Saijun Wu and Dr. Yizun He from the Fudan University (Shanghai), and is structured as follows. In Sec. 3.2 we briefly review the microscopic theoretical description of photon-mediated dipole-dipole interactions, which accounts for atomic positions, near-field interactions, and multiple scattering of light, and which serves as the basis for the microscopic simulations of spin-wave dynamics. In Sec. 3.3 we describe the RG approach, which enables one to predict a universal inhomogeneous broadening function for a disordered medium. From here, we then formulate a simple, approximate, *single-atom* model for the spin-wave dephasing dynamics. In Sec. 3.4, we present detailed numerical simulations of the spin-wave dynamics from dilute to high-density media, which show both the initial exponential dephasing and non-exponential behavior at later times. We also compare these results with the RG approach, which exhibits good quantitative agreement in all regimes. We conclude and provide an outlook in Sec. 3.5.

3.2 Microscopic model of atom-light interaction dynamics

We consider a minimal model consisting of N identical 2-level atoms at fixed, random positions $\{\mathbf{r}_i\}_{i=1,\dots,N}$ that are uniformly distributed within a spherical cloud. The ground and excited states $|g_j\rangle$ and $|e_j\rangle$ have an electric dipole transition characterized by resonance frequency $\omega_0 = ck_0$ and wavelength $\lambda_0 = 2\pi/k_0$, and a single-atom excited-state spontaneous emission rate given by Γ_0. We also define a dimensionless density in terms of the number of atoms per cubic wavelength $\eta = \lambda_0^3 N/V$, where $V = \frac{4}{3}\pi R^3$ is the volume of the ensemble and R its radius.

As it has been extensively discussed in the previous chapters, the effects of photon-mediated dipole-dipole interactions, multiple scattering, and wave interference in spontaneous emission are captured by an effective atomic Hamiltonian (2.1), where the photon-mediated interactions between atoms are described by the free-space Green's tensor $\mathbf{G}_0(\mathbf{r}, \omega_0)$ introduced in Eq.(1.7). Fixing the orientation of the atomic dipole matrix element, $\boldsymbol{\wp} = \hat{\mathbf{x}}$, it is convenient define $\theta_{j\ell}$ as its angle with respect to $\mathbf{r}_{j\ell}$. Doing so,

the Hamiltonian $H = \sum_{j\ell} H_{j\ell}\sigma_{eg}^{j}\sigma_{ge}^{\ell}$ is characterized by the coefficients

$$H_{j\ell} = -\frac{3\Gamma_0}{4}e^{ik_0 r_{j\ell}}\left[\frac{3\cos^2\theta_{j\ell}-1}{(k_0 r_{j\ell})^3} - i\frac{3\cos^2\theta_{j\ell}-1}{(k_0 r_{j\ell})^2} - \frac{\cos^2\theta_{j\ell}-1}{k_0 r_{j\ell}}\right]. \tag{3.1}$$

Important to later discussions, however, let's recall that the real part of the Green's function (describing coherent interactions) contains a $\sim 1/r^3$ near-field component, which dominates at small inter-atomic distances ($k_0 r < 1$). This near-field interaction explicitly reads:

$$H_{j\ell}^{\text{near}} = -\frac{3\Gamma_0}{4(k_0 r_{j\ell})^3}\left(3\cos^2\theta_{j\ell}-1\right). \tag{3.2}$$

The dissipative part instead describes collective spontaneous emission as arising from wave interference of the emitted light, while in the limit of a single atom, predicts the known spontaneous emission rate of $\Gamma_0 = \omega_0^3 d_{eg}^2/3\pi\hbar\varepsilon_0 c^3$, with d_{ge} being the amplitude of the dipole matrix element for the atomic transition. Generally, the presence of dissipation requires a master equation treatment [87, 88, 191, 221], but the non-Hermitian Hamiltonian (2.1) is sufficient to describe the single-excitation regime of interest in our work, which generally reduces to solving a set of classical coupled dipole equations of motion [55, 80, 82, 90, 98, 104, 114, 211, 212], as discussed also in Appendix A.

We will specifically be interested in applying the Hamiltonian (3.1) above to investigate the dynamics of a single-excitation "timed Dicke state" or spin wave, defined as

$$|\mathbf{k}\rangle = \frac{1}{\sqrt{N}}\sum_j e^{i\mathbf{k}\cdot\mathbf{r}_j}|e_j\rangle. \tag{3.3}$$

These collective states with well-defined wavevectors constitute a natural basis to describe light-matter excitations. For example, phase-matched spin waves with $|\mathbf{k}| \approx k_0 = \omega_0/c$ are naturally and easily excited by an incoming resonant short pulse. By reciprocity, it is well known that they also efficiently emit into a narrow, well-defined direction centered around $\mathbf{k}$ [45], with a collectively enhanced rate [55, 98, 188, 211, 212, 222–225], $\Gamma^{\text{coll}}_{|\mathbf{k}|\sim k_0}/\Gamma_0 = 1+\overline{D}/4$, which linearly scales with the average optical depth of the medium. This narrow emission occurs due to constructive interference of the emitting atoms along the $\mathbf{k}$ direction, and forms the basis of collective enhancement at the heart of efficient atom-light interfaces [1, 56] and the applications mentioned in the introduction. This behavior can be equally

derived by microscopic theories [188] or by the macroscopic MBE [55, 222, 223].

It should be noted that phase-matched spin-wave excitations undergo non-trivial macroscopic spatio-temporal propagation dynamics [100, 213], which is already an interesting problem by itself. This makes it challenging to quantify the magnitude and effects of microscopic dephasing, due to the difficulty in defining an ideal time-evolving reference state to compare to, if dephasing could hypothetically be eliminated. As discussed in the previous chapter (Sec. 2.3), an elegant, robust solution to this problem was proposed in Ref. [190], with experimental realization based on a series of time-domain spin-wave control techniques [188, 189].

Let's briefly recall that the experimental technique relies on sending a series of very short (sub-ns) pulses that cyclically drive an additional auxiliary transition deterministically shift the spin wavevector before the collective emission has a significant effect. The net effect is that the norm and the direction of $\mathbf{k}$ can be controlled coherently. While the directional control is one of the key ingredients to precisely explore the superradiant dynamics [188, 189], here we will focus on the generation of highly mismatched spin waves, simply labeled with $\mathbf{k}$ and with $|\mathbf{k}| \neq k_0$. The process can also be reversed by exchanging the order of the control pulses. In particular, one can map a phase-mismatched spin-wave back to a matched one, for convenient optical measurements. The peak intensity emitted by this matched spin-wave, and specifically the dependence on the amount of time that the system spends in the mismatched state, directly reveals the magnitude of microscopic dephasing, as detailed in the previous chapter and in Ref. [190].

The mismatched spin-waves constitute elegant initial states to investigate microscopic dephasing dynamics, due to the absence (on average) of macroscopic spatio-temporal dynamics. For example, these states neither couple to light efficiently nor have any preferred emission or propagation direction. Due to the lack of any direction in which the emitted field (averaged over random configurations) interferes, the average initial spontaneous emission rate of this state reduces to the single-atom value $\Gamma^{\text{coll}}_{|\mathbf{k}|\neq k_0} = \Gamma_0$ [214]. Since this state does not exhibit any background macroscopic dynamics, $|\mathbf{k}\rangle$ itself serves as a reference to compare against the actual time-evolved state.

Specifically, we will be interested in the time evolution under the dipole-dipole Hamiltonian (2.1) as given by $|\mathbf{k}(t)\rangle = e^{-iHt}|\mathbf{k}\rangle$. Since the initial state contains only a single excitation, as argued above, the dynamics can be efficiently evaluated numerically, with the resulting equations of motion

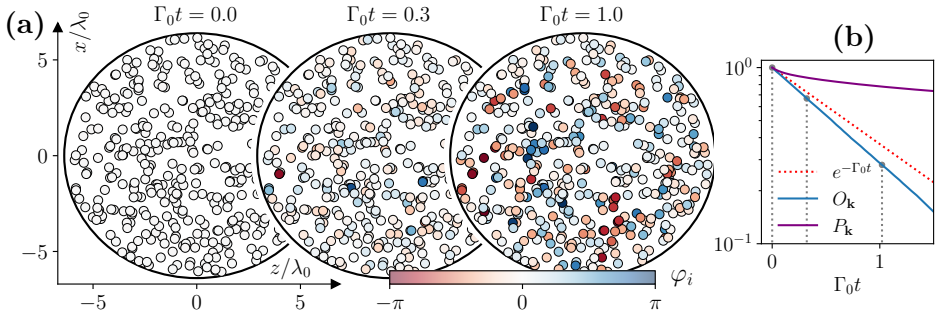

Figure 3.2: (a) Snaphots of the time evolution of a mismatched spin wave. We initially prepare a mismatched spin wave $|\mathbf{k}\rangle$ ($|\mathbf{k}| = 6.0k_0$) in a particular configuration $\{\mathbf{r}_j\}$ of a disordered gas at density $\eta = 10$, $N = 10^4$ atoms and radius $R/\lambda_0 \sim 6$. The state is then let to evolve under the dipole-dipole Hamiltonian (2.1) and the projection over the initial state is computed, $\langle \mathbf{k}|\mathbf{k}(t)\rangle = \sum_j |f_j| e^{i\varphi_j}$, extracting the time dependent amplitudes and phases in the single atom basis. To create the snapshots above we consider all the atoms contained in a slice of size $\Delta y = R/35$, plot their position along the xz plane, and color them according to their accumulated phase in time evolution φ_j, as a consequence of the interaction, for different times. The global effect of this dephasing is represented in (b) where we plot the global overlap $O_{\mathbf{k}} = |\langle \mathbf{k}|\mathbf{k}(t)\rangle|^2$ (blue curve) and population $P_{\mathbf{k}} = \langle \mathbf{k}(t)|\mathbf{k}(t)\rangle$ (purple) of the same mismatched spin-wave. Quantifying the deviation of the overlap with respect to the predicted decay $e^{-\Gamma_0 t}$ (red dotted line) is the main purpose of this work.

equivalent to classical coupled dipole equations (see Appendix A). As in chapter 2, with the time-dependent state we can construct two quantities of interest,

$$\begin{aligned} P_{\mathbf{k}}(t) &= \langle \mathbf{k}(t)|\mathbf{k}(t)\rangle \\ O_{\mathbf{k}}(t) &= |\langle \mathbf{k}|\mathbf{k}(t)\rangle|^2. \end{aligned} \tag{3.4}$$

The first quantity $P_{\mathbf{k}}(t) \leqslant 1$ monotonically decreases and gives the total remaining excited state population at any time t, with the rest having been irreversibly lost due to (collective) spontaneous emission. The second quantity, $O_{\mathbf{k}}(t)$, on the other hand, quantifies the overlap with the initial spin wave, and thus describes the survival of the spin-wave order. Importantly, as discussed more in concrete in the previous chapter (see Sec. 2.3), the survival ratio and its time dependence are measurable quantities in the experiments. While we will present a more systematic analysis in Sec. 3.4, we provide a visual example of the physics encoded in $P_{\mathbf{k}}(t)$ and $O_{\mathbf{k}}(t)$ in Fig. 3.2. In particular, we simulate the dynamics of an initial spin wave $|\mathbf{k}\rangle$, with $|\mathbf{k}| = 6k_0$, in a particular configuration $\{\mathbf{r}_j\}$ of a disordered gas

of $N = 10^4$ atoms with density $\eta = 10$, and in a spherical volume of radius $R/\lambda_0 \approx 6$. The evolved state $|\mathbf{k}(t)\rangle$ under Eq. (2.1) is calculated for several specific times t. In Fig. 3.2a we consider all the atoms contained within a slice $\Delta y = R/35$ of the center of the cloud, and plot their positions in the x-z plane. The colors represent the accumulated phase of each atom relative to its initial value $e^{i\mathbf{k}\cdot\mathbf{r}_j}$, with a strong dephasing evident at time $\Gamma_0 t = 1.0$. In Fig. 3.2b, we then plot $P_{\mathbf{k}}(t)$ (purple) and $O_{\mathbf{k}}(t)$ (blue) as calculated for the entire ensemble, along with the single-atom spontaneous emission $e^{-\Gamma_0 t}$ for reference (dashed red). It can be seen that while the initial decay of the total excited population $P_{\mathbf{k}}(t)$ occurs at a rate $\sim \Gamma_0$ (confirming the absence of collective enhancement) before slowing down, the spin wave survival ratio $O_{\mathbf{k}}(t)$ decays significantly faster than Γ_0, due to the dephasing illustrated in Fig. 3.2a.

To practically study the dephasing dynamics of a mismatched excitation, it is important to realize that the condition for mismatching actually depends on system size. In a sufficiently small system $R \to 0$, intuitively, phase differences $e^{i\mathbf{k}\cdot\delta\mathbf{r}}$ between atoms become negligible and all spin waves begin to resemble the symmetric $|\mathbf{k} = 0\rangle$ state. Such a state then has superradiant properties reminiscent of the Dicke limit [45, 86]. To check the degree of phase mismatch, we evaluate the instantaneous average decay rate, $\Gamma_{\mathbf{k}} = -2\mathrm{Im}\langle\mathbf{k}|H|\mathbf{k}\rangle$, and check that it is sufficiently close to Γ_0. In Fig. 3.3, we plot the decay associated to a particular spin-wave $|\mathbf{k}\rangle$, for different densities, atom number and radii. These decay rates generically show two peaks at $\pm k_0$, which are associated with modes that efficiently emit because of the phase-matching condition. It can be seen that these peaks become narrower as the system size is increased (either at fixed density or fixed atom number), while for spin wavevectors that lie sufficiently far from these peaks the spin waves have a decay rate that indeed approaches Γ_0. We observe in Fig. 3.3 that our specific choice $|\mathbf{k}| = 6k_0$ fulfills our mismatching requirement $\Gamma_{\mathbf{k}} \sim \Gamma_0$ for the ranges of system sizes and densities to be explored in this work.

3.3 A Renormalization group approach

While the microscopic model (Eq. (2.1)) can be numerically solved for moderate atom number, its complexity scales directly with the number of atoms N, and with the number of configurations needed to obtain disorder-averaged results. Furthermore, the exact numerics does not directly elucidate the underlying physics. Motivated by that, here we introduce

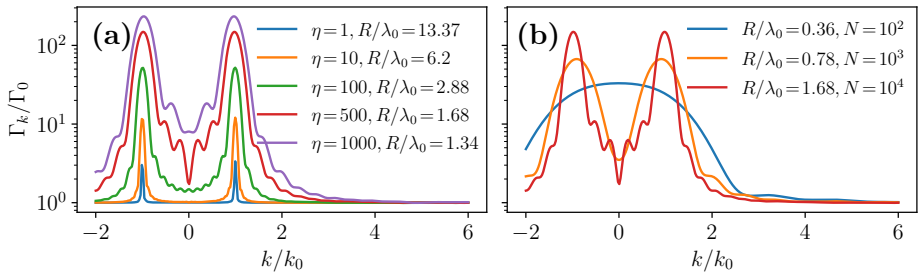

Figure 3.3: Average decay rate $\Gamma_{\mathbf{k}} = -2\mathrm{Im}\langle \mathbf{k}|H|\mathbf{k}\rangle$ of a spin-wave with momentum $\mathbf{k} = (0, 0, k)$ for (a) different densities η of a spherically uniform atomic cloud of $N = 10^4$ atoms. In (b) we evaluate the same quantity but keeping the density fixed to $\eta = 500$ and varying the number of atoms and the radius of the cloud. All the curves are averaged over 200 realizations.

a simple model, based on a strong-disorder RG approach, which clearly identifies the role that near-field interactions have on the dynamics, and which allows the effects of such interactions to be captured by a simple *effective, single-atom* theory.

In the previous chapter, a theory to understand the short-time dephasing rate of a spin wave for dilute ensembles with densities $\eta \lesssim 1$ was developed. It was then found that the dephasing is primarily attributable to a small fraction of atomic pairs separated by a distance much smaller than the optical wavelength, $k_0 r < 1$ (highlighted in Fig. 3.1(a)), which strongly interact via their near fields (Eq. (3.2)). The $\sim 1/r^3$ scaling of the near field implies (in three dimensions) that the presence of other atoms is just a weak perturbation on top of the strong pairwise interaction, such that the pair can be separately and approximately diagonalized. In the single-excitation manifold, diagonalizing the near-field interaction (3.2) of a pair yields symmetric and anti-symmetric eigenstates, $|\pm\rangle = (|eg\rangle \pm |ge\rangle)/\sqrt{2}$, which experience opposite frequency shifts $\omega_\pm = \pm\frac{3\Gamma_0}{4k_0^3 r^3}(1 - 3\cos^2\theta)$ relative to the bare atomic transition frequency.

The time evolution for the two-body problem can now be studied in terms of its normal modes. Concretely, in the single atom rotating frame $e^{-i\omega_0 t}$, an initially prepared two-body spin-wave $|\mathbf{k}\rangle$, will evolve as $\langle \mathbf{k}|\mathbf{k}(t)\rangle = e^{-i\omega_+ t}|c_{\mathbf{k}}^+|^2 + e^{-i\omega_- t}|c_{\mathbf{k}}^-|^2$, having defined the projections $c_{\mathbf{k}}^\pm = \langle \mathbf{k}|\pm\rangle$. Although the magnitude of $\mathbf{k}$ might be constrained in an experiment, we can take the conceptual limit where $k \to \infty$, or infinite mismatch. This implies that the phase $e^{i\mathbf{k}\cdot\mathbf{r}_j}$ of each excited atom is

effectively random (being infinitely sensitive to the specific atomic position), which implies that the actual spin wave should have on average equal overlap with the $\pm$ eigenstates, i.e. that $|c_{\mathbf{k}}^{\pm}|^2 \to 1/2$. The dynamics can therefore be equivalently modeled by replacing the two original atoms with two new atoms of new resonance frequencies $\omega_{\pm}$, that now do not interact anymore through the near field, but evolve with their "free" inhomogeneous phases $e^{-i\omega_{\pm}t}$ (see Fig. 3.1(a)).

In Ref. [190], the short-time dynamics of a many-atom, dilute ensemble were approximated by identifying a small fraction of close-by atomic pairs that evolved with the phases $e^{-i\omega_{\pm}t}$ as argued above, while the remaining atoms were assumed to undergo no evolution. By taking the position dependence of the function $\omega_{\pm}(\mathbf{r})$ and combining with the known distribution function of separations $\mathbf{r}$ of nearest neighbors in a random ensemble, an initial decay of the spin-wave survival order was predicted and measured to be exponential, $|O_{\mathbf{k}}(\delta t)|^2 = e^{-\Gamma_{\mathbf{k}}\delta t}$, with a density-dependent rate $\Gamma_{\mathbf{k}}/\Gamma_0 = 1 + \xi\eta$, where $\xi = 1/6\pi\sqrt{3}$ for two-level atoms.

Now, in a dense ensemble (Fig. 3.1(b)) or at longer evolution times, the basic picture of replacing close-by atomic pairs with new effective atoms of renormalized frequencies do not change. However, a key realization is that after an atom has been renormalized, it can still see another atom close by with which it can strongly interact (again highlighted by red circles in Fig. 3.1(b)). This allows yet another renormalization step to take place, which now will involve the diagonalization of a pair of atoms with the effective frequencies previously obtained. Whereas only a small fraction of atoms dictates the initial decay in a dilute ensemble, here, we must specify a general procedure valid for any density, to repeatedly and hierarchically identify the single most strongly interacting pair (including the possibility that the pair contains already renormalized atoms) and replace them with two new effective atoms.

Starting from that overall intuition, we now formulate the general principles and assumptions underlying our proposed RG scheme, before presenting a more detailed description of its implementation. We also present the principles of the RG scheme in a manner that goes beyond the particular goal of interest here, involving the study of dephasing dynamics. Succinctly put, our RG scheme consists of three principles:

1) The system dynamics is exactly described by the total Hamiltonian of Eq. (3.1). Although we have provided the matrix elements in the basis given by individually excited atoms $|e_j\rangle$, formally we are free to choose any other basis. In our RG scheme, we thus choose to work in

the basis defined by the eigenstates of just the near-field interaction H^{near}, as given in Eq. (3.2). Note that this is simply a choice of basis, and in particular, makes no assumptions about the relative contributions of the near- versus far-fields to the system dynamics.

2) We assume that the many-atom eigenvalue distribution of H^{near} can be approximately obtained by a series of diagonalizations over atomic pairs, through a procedure specified below. The pairwise diagonalization, which significantly reduces the complexity, is motivated by the fact that the near field between a close-by atomic pair can dominate over the near-field interactions between this pair and all other atoms combined. While this is an approximation, we can numerically verify that the agreement between the approximate and exact eigenvalue distribution is nearly perfect (e.g., see Fig. 3.4 and the related discussion).

3) We now arrive at the third principle, the only one that cannot be fully justified. Strictly speaking, the eigenstates of H^{near} will be somewhat delocalized over a set of atoms, as dictated by our identification of strongly interacting pairs. However, we *assume* that in terms of their interaction with light (via the far-field dipole-dipole interactions and from any possible external fields), these eigenstates respond effectively as if they were perfectly localized point dipoles. In particular, under this assumption, the original system becomes optically equivalent to a set of point dipoles that only interacts via the far fields, and which has a resonance frequency distribution corresponding to the eigenvalue distribution from (3.2). While the degree of validity of this approximation is hard to analyze on formal grounds, a partial justification of why it might work well is given in Ref. [119].

With these principles in mind and having anticipated that RG can involve the renormalization of atoms that have already been renormalized in previous steps, here, we consider the more general case of two inhomogeneous atoms of general resonance frequencies of ω_i and ω_j, interacting via the near field, as described by the two-body Hamiltonian in the single excitation sector,

$$H_{j\ell}^{2b} = \langle \omega_{j\ell} \rangle \mathbb{1} + \begin{pmatrix} \delta\omega_{j\ell} & H_{j\ell}^{\text{near}} \\ H_{j\ell}^{\text{near}} & -\delta\omega_{j\ell} \end{pmatrix}. \tag{3.5}$$

For convenience, we have defined $\langle \omega_{j\ell} \rangle = (\omega_j + \omega_\ell)/2$, $\delta\omega_{j\ell} = (\omega_j - \omega_\ell)/2$. To quantify the strength of the interaction, we define the ratio between

the off-diagonal and the diagonal elements, $\mathcal{K}_{j\ell} = \mathcal{L}_{j\ell}|H^{\text{near}}_{j\ell}|/(|\delta\omega_{j\ell}| + 1)$, where the matrix $\mathcal{L}$ keeps the information of whether a pair of atoms has already been renormalized ($\mathcal{L}_{j\ell} = 0$) or not ($\mathcal{L}_{j\ell} = 1$). This prevents a pair of renormalized atoms from being renormalized between themselves multiple times (although each atom from the pair can be renormalized with other atoms). Intuitively, a large value of $\mathcal{K}_{j\ell}$ (which requires $\mathcal{L}_{j\ell} = 1$) means that the strength of the interaction is able to further split the original frequency difference $\delta\omega_{j\ell}$. Thus, the most strongly interacting pair is identified as that with the largest value of $\mathcal{K}_{j\ell}$ (red circles in Fig. 3.1(b)). Once identified, the full diagonalization of (3.5) gives two eigenvalues, $\omega_\pm = \langle\omega_{j\ell}\rangle \pm \sqrt{\delta\omega^2_{j\ell} + \left(H^{\text{near}}_{j\ell}\right)^2}$. The pair can be therefore replaced by an approximately equivalent one, made of two atoms with the new resonance frequencies $\omega_\pm$ and that do not interact anymore through the near field (setting $\mathcal{L}_{j\ell} = 0$).

Repeated application of this algorithm, which constitutes the renormalization group (RG) flow, continues until all near-field interactions have been removed ($\mathcal{L}_{jl} = 0$ for all pairs) and the atoms have been assigned the new effective frequencies $\{\omega_i\}$. In particular, this does allow for pairs with small values of $K_{j\ell} < 1$ to be renormalized, and we do not impose a cutoff to the RG based on the value of $K_{j\ell}$. This formally implements the principles of our RG approximation described earlier, where our goal is to describe the system in terms of the (approximately calculated) eigenstates of the near field. The actual numerical implementation of RG thus exhibits a complexity of $\sim N^2$ steps of renormalizing atomic pairs. However, as we will see in the next paragraph, RG gives rise to a universal distribution $P(\omega)$ of new effective resonance frequencies that is independent of atom number for sufficiently large N. This distribution can thus be used for all future calculations at no complexity cost, e.g., in cases where N is too large to make the direct numerical implementation feasible.

When the RG scheme is applied to multiple realizations of randomly distributed ensembles of atoms, we can build up the probability distribution $P(\omega)$ of the effective frequencies, which we illustrate in Fig. 3.4. As the near-field interaction only depends on distance through the dimensionless parameter $(k_0 r)^{-3}$, the distribution when rescaled by density, $P(\omega/\eta)$, should be a universal function for a sufficiently large number of atoms and sufficiently large geometry, where boundary effects are negligible. We can directly confirm this numerically in Fig. 3.4, where we plot $P(\omega/\eta)$ obtained from RG for various densities.

The high-frequency tails of $P(\omega)$ correspond to the most strongly

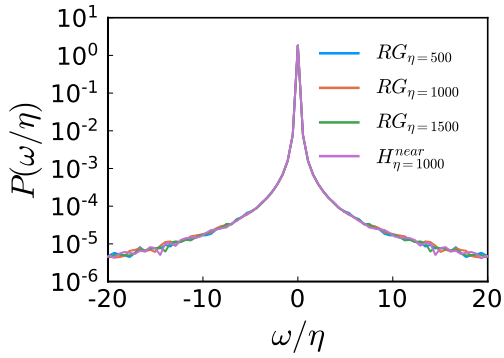

Figure 3.4: Universal probability distribution of normalized frequencies ω/η. We apply the RG approach to spherical samples of $N = 2500$ atoms at dimensionless densities $\eta = 500, 1000, 1500$ to extract the new effective frequencies $\{\omega_i\}$, sampling approximately $\sim 10^3$ different configurations at each density to build the probability distribution $P(\omega/\eta)$. The purple solid line instead corresponds to the exact numerical spectrum of the near-field interaction Hamiltonian. This is obtained considering an ensemble of atoms (same parameters as before) and diagonalizing H^{near} (defined in Eq. (3.2)) to get the eigenfrequency statistics.

interacting pairs, which are renormalized at the beginning of the flow. This perfectly matches the simpler theory presented in [190] for dilute atoms, based on the probability distribution of nearest neighbors, where it was found that asymptotically

$$P(\omega) \sim_{\pm\infty} \xi\eta \frac{1}{2\pi\omega^2}. \tag{3.6}$$

The central part of the distribution $P(\omega)$ instead consists of atoms that have been renormalized multiple times. In this sense, the presented RG scheme and the resulting probability distribution is the correct way to capture the near field induced inhomogeneous broadening of the medium and the induced dephasing rate of spin-waves in dense media, as we are going to discuss.

Formally, the RG procedure amounts to approximately diagonalizing the near-field part of the Hamiltonian (2.1) (an $N \times N$ matrix), by repeatedly identifying and diagonalizing a dominant interacting pair of atoms (a 2×2 block). We can quantify the error by comparing the resulting frequency distribution $P(\omega)$ obtained by RG, with the eigenvalue distribution obtained by exact, numerical diagonalization of the real, symmetric $N \times N$ Hamiltonian H^{near} (Eq. (3.2)). It can be seen in Fig. 3.4 that the two are essentially indistinguishable, which validates principle 2) of the RG scheme.

As anticipated in principle 3), at the end of the RG flow, the resulting new effective (point-like) atoms can still interact through the far-field, which in general cannot be ignored or assumed to be a small effect. From here, one can solve the far-field dynamics in this new basis (which now no longer has near-field interactions). This was done for example in [119] to study the refractive index, finding excellent agreement between the optical response that can be calculated exactly from the full Hamiltonian of Eq. (3.1) and the one of an inhomogeneously broadened medium as obtained by the RG treatment.

In our particular problem of interest involving near-field induced dephasing, we essentially eliminate the effect of far-field interactions, due to the specific choice of a phase-mismatched spin wave as the initial state. We specifically recall that mismatched excitations are naturally decoupled (in an average sense) from free space, with no particular direction of emission and a decay rate Γ_0 free of collective enhancement. We will indeed see in the next section that far-field effects are essentially unnoticeable in the dephasing of mismatched spin waves while RG predicts the dephasing rate with great quantitative accuracy. Since decay can be treated separately now, RG results can be applied to predict the time evolution of a spin wave in an effective single-atom picture, focusing on the spin-wave survival ratio $O_{\mathbf{k}}(t)$. In particular, while the coherence of a single, isolated atom (without the rotating frame) is expected to evolve as $\langle\sigma_{ge}(t)\rangle = \langle\sigma_{ge}(0)\rangle e^{-i(\omega_0 - i\Gamma_0/2)t}$, the distribution in resonance frequencies of the new effective medium will result in an uncertainty of accumulated phase in time

$$O_{\mathrm{RG}}(t) = \left|\int d\omega P(\omega) e^{i\omega t}\right|^2 e^{-\Gamma_0 t}, \tag{3.7}$$

thus introducing microscopically-driven dephasing due to inhomogeneous broadening. We emphasize that the simplicity of Eq. (3.7) arises from the elimination of macroscopic dynamics via our initial phase-mismatched state.

3.4 Spin-wave dephasing

We now present the exact numerical simulations and analysis of the time evolution of a mismatched spin wave for densities ranging from dilute ($\eta \ll 1$) to dense ($\eta \gg 1$), which we will then compare with the simple RG prediction of Eq. (3.7). To be concrete, we take an initial state consisting of a highly mismatched spin wave (Eq. (3.3)) with momentum $|\mathbf{k}| = 6k_0$,

$\hat{x}-$polarized and directed along $\hat{z}$, in an ensemble of $N = 10^4$ atoms. Then, the time evolution of the total excited-state population $P_{\mathbf{k}}(t)$ and of the overlap with the initially prepared spin-wave order $O_{\mathbf{k}}(t)$ is calculated for $N_s = 500$ realizations of the disordered gas and averaged, as indicated by $\langle P_{\mathbf{k}} \rangle$ for example. Numerical results are represented in Fig. 3.5, where we also plot our prediction for the time evolution of the overlap, O_{RG}, made in Eq.(3.7) (orange dash-dotted lines), based on the effective single-atom theory described in the previous section. We first focus on the short-time

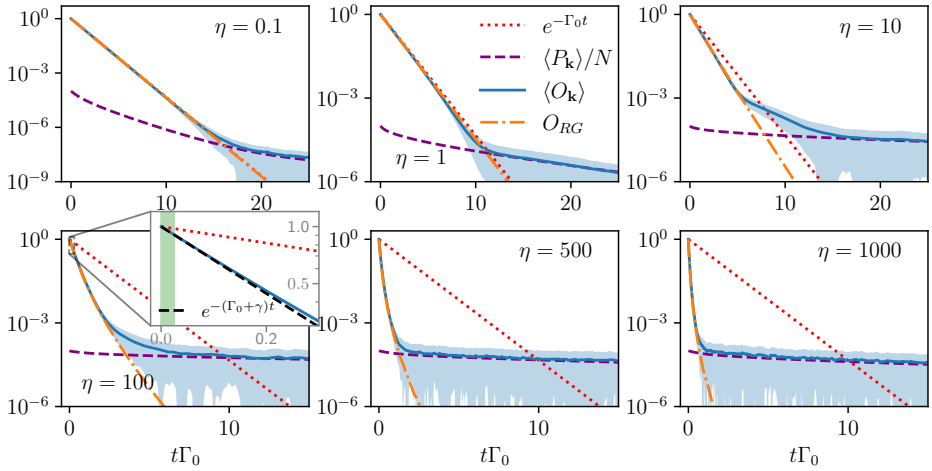

Figure 3.5: Time evolution of an initially prepared ideal mismatched spin-wave ($|\mathbf{k}| \neq k_0$), at different values of the dimensionless density, from small, $\eta = 0.1$ to high $\eta = 1000$. The blue line is the average time evolution of the overlap $O_{\mathbf{k}}$ (see Eq.(3.4)) over different realizations of the disordered gas, while the blue shaded region corresponds to the standard deviation. The red dotted line shows an exponential decay with a rate Γ_0, as predicted by treating the atomic medium as smooth (MBE). The purple dashed line is the population of the time evolved state divided by the atom number, $P_{\mathbf{k}}/N$. Finally, the orange line is the overlap O_{RG} as predicted by RG theory (see Sec. 3.3). We simulate the time evolution of $N = 10^4$ atoms, to guarantee that, at the maximum density $\eta = 1000$, the radius of the uniformly distributed spherical cloud is $R/\lambda_{eg} = 1.34 > 1$, such that the cloud is not subwavelength. All the quantities are averaged over $N_s \sim 500$ different atomic samples. At density $\eta = 100$, the inset shows the short-time exponential dynamics. The interval over which we fit for an exponential $e^{-(\Gamma_0+\gamma)t}$ (dashed black curve) is highlighted in green and corresponds to $\Gamma_{\mathbf{k}} t < 0.1$, while at longer times the overlap deviates from this simple behavior, as predicted by our RG approach.

dynamics. As introduced in the previous section, the short-time decay of a

spin-wave is predicted to be exponential [190], $\langle O_{\mathbf{k}}(\delta t)\rangle \sim e^{-\Gamma_{\mathbf{k}}\delta t}$, within a time interval $\Gamma_{\mathbf{k}}\delta t \ll 1$. The rate $\Gamma_{\mathbf{k}} = \Gamma_0 + \gamma$ is given by the sum of the single-atom emission rate, as predicted by the macroscopic MBE, and an additional density-dependent dephasing rate, $\gamma = \Gamma_0\xi\eta$, with $\xi = 1/6\pi\sqrt{3}$. As shown in the inset of $\eta = 100$ (Fig. 3.5), for example, the microscopic dynamics reveal a short-time decay of the spin-wave order that is distinctly faster than the MBE prediction. The decay becomes even more evident at higher densities ($\eta = 10^2, 10^3$). We can confirm the density dependence in the short-time decay rate $\Gamma_{\mathbf{k}}$ by fitting the curve $\langle O_{\mathbf{k}}\rangle$ for each density in the short-time window, defined by $\Gamma_{\mathbf{k}}\delta t < 0.1$, to an exponential of the form $e^{-(\Gamma_0+\gamma)t}$, and plotting the dependence of the fit parameter γ versus density parameter η in Fig. 3.6(a). We also plot the prediction $\gamma = \Gamma_0\xi\eta$ in red. It is important to observe that within our defined "short time" interval, already $\sim 10\%$ of the initial spin-wave order is lost. An excellent agreement is observed over a large range of densities, both changing size and number of atoms (respectively blue squares and circles) of a random gas, confirming that this effect does only depend on the dimensionless density parameter η, as predicted and experimentally checked in the previous chapter. At longer times and higher densities, the decay of spin-wave order noticeably deviates from exponential. Despite its simplicity, our single effective atom model based on RG (Eq. (3.7)), displays excellent agreement beyond the short-time interval. Viewed from the RG perspective, this non-exponential contribution comes from the frequency components near the center of the inhomogeneous broadening probability distribution $P(\omega/\eta)$ (Fig. 3.4), corresponding to atoms that are renormalized multiple times.

Interestingly, at even longer times, it can be seen that for each density, the average $\langle O_{\mathbf{k}}\rangle$ deviates from our prediction and saturates to a value that barely decreases over the range of times plotted. We furthermore observe numerically that this value closely coincides with the total excited state population remaining divided by the atom number, $P_{\mathbf{k}}(t)/N$ (dashed purple curves). The slow decay of population $P_{\mathbf{k}}(t)$ at long times is an effect that has been studied extensively in recent years, and is known as late-time subradiance [97–103]. While a microscopic derivation is difficult, a heuristic argument can be made that the remaining population should be roughly equally distributed throughout the ensemble, given a smooth initial distribution. Furthermore, given the randomness of the dynamics, this population will be statistically evenly distributed among any N extended modes that can be defined for the system, such as our spin-wave mode of interest.

As far as we can numerically check (e.g., up to $N = 10^4$ atoms for a

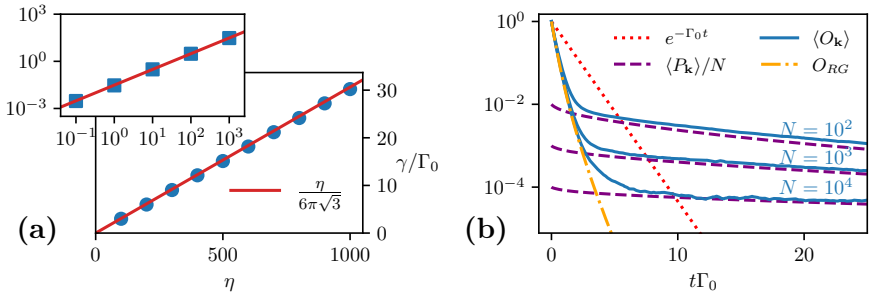

Figure 3.6: (a) Short-time dephasing rate vs. dimensionless density η. Blue dots are extracted from an exponential fit at short times ($\langle O_{\mathbf{k}}\rangle \sim e^{-\Gamma_{\mathbf{k}}\delta t}$), within the time interval $\Gamma_{\mathbf{k}}\delta t = 0.1$, of the full time evolution of a mismatched spin-wave ($|\mathbf{k}| = 6k_0$) at different densities $0.1 \leqslant \eta \leqslant 10^3$. The red line is instead the theoretical prediction for the short-time dephasing rate $\gamma = \Gamma_0\xi\eta$, discussed in the main text. Simulations are performed with a cloud of atoms of fixed size ($R/\lambda_{eg} = 1.34$) and averaging over $N_s \sim 500$ realizations. (inset) The same short time dephasing rate is evaluated (square dots), but now to explore the low-density regime we simulate the spin-wave dynamics in an ensemble with a fixed number of atoms, $N = 10^4$ (again averaged $N_s \sim 500$ times) and varying the radius of the cloud. (b) Numerical simulations of the time evolution of the averaged overlap $\langle O_{\mathbf{k}}\rangle$ (solid blue lines) for a mismatched spin-wave ($|\mathbf{k}| = 6.0k_0$) compared with the RG prediction O_{RG} (orange dash-dotted line), and the total excited population divided by atom number, $\langle P_k\rangle/N$ (purple dashed line). The simulations consider a system of fixed density $\eta = 100$, but different atom number $N = 10^2, 10^3, 10^4$.

density of $\eta = 100$ in Fig. 3.6(b)), we see that the RG prediction O_{RG} follows the actual spin-wave survival ratio $O_{\mathbf{k}}$ for increasingly long times as N is increased, due to the decrease in the saturation value $P_{\mathbf{k}}/N$. This strongly suggests that the single-atom RG prediction should be interpreted as the correct description of the dephasing dynamics in the thermodynamic limit when the late-time population in any one mode $\sim 1/N$ becomes negligible.

3.5 Conclusions

In summary, we have developed an effective single-atom theory that describes well the non-exponential dephasing dynamics of optical spin waves in disordered atomic media, including at high densities and at long times. This theory is based upon the technique of strong disorder renormalization group, which treats the potentially strong near-field interactions in such a medium in a non-perturbative way.

We envision that our predictions, particularly in the high-density regime, could be immediately explored using solid-state emitter ensembles such as rare-earth-doped crystals [73, 226–228], where many atoms per cubic wavelength are typical. Separately, the remarkable accuracy by which RG is found to reproduce the dephasing dynamics suggests that it can be a powerful tool to quantitatively investigate and understand other microscopic optical phenomena in disordered systems.

CHAPTER 4

Refractive index of 3D array

4.1 Introduction

This chapter covers recent collaborative efforts with Francesco Andreoli, Bennet Windt, and Dr. Gian Marcello Andolina, members of the TQNP group at ICFO. The results are being drafted into a manuscript.

Ultrahigh index, low-loss optical materials at telecom or visible frequencies would have potentially game-changing implications for optical technologies and light-based applications. Notably, the reduction in the optical wavelength $\lambda = \lambda_0/n$ compared to the free-space value λ_0 could lead to unprecedented opportunities associated with field confinement and focusing. For example, nanoscale resonators and waveguides could lead to strong optical nonlinear interactions at the single-photon level, compact metasurfaces such as for wavefront shaping, and optical circuitry with the same physical footprint as electronic transistors. The reduction in wavelength could also be useful for nanoscale microscopy and optical lithography, processes that are fundamentally limited by the diffraction limit. Despite these remarkable implications, known optical materials at telecom and visible wavelengths ubiquitously have an index of order unity. Interestingly, very little research has been done on why such a limitation might arise [203]. For example, using Kramers-Kronig relations and a sum rule, one recent work places an elegant bound between the maximum index a material can have and the bandwidth over which a large index can be maintained [202], but does not directly address how large the index can be. Here, we introduce a minimal model that elucidates how large we *might expect* an index to become, under ideal circumstances, and anticipate the possible fundamental mechanisms that could limit its indefinite growth, leaving their exploration

for future work. As a starting point for a bottom-up model, let's recall that the basic building block of a material – individual atoms – can have an extraordinarily large and universal response to light when isolated. As discussed in Ch. 1, an isolated atom can exhibit a scattering cross-section of $\sim \lambda_0^2$ when illuminated by photons resonant with an electronic transition of wavelength λ_0. Given that a typical transition wavelength $\lambda_0 \sim 1$ μm is much larger than the typical spacing between atoms in a solid (of the order of the Bohr radius, $a_0 \sim 0.05$ nm), one might wonder why the large atomic density in a solid does not provide a strongly multiplicative response to light. Indeed, we anticipated in Ch. 1 that such a huge response is predicted by the standard macroscopic theory of light-matter interaction (MBE). In particular, let's recall that such theory states that the refractive index should depend on the product of the susceptibility of a single atom and the particle density as $n(\omega) \sim \sqrt{\chi_0(\omega) N/V} \sim \sqrt{\eta}$ ("refined" approaches such as Drude-Lorentz or the Lorentz-Lorenz models actually reach the same conclusions [119]). The large near-resonant susceptibility of an individual atom then leads to a value of the maximum index of $n \sim 10^5$ at solid densities, as illustrated by the black curve in Fig. 4.1, which is in contrast with typical values of $n \sim 1$ in real-life material, as highlighted by the green region. As discussed in Ch. 1, this scaling comes from the assumption that atoms interact with the optical field independently, neglecting the possible complex behavior associated with wave interference and multiple scattering of light between emitters at fixed discrete positions, which cannot strictly be correct.

Indeed, as highlighted in the rest of this thesis, intuitively, a proper theory for the index must also account for strong, non-perturbative multiple scattering of light. This is expected to be important once the inter-atomic distance becomes smaller than the resonant transition wavelength, $d \lesssim \lambda_0$ (see Fig. 4.1b), such that the individual atomic scattering cross-section start to overlap. A complete theory must also account for the fact that at sufficiently high densities, one reaches the "quantum chemistry" regime highlighted in Fig. 4.1. Here, atomic orbitals strongly hybridize (Fig. 4.1c), and the many-body quantum chemistry problem would have to be combined with multiple scattering.

This chapter covers part of this theory, exploring the maximum possible attainable index from a purely electrodynamical standpoint at densities where quantum chemistry effects can be ignored.

The highly non-perturbative nature of light scattering and optical properties in dense collections of near-resonant atoms in the quantum optics regime of well-separated atoms has attracted significant attention

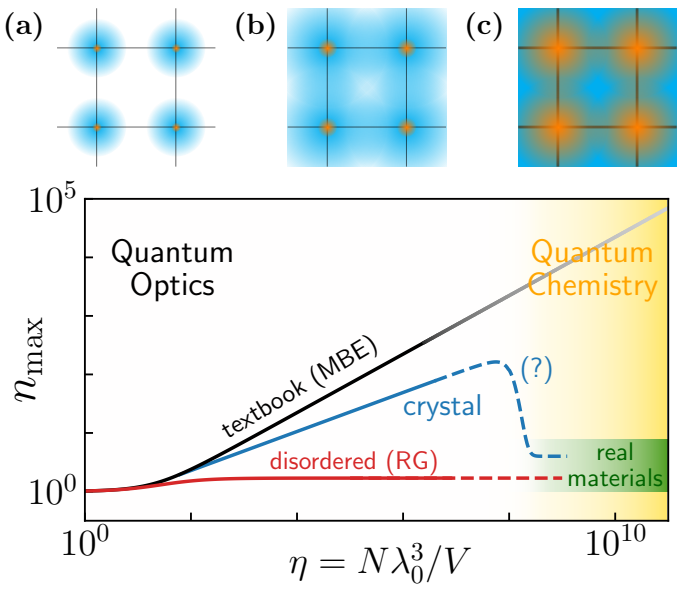

Figure 4.1: Schematic plot of the maximum real part of the refractive index versus density of atoms N/V (in units of the wavelength λ_0 of an atomic transition). Conventional textbook theories predict a maximum index that scales with density as $n \sim (N\lambda_0^3/V)^{1/2}$. In the "quantum optics" regime, atoms are sufficiently far enough part that they can be considered isolated objects, which only interact via the electromagnetic field. For sufficiently high densities, one enters the "quantum chemistry" regime where the overlap of electronic orbitals between different atoms becomes non-negligible and chemical interactions occur. The effects of non-perturbative multiple scattering were investigated for a disordered atomic medium in the quantum optics regime in Ref. [119], where it was found that the maximum index was limited to $n \approx 1.7$ (red curve). Here, we show that a perfect crystal exhibits a purely real index scaling as $n \sim (N\lambda_0^3/V)^{1/3}$ in the quantum optics regime (solid blue curve). The maximum index should be ultimately limited by the onset of quantum chemistry (dashed blue curve) and approach typical values of real materials $n \sim 1$, highlighted by the green region. We also schematically represent the three different regimes of the problem, at varying d. (a) At $d \gg \lambda_0, a_0$, atoms are far apart from each other and each one independently respond to light, with the cross section $\sigma_0 \sim \lambda_0^2$ (cyan shaded region) of an isolated atom in free space. (b) At $\lambda_0 > d > a_0$, intuitively, as the optical cross sections start to overlap, multiple scattering and wave interference need to be taken into account. (c) At $\lambda_0 \ll d \sim a_0$, also the electronic orbitals (orange) starts to overlap and a quantum chemistry approach is therefore required.

in recent years. In the context of disordered ensembles, for example, it has been theoretically predicted and experimentally observed that dense media can have a significantly weaker optical response than predicted by standard formulas. The maximum refractive index of a disordered atomic medium was predicted to saturate at $n \approx 1.7$ regardless of how high the atomic density becomes [119] (solid red curve of Fig. 4.1). In particular, the same non-perturbative strong disorder renormalization group theory used to identify inhomogeneous broadening coming from near-field interactions discussed in Ch. 3, was also shown to be the limiting mechanism for the index growth.

The case of perfectly ordered and equivalently dense atomic lattices, however, is expected to be quantitatively and qualitatively different, as a consequence of the discrete translational invariance. In concrete, according to Bloch's theorem, the atomic excitations are organized in bands with a well-defined dispersion relation and moreover, the physics of diffraction and directional constructive/destructive interference should play a prominent role. Light scattering with regular atomic structures has been studied in the past, in various dimensions. Indeed, as anticipated in Sec. 1.2.2 and relevant to this chapter, it has been theoretically predicted [82, 84, 140] and experimentally observed [163] that a 2D array of atoms in free space can in principle act as a perfect mirror for a weak resonant, incident plane wave, while providing a significant ($\sim \pi/2$) transmission phase shift around resonance (see Fig. 1.8). This effect arises from the strong collective response and constructive interference of the emission from the array. As light is fundamentally prohibited from being absorbed or scattered into random directions, the array and the field then see each other as single-mode systems. Moreover, the fact that the atoms are ordered and that each constituent 2D layer has a single-mode response should lead to the largest index possible, as the lattice constant is decreased. Indeed, the importance of having a single mode response is already suggested in Ref. [202]. At the same time, in Ref. [203], it is presciently predicted that "on a more futuristic level, the writing is on the wall – the way to increase the index is to somehow develop a stoichiometric high-density arrangement of atoms."

The central result of this chapter is that in the quantum optics regime before quantum chemistry can occur, the maximum index of a perfect lattice grows with the density as $n_{\max} \propto \lambda_0/d = \eta^{1/3}$, and is furthermore perfectly real.

The chapter is organized as follows. In Sec. 4.2 the general method to calculate the band structure of an infinite 3D lattice is discussed while leaving the detailed calculations to Appendix C. In Sec. 4.3 we then show

that this band structure directly gives the phase of transmitted light and the index as seen by a field from the outside of a finite 3D array. Finally, in Sec. 4.5, we speculate that at even higher densities, once the lattice constant decreases to a sufficient level, $d \sim a_0$, where atomic orbitals start to overlap, new quantum chemical interactions necessarily appear. Their possible effect on the refractive index problem is discussed.

4.2 The band structure

In order to achieve our goals, it is necessary to learn how to evaluate the refractive index from the "spin model" formulation of light-matter interaction provided in Chapter 1 and extensively used during the rest of the thesis. To capture the linear optical response, it will be sufficient to consider only a single excitation in our system, exactly described, as argued, by the Hamiltonian (1.12). The input-output equation (1.8) instead, tells us that once we solve for the atomic degrees of freedom, the electrical field can be always reconstructed with just the information on the probe field and the state of the atoms. This already suggests that not only should be possible to extract an index directly from the transmitted field, but more importantly that there should be some relation between how atomic excitation and the electrical field propagate.

The natural language for studying the propagation of an excitation in a systems characterized by a discrete translational invariance is the one of spin waves, Bloch theorem and band structures. For an infinite periodic Bravais lattice (single atom per unit cell) the single excitation eigenstates are, due to Bloch theorem, spin waves with definite momentum (Bloch modes)

$$|\mathbf{k}\rangle = \sum_j e^{i\mathbf{k}\cdot\mathbf{r}_j}\sigma_{eg}^j|g\rangle \tag{4.1}$$

where $\mathbf{k} = (k_x, k_y, k_z)$ is the associated Bloch vector, chosen to be in the first Brillouin zone $[-\pi/d, \pi/d]^3$, and d is the lattice constant. The associated eigenvalues for such a spin wave can be calculated as $H|\mathbf{k}\rangle = \left(J_\mathbf{k} - i\frac{\Gamma_\mathbf{k}}{2}\right)|\mathbf{k}\rangle$. This allows to find, for every $\mathbf{k}$, a complex eigenvalue where, the real (imaginary) part correspond to the frequency (decay rates) of the excitation, given by

$$J_\mathbf{k} = \omega_0 + \mathrm{Re}(\chi_\mathbf{k}) \tag{4.2}$$

$$\Gamma_\mathbf{k} = \Gamma_0 - 2\mathrm{Im}(\chi_\mathbf{k}), \tag{4.3}$$

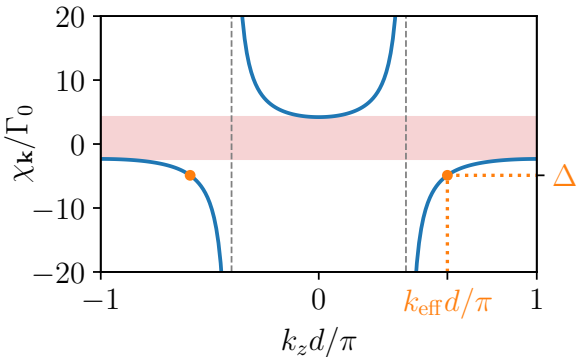

Figure 4.2: Unidirectional band structure for a propagating spin waves $|\mathbf{k}\rangle$, with $\mathbf{k} = (0, 0, k_z)$ along the $\hat{z}$ direction, for a simple cubic sub-wavelength array of lattice constant d/λ_0=0.2. The numerical evaluation is done fixing the polarization of the atoms to be perpendicular to the propagation direction such that $\wp = \hat{\mathbf{x}}$. The dashed vertical lines corresponds to the light cone $k_z = \pm k_0$. The red shaded region shows the presence of a bandgap, where no propagating modes are allowed.

and can be obtained performing the sum:

$$\chi_{\mathbf{k}} = -\frac{3\pi\Gamma_0}{k_0} \sum_{\mathbf{r}\neq 0} e^{i\mathbf{k}\cdot\mathbf{r}} \wp^* \cdot \mathbf{G}_0(\mathbf{r}, \omega_0) \cdot \wp. \tag{4.4}$$

It is important to notice that the sum to compute in (4.4) is poorly convergent in real space, due to the long-range nature of the interaction; an established technique to resolve this issue, Fourier transforming the sum in momentum space, where convergence is expected to be faster, is presented in Ref. [171, 229–231] and reviewed in details in Appendix C.

In the following, we will study the propagation of a single atomic excitation inside a 3D infinite array of atoms, polarized along with $\hat{\mathbf{x}}$, in a simple cubic lattice and in the sub-wavelength regime. We furthermore focus on the propagation along with the $\hat{\mathbf{z}}$ direction. The resulting band structure, obtained performing the sum (4.4), is plotted in Fig. 4.2, which we now discuss in detail. Intuitively, since in an infinite lattice the atoms occupy the whole space, without boundaries, there cannot be any coupling with free-space modes of the electromagnetic field and thus, we expect the decay rates in Eq. (4.3) to be exactly zero, i.e. $\Gamma_{\mathbf{k}} = 0$. Indeed, as shown in Ref. [229] when the reduced atomic system of Eq. (2.1) is diagonalized, one finds that the eigenvalues are purely real and thus describe purely lossless excitations, even though the Hamiltonian itself is non-Hermitian. It is important to notice that the full atom-light Hamiltonian that describes

exactly the system is Hermitian, and thus the coupled system would be diagonalizable by a set of polariton modes with no decay. That also the diagonalization of the effective Hamiltonian produces lossless polariton modes reflects the fact that Eq. (2.1) is an exact description of atom-light interactions in the limit that the speed of light is infinite. The conclusion is that we expect the polariton propagation inside the medium to be exactly described by the spin-wave band structure and that absorption cannot occur within the bulk of a (unity filled) 3D lattice, or equivalently, that $\mathrm{Im}(\chi) = 0$. This of course contradicts the prediction of MBE, which implies huge absorption ($Im(\chi) \sim \sqrt{\eta}$).

Now, when the idea that propagation inside the lattice is fully determined by a real band structure is combined with the fact that light scattering on a sub-wavelength lattice needs to happen in the same direction imposed by an incoming field (as all but one scattering orders are suppressed), implies that for a sufficiently big, but finite array, light propagation in the bulk will be fully determined by the band structure along the same direction. In concrete, as represented in Fig. 4.2 when illuminated by light at a particular detuning Δ respect to the resonant frequency ω_0, and directed along with $\hat{\mathbf{z}}$, the dispersive nature will force the system to excite spin waves with wavevector that satisfy energy conservation, i.e. $\omega_{\mathbf{k}} = \Delta$. When the solutions are given by $\pm k_{\mathrm{eff}}(\Delta)$, being lossless, the spin waves can travel without dissipation and emerge either from the other side of the finite lattice (transmitted) or backward (reflected), such that $T + R = 1$ as anticipated. Moreover, we notice the presence of a bandgap (red shaded region in Fig. 4.2), a range of frequencies in which the spin-wave cannot propagate and thus necessarily needs to be reflected in the finite case, $R = 1$.

Having anticipated that we intuitively expect propagation of the light-matter excitation to be exactly described by the band structure, one could in principle evaluate the phase refractive index just by the ratio between the effective wavevector inside the array versus the free space one:

$$n = \frac{k_{\mathrm{eff}}}{k_0} \tag{4.5}$$

The equation written above implies an unbounded scaling of the refractive index versus the atomic density. Indeed, focusing on the maximum achievable index, for momenta close to the edge of the Brillouin zone, where $k_{\mathrm{eff}} \sim \pi/d$, the refractive index is expected to scale as $n = \lambda_0/2d \sim \eta^{1/3}$ (blue solid line in Fig. 4.1). However, as anticipated, such scaling cannot be sustained at the densities of real-life materials, where atoms sit a few

Bohr radii from each other and where the atomic orbitals are expected to strongly hybridize. Taking a conservative value for the distance between the atoms, e.g. $d \sim 10^2 a_0$, where one expects quantum chemistry to be negligible, but still small ($d \gg \lambda_0$) such that multiple scattering of light to strongly contribute to the light response, quantum optics allows in principle to have a lossless medium of index $n_{\max} = \lambda_0/2d|_{d\sim 10^2 a_0} \sim 100$.

We have seen that the study of an infinite 3D lattice leads to a number of remarkable properties, which should be inherited by a sufficiently big, but finite, array. In particular:

- The fact that lossless mode can propagate through the lattice and that sub-wavelength lattice can only have a single order of diffraction leads to the exciting prediction that a large, but finite, 3D lattice, with a lattice constant, $d < \lambda_0$, should always respond to light in a purely dispersive way. In other terms, for a suitable input mode, transmittance and reflectance should always add to one ($T + R = 1$).

- For this reason, within the range of frequencies characterized by the bandgap, we expect 100% reflection, due to the impossibility for the spin-waves to propagate through the lattice.

- The atomic band structure, if it is indeed equivalent to the band structure as seen by light, should predict the accumulated phase of the light transmitted through the array and thus the index.

These predictions motivate the study of light propagating through a finite-sized lattice, which allows the transmission/reflection coefficients and the effective index of light to be deduced (e.g., the transmission phase) and compared to the atomic band structure calculation, which will be done in the following section.

4.3 The transmission coefficient

In the previous section, we have characterized the mixed light-matter excitations that emerge in a 3D lattice of two-level atoms interacting with the quantized radiation field. Now, we discuss how to study numerically the linear transmission and reflection properties of a weak probe field through a finite 3D array, and consequently how to evaluate its phase refractive index, directly from the computed transmitted light.

First, an external incoming light field $\mathbf{E}_{in}$ can drive an arbitrary collection of atomic dipoles in free space, as specified by the atomic Hamiltonian

$$\begin{aligned} H_{\text{at}} &= -\hbar\Delta \sum_j \sigma_{ee}^j - \hbar \sum_j \left(\Omega_j \sigma_{ge}^j + \text{h.c.}\right) \\ \Omega_j &:= \frac{d_{eg}}{\hbar} \wp_j^* \cdot \mathbf{E}_{\text{in}}(\mathbf{r}_j) \end{aligned} \tag{4.6}$$

Here, as in the previous section, $\Delta = \omega_p - \omega_0$ is the detuning of the probe field frequency ω_p with respect to the transition frequency. Moreover, the defined Rabi frequencies Ω_j only depend on the value of the external field at the discrete, fixed atomic positions.

As discussed in Ch. 1 the full dynamics of light emission and re-scatter of a single photon through the ensemble can be related to an effective model containing only the atomic degrees of freedom and the incident field, prescribed by the Hamiltonian $H_{at} + H$ (see (1.12)).

Moreover, the total electrical field can be then reconstructed with an input-output relation (1.8). Evaluating the field at each point $\mathbf{r}$ can be computationally expensive, however, in experiments, one often cares only about the projection of this field in a particular spatial mode, such as a Gaussian. In Ref. [164] it is sown that as long as the input field does not contain any evanescent component (or they are negligible), the projection of the input-output equation on the same mode lets us define the quantum operator associated with the detector which is simply given by:

$$\mathbf{E}_{\text{det}} = \mathbf{E}_{\text{in,det}} + i d_{eg} \sqrt{\frac{k_0}{2\hbar\varepsilon_0 F_{\text{det}}}} \sum_j \mathbf{E}_{\text{det}}^*(\mathbf{r}_j) \cdot \wp\, \sigma_{ge}^j \tag{4.7}$$

where $\hat{E}_{\text{in,det}}$ is the input field projected in the detection mode and $F_{\text{det}} = \int_{z=\text{const}} d^2 r \mathbf{E}_{\text{det}}^*(\mathbf{r}) \cdot \mathbf{E}_{\text{det}}(\mathbf{r})$ is a normalization constant. With the equation (4.7) it is possible to reconstruct the projection of the output field in the detection mode just solving for the atomic degrees of freedom. In the absence of atoms this equation is simply stating that the outgoing and the incoming field are the same. We typically want to probe the system with a classical Gaussian-like beam and to recollect light in the same mode

The field that we chose is a Gauss-Laguerre mode, a solution of Maxwell's equation in the paraxial approximation ($\text{w}_0 \gg \lambda$) [80, 84].

$$\mathbf{E}_{\text{in}}(\mathbf{r}, z) = \mathbf{E}_0 \frac{w_0}{w(z)} e^{i\left(k_0 z - k_0 \frac{r^2}{2R(z)} - \varphi(z)\right)} e^{-\frac{r^2}{w^2(z)}}, \tag{4.8}$$

with the usual beam parameters

$$\begin{aligned} w(z) &= w_0\sqrt{1+\left(\tfrac{z}{z_R}\right)^2} \qquad z_R = \tfrac{w_0^2 k_0}{2} \\ R(z) &= z\left[1+\left(\tfrac{z_R}{z}\right)^2\right] \quad \varphi(z) = \arctan\tfrac{z}{z_R} \end{aligned} \tag{4.9}$$

where w_0 is the beam waist. In particular one wants to avoid the regime where the paraxial limit breaks down. While the non-paraxial limit can be formally solved [164], physically it makes it more difficult to compare the numerically obtained refractive index to the band structure calculation. This is because the tightly focused beam has a lot of wavevector components, whereas we would like something as close to the plane-wave limit as possible in order to map a light wave with a definite momentum into a spin-wave with a definite momentum.

In the weak driving regime, one can look for a solution $|\psi\rangle$ in the single excitation sector. Defining the expectation values of the atomic coherences as $\langle\hat{\sigma}^i_{eg}\rangle = \sigma^i_{eg}$, the atomic equation of motion reads:

$$\begin{aligned} \partial_t \sigma^j_{ge} &= i\Delta\sigma^j_{ge} + i\Omega_j - i\Gamma_0 \sum_\ell g_{j\ell}\sigma^\ell_{ge} \\ g_{j\ell} &= -\frac{3\pi}{k_0}\wp^* \cdot \mathbf{G}_0(\mathbf{r}_j, \mathbf{r}_\ell, \omega_{eg}) \cdot \wp. \end{aligned} \tag{4.10}$$

Driving the system we look in particular for a stationary solution, $\langle\dot{\sigma}^i_{eg}\rangle = 0$, given by

$$\boldsymbol{\sigma}_{ge} = \mathcal{M}^{-1}\boldsymbol{\Omega} \qquad \mathcal{M}_{ij} = -\Delta\delta_{ij} + \Gamma_0 g_{ij}. \tag{4.11}$$

Looking at the expectation value ($\langle\hat{E}_{out}\rangle = \langle\psi|\hat{E}_{out}|\psi\rangle$) of the projection (4.7) over the atomic states and normalizing respect to the input field the transmission coefficient associated to this input mode can be written down as

$$t(\Delta) = 1 + i\frac{3\pi\Gamma_0}{2k_0^2 F_{in}} \sum_{j,\ell} E^*_j \mathcal{M}^{-1}_{j\ell} E_\ell. \tag{4.12}$$

For simplicity, we introduce the scalar field amplitude

$$E_j = \wp^* \cdot \mathbf{E}_{\text{in}}(\mathbf{r}_j) = \frac{\hbar}{d_{eg}}\Omega_j, \tag{4.13}$$

and the normalization constant

$$F_{\text{in}} = \int_{z=\text{const}} d^2 r \mathbf{E}^*_{in}(\mathbf{r}) \cdot \mathbf{E}_{in}(\mathbf{r}), \tag{4.14}$$

which ensures that the input field carries only one photon. The reflection coefficient is instead obtained by projecting on the backward propagating input mode, $\mathbf{E}_{in}(\mathbf{r})^*$:

$$r(\Delta) = i\frac{3\pi\Gamma_0}{2k_0^2 F_{in}}\sum_{j,\ell} E_j \mathcal{M}^{-1}_{j\ell} E_\ell. \tag{4.15}$$

From the evaluation of the transmission coefficient, one can readily define a phase refractive index, as we are going to show. An electromagnetic wave propagating in a medium of length L with a refractive index n will have a transmission coefficient $t(\Delta) = |t(\Delta)|e^{i\varphi}$, which is just the product between the transmission amplitude and φ, the imprinted phase shift. In a macroscopic description, the latter is simply the difference between the phase acquired by the incoming field in free propagation, $k_0 L$, and the one within the medium, $k_{\text{eff}}L$, described by an effective momentum [90, 91]. Generally k_{eff} can be complex, which accounts for dispersion and dissipation. The (generally complex) phase refractive index can therefore be defined as the ratio:

$$n(\Delta) = \frac{k_{\text{eff}}}{k_0}(\Delta) = 1 - i\frac{\log(t)}{k_0 L} \tag{4.16}$$

While the formalism is quite general, in the following section we will numerically evaluate the transmission and refractive index of a 3D array.

4.4 Finite 3D array

Having elucidated the basic formalism and tools, in this section we will evaluate the refractive index of a sufficiently big, but finite, perfectly filled 3D array of 2-level atoms ($\hat{x}$ polarized) in a simple cubic lattice. In particular, we will show that the optical response of the system can be related to the spin-wave band structure of the infinite lattice described before.

Practically we will look at transmission of a Gaussian beam, Eq. (4.8), for which the beam waist is chosen to be $w_0/\lambda_0 = 0.3(N_x - 1)d/\lambda_0$; for the parameters that will be used in the simulations, $N_{x,y} = 50$ and for lattice constant $d/\lambda_0 \leqslant 0.2$ one gets a focal spot of $w_0/\lambda_0 \sim 3$. The factor 0.3 is just a reasonable choice to have the input field mostly inside the array but still have a beam waist large enough to treat it as a paraxial field with a well-defined wavevector along $\hat{z}$ [84, 164]. For these parameters, the overall results of the numerical simulations are presented in Fig. 4.3, which are now

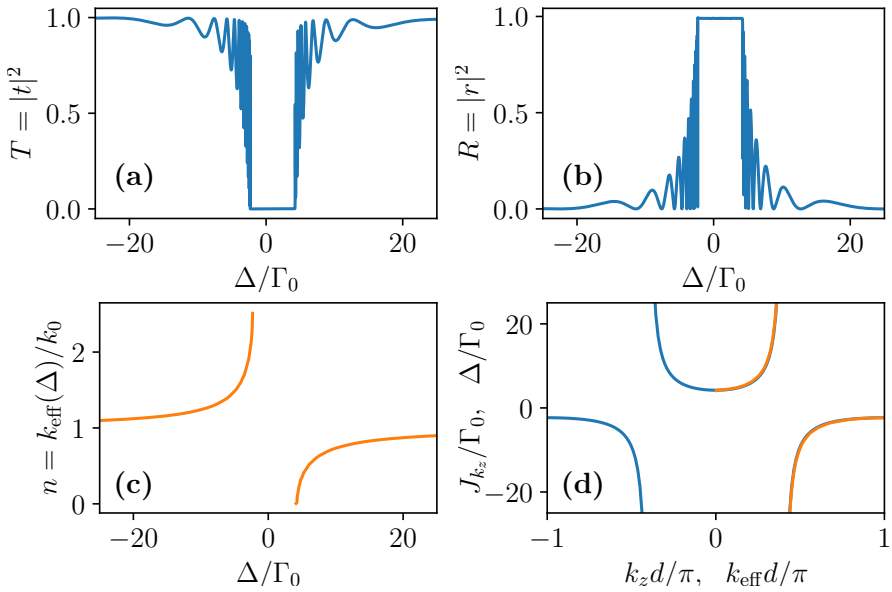

Figure 4.3: (a) Transmittance $T = |t|^2$ and (b) reflectance $R = |r|^2$ spectrum calculated respectively with the transmission and reflection coefficients defined in Eq. (4.12) and Eq. (4.15), for a 3D array of $N = 50^2 \times 25$ atoms of lattice constant $d/\lambda_0 = 0.2$, illuminated by a weak Gaussian field of waist $w_0/\lambda_0 \sim 3$. (c) Phase refractive index, numerically calculated extracting the phase acquired by the transmission coefficient, as defined in Eq. (4.16). The curve also represent the effective momentum of light as seen from outside the medium, as a function of the dimensionless detuning. (d) The blue solid line is the same unidirectional band structure for an infinite array presented in Fig. 4.2. On top of it, the orange solid line is the same line plotted in (c) but now inverted, i.e. plotting the detuning as a function of the numerically evaluated effective wavevector.

discussed. In Figs. 4.3a and 4.3b the squared transmission and reflection coefficients are respectively plotted. As predicted in the previous section, as a consequence of the purely dispersive behavior of the medium ($\text{Im}\chi = 0$), and the single-mode response of a dense sub-wavelength array, transmission and reflection always add up to one ($T+R=1$) over the whole spectrum. Moreover, a stopband in light transmission is present. In that frequency range, the band structure shows us that the spin-waves cannot propagate and for sub-wavelength lattice constant light can only be re-emitted in the reflection mode, achieving nearly 100% reflection. Outside the gap, the transmitted spectrum shows peaks, associated with resonant modes of the finite-size atomic "slab" (in particular, the ends of the medium constitute

mirrors that form a low-finesse cavity).

The phase refractive index is then directly extracted from the phase of the numerically evaluated transmission coefficient, as defined in Eq. (4.16), and plotted in Fig. 4.3c as a function of the dimensionless detuning of the input field. First, outside the bandgap, where light can be transmitted, the index is found to be perfectly real, as predicted in the previous section. Again, n can be interpreted as the ratio between the effective wavevector of light traveling through the medium and the free space one, $n = k_{\text{eff}}/k_0$. Importantly, $k_{\text{eff}}(\Delta)$ is a function of the detuning of the incoming beam. In a dispersive environment, such detuning simply constitutes the energy difference that the probe needs to provide (respect to ω_0) in order to excite such an effective mode. Inverting this relation, i.e. obtaining the energy of the mode $\Delta(k_{\text{eff}})$ as a function of the wavevector, one intuitively gets a band structure, this time numerically evaluated and again effectively, the band structure as seen from the outside by light. To conclude, when the effective band structure is superimposed on the spin-wave band structure discussed in the previous section, as done in Fig. 4.3d, we observe an excellent agreement. This result shows that, for a large enough system, the light dispersion inside the medium is indeed characterized by the spin-wave band structure.

The equivalence between the index and the band structure also implies that, as clearly visible in Fig. 4.3c, at a particular detuning of the input field, one can excite a spin wave of wavevector $k_{max} = \pi/d$, thus reaching the maximum refractive index achievable in an ideal 3D array of atoms at that particular lattice constant

$$n_{max} = \frac{k_{max}}{k_0} = \frac{\lambda_0}{2d} \tag{4.17}$$

As a function of the dimensionless density, $\eta = (\lambda_0/d)^3$, the maximum refractive index goes like $n_{max} \sim \eta^{1/3}$ and is furthermore real, in agreement with the band structure argument provided in the previous section while in contrast with Maxwell-Bloch prediction.

4.5 Quantum chemistry

We have shown that a 3D unity-filled lattice has a maximum refractive index that is purely real and scales as $n \sim \lambda_0/2d \sim \eta^{1/3}$. This unbounded increase suggests that the low index of real materials should be caused by other physical mechanisms that can alter the perfect interference and the dispersive response of an ideal 3D array.

An interesting question, which we aim to pursue in the future, is what crucial ingredients are missing from the spin model treatment of light-matter interaction, which are relevant for real-life materials and are responsible for saturation of the refractive index. On one hand, real-life materials could be affected by dephasing, disorder, static inhomogeneities, or coupling of electronic transitions to other degrees of freedom (e.g., phonons, yielding an effective bath). Minimal models of these effects could be incorporated into the spin model, to understand their effects on n, for example as an additional decay rate on top of the dispersive response of a 3D array.

Another possibility, more fundamental and interesting, is chemistry, e.g. the interaction and hybridization of atomic orbitals. While a full "quantum chemistry" calculation is beyond the scope of this thesis, it is possible that the initial onset of chemical effects might be captured in a perturbative manner in our spin model. Here we discuss the key assumption and the minimal set of chemical interactions that are expected to affect the optical response of a 3D array of atoms.

As anticipated, one can focus on a regime of large d/a_0 and try to identify which physical mechanism turns on first as well its magnitude by making the lattice constant smaller compared to the Bohr radius. To the lowest order, there is no overlap between the electronic orbitals centered at different atomic sites and the problem reduces to the quantum optical limit discussed in the previous sections. For simplicity, one can consider the paradigmatic case of hydrogen atoms as the solution for the electronic orbitals is known. Furthermore, as in the previous discussion, the driving field is taken to be weak. Thus, along with the d/a_0 expansion, we can then restrict to the lowest bands (those reducing to 1s and 2p hydrogen levels in the isolated atom limit, respectively our ground and excited state), and further assume that only a single electron is excited to the p-orbital band. Again restricting to this regime is sufficient to probe the linear refractive index.

Here, we speculate on one limitation to the index that can emerge purely due to quantum chemistry on the ground state (all atoms in the 1s orbital), in the form of density-density correlations. For large d/a_0, the first effect allowed by chemistry is the tunneling of an electron to a neighboring nucleus. The complex dynamics and the interaction of charge and spin of electrons in a material are thought to be captured by the well-known, minimal (yet physically rich), Fermi-Hubbard model. The model, while offering great simplification to the full many-electron Hamiltonian, captures the competition between the kinetic energy of the electron, that makes it tunnel to the nearest neighbor with a hopping amplitude t and a local

repulsion $U > 0$ which penalizes double occupation ($n_{i\sigma} = c^+_{i\sigma} c_{j\sigma}$) of sites

$$H = -t \sum_{<ij>} \sum_{\sigma} c^+_{i\sigma} c_{j\sigma} + U \sum_i n_{i\uparrow} n_{i\downarrow}. \tag{4.18}$$

As the overlap directly depends on the distance between the lattice sites, also the energy scales depend on d/a_0. While the evaluation of t and U from first principles can be challenging, a straightforward approximation is to take the hopping term as the overlap between two $1s$ hydrogen wavefunction centered at two consecutive lattice sites, such that $t(d/a_0)$ will intuitively decay exponentially as d/a_0 gets bigger. On the other end the energy cost of having two electrons occupying the same lattice site is the same as the ionization of the donor. This is roughly independent of d and for hydrogen is $U \sim 13.6$ eV. An array of hydrogen atoms corresponds to the half-filling limit of the Fermi-Hubbard model, in which case the absence of tunneling would lead to exactly one electron per nucleus as the ground state. For small but non-zero tunneling ($t \ll U$), so-called holon-doublon pairs can emerge, in which one nucleus has no electrons and a neighboring one contains two. This represents the onset of density-density correlations induced by chemistry, within the Fermi-Hubbard model. Thus the typical configuration we wish to take into account is illustrated in Fig. 4.4a, where with a generally low probability (intuitively $\sim (t/U)^2$) one can find a holon-doublon pair in an otherwise perfect array (one electron per site).

The realization now is that holon-doublon pairs are expected to strongly affect the optical response. Because of their small population, it generally makes sense to consider just the effect of a single holon-doublon pair, in an otherwise perfect crystal (one electron per site). Importantly, the holon (nucleus with no electron) and the doublon (a negatively charged ion) have a completely different response to light and in particular, do not efficiently couple to light near resonance with the first excited state of neutral hydrogen. As a result, at large d/a_o, one can model a holon-doublon pair as two consecutive defects (empty sites) of the perfect array, as illustrated in Fig. 4.4b. Intuitively, as a defect explicitly breaks the discrete translational invariance, it opens up different scattering channels, which ultimately can be interpreted as additional decay (Γ' in Fig. 4.4b) on top of the purely dispersive and single-mode behavior of unity-filled 3D array. It will be therefore crucial for the future to study the optical response of an array with holes and their effect on the refractive index. While a more quantitative and precise study of the complex dynamics of correlated electrons is needed in the future, we stress that the general approach, as conveyed in this section, will be to incorporate complex quantum chemistry

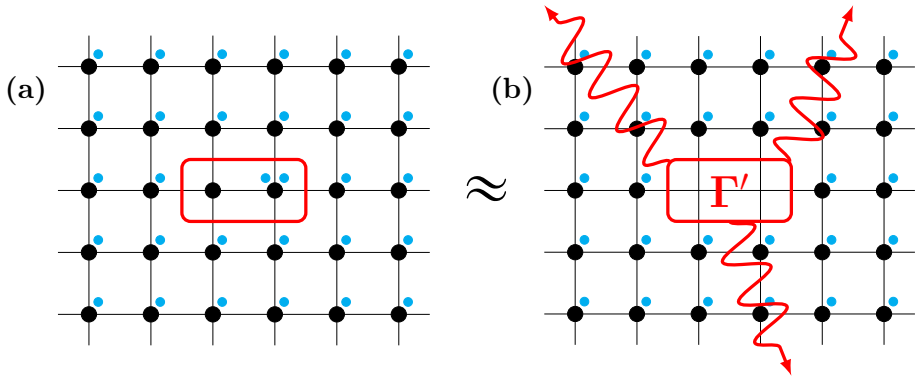

Figure 4.4: (a) Due to the overlap of electronic orbitals, qualitatively an electron can tunnel to a nearest neighbor atom to form an holon-doublon pair. (b) From the perspective of the incoming photon this pair can be approximated as two consecutive defects in a otherwise perfect array of well separated atoms. A defect breaks the perfect interference and can scatter light into other modes, effectively introducing an additional effective decay rate Γ'.

and condensed matter effects into quantum optics in a simple effective way. Overall, this future work, besides trying to answer the fundamental question of why the refractive index of real-life material of order $n \sim 1$, should also both inspire new efforts to realize ultra-high index material but also discover new optical phenomena at the interplay between collective optical phenomena, multiple scattering, solid-state physics, and quantum chemistry.

CHAPTER 5

Conclusions & Outlook

The interface between light and atomic ensembles is an important platform for the development of quantum technological applications while exposing many fundamental and contemporary physical questions that are yet to be completely answered. In the introduction of this thesis, it was discussed how MBE are generally considered the standard approach both to describe light-matter interaction and excitation propagation dynamics in cold atoms ensembles in terms of smooth fields. Within MBE, the efficiency of the interface between a single photon and an ensemble of cold atoms is fundamentally limited by the competition between spontaneous and collective emissions. While the first happens at the rate of a single atom in free space Γ_0 and covers the whole 4π solid angle, collective emission in a well-defined direction happens at an enhanced rate $\Gamma_{\mathbf{k}}^{\text{coll}} = \Gamma_0(1 + \mathrm{D}/4)$. This gives a branching ratio between "good" and "bad" emission, and thus an efficiency, which is simply proportional to the optical depth $\Gamma_{\mathbf{k}}^{\text{coll}}/\Gamma_0 \sim \mathrm{D}$, which ultimately sets the performance of quantum applications such as photon storage [54]. Importantly, this ratio remains fundamentally limited by spontaneous emission.

As argued, while MBE captures the strong collective resonant emission that characterizes an efficient light-matter interface at high D, it explicitly neglects microscopic effects like multiple scattering arising from dipole-dipole interaction. Beyond MBE, these effects are important because they have been predicted to give rise to interesting phenomenology and could potentially affect the performance of applications.

Importantly, the fundamental dipole-dipole interaction, emerging from photon exchange processes between the emitters, can be self-consistently taken into account in a "spin model" treatment of light-matter interaction with atomic media, which has been reviewed in Ch. 1. This approach has

attracted a lot of attention in the past years, especially in trying to answer the two fundamental questions that were posed at the beginning of this thesis:

- Is there some new and exciting physics beyond MBE?
- Are the performance of quantum technology simply limited by the optical depth as MBE would predict? Can we do better?

These questions, of crucial importance in the field of quantum optics but far from being completely answered, were tackled during the three main chapters of this thesis. Here, we provide a general overview of the obtained results and some perspectives on future directions that would be interesting to explore.

In Ch. 2 two important results were obtained. First, an innovative method has been demonstrated to coherently manipulate the wavevector of the atomic spin-wave excitations. As argued in the main text, the coherent manipulation of the matching condition between the atomic excitation with the free space radiation can be used to suppress the strong macroscopic collective dynamics (well captured by the MBE) and opens up the possibility of probing microscopic correlations in cold atomic ensembles.

Second, with this experimental technique, a density-dependent dipolar dephasing rate of optical spin waves has been measured. Moreover, the additional decoherence contribution has been described by a simple quantitative theory that captures the role of strongly interacting pairs in the medium. Importantly, while well-known error sources such as Doppler broadening due to atomic motion and dephasing due to magnetic field inhomogeneities are generically considered "technical", as they can be reduced by cooling down the atoms or better shielding the atomic cloud, here, as the strong near-field resonant dipole interaction between closely spaced pairs of atoms is a universal property of dense atomic ensembles [102, 104, 110, 174] and is therefore fundamental to a randomly positioned atomic gas.

The unraveled dephasing effect on spin-wave order is therefore expected to be of direct relevance to the performance of quantum light-matter interfaces. Indeed, recalling that the efficiency of the light-atoms interface, i.e. the branching ratio between 'good" and "bad" emission, fundamentally limited by Γ_0, here should be accordingly modified as $\sim \mathrm{D}/(1+\xi\eta)$ to take into account the enhanced decoherence rate by the $(1+\xi\eta)$ factor. The correction can be of course significant if the local density of the atomic sample is high. This suggests that there could be upper bounds on the maximum atomic densities tolerable to reach a given fidelity or limit on the

minimum system size, which has implications in efforts to make compact quantum devices based upon ensembles. More experimental and theoretical studies should be therefore done in the high-density regime.

Finally, to overcome the limitations imposed by dephasing, one might resort to atomic arrays [83], where the fluctuations of near-field interactions are controlled, as has been experimentally demonstrated recently [163] and where phase coherence is protected by the symmetry (see Ch.4). Furthermore, arrays of atoms offer the intriguing possibility of even suppressing spontaneous emission in the first place. Indeed, because of the destructive interference in collective spontaneous emission, mismatched spin waves have the important property to be "subradiant", i.e. their decay rate approaches zero. Subradiant states have been shown, for example, to provide a basis to store and retrieve a single photon with exponentially better performance compared to what MBE would predict [90]. For these reasons, the ability to reversibly generate and retrieve mismatched spin waves is therefore anticipated to have important applications in atomic array setups, where it could be readily used to access this class of states, which are otherwise generally decoupled from free space radiation and difficult to probe.

Motivated by the result of the previous chapter it was natural to ask ourselves if the particular scaling with the density also holds outside the experimentally achievable regime of parameters. For this reason, in Ch. 3 dephasing has been studied in the high-density and long times regime, simulating the relaxation dynamics of a mismatched spin wave for up to $N = 10^4$ atoms. While such a strongly correlated system is generally complex to solve, here, we have developed an effective single-atom theory that describes well the non-exponential dephasing dynamics of optical spin waves in disordered atomic media. The theory, based upon the technique of strong disorder renormalization group (RG), treats the strong near-field interactions in such a medium in a non-perturbative way. An important result is that at the end of the RG flow, the technique maps the initial complex interaction between discrete point-like atoms into an inhomogeneous broadening of the two-level transition, characterized by a probability distribution. This suggests that MBE can be refined to capture the near field correlations build-up by including by hand inhomogeneous broadening. This approach, as shown in Ch. 3, can be tested against the full exact simulation of light and atomic excitation dynamics. While here this approach has been used to capture, with an excellent agreement, the dephasing dynamics that emerged from exact simulations, in a previous work [119], the refractive index and its saturation at high densities as been unraveled.

For these reasons, RG can be a powerful tool to quantitatively investigate and understand other microscopic optical phenomena in disordered dense systems.

In concrete, as argued in Ch. 3, the developed approach could be immediately explored using solid-state emitter ensembles such as rare-earth-doped crystals [73, 226–228], where many atoms per cubic wavelength are typical. Moreover, recently it has been predicted that dipole-dipole interaction in dense ensembles contributes to narrowing the EIT transparency window [232], which is expected to reduce the storage efficiency of slow light as an EIT-based quantum memory application (see Ch. 1). In parallel, as demonstrated in Ch. 3, we also face the unprecedented possibility of actually simulating the dynamics, and more in concrete the storage and retrieval capabilities of realistic atomic ensembles ($N \sim 10^4$), at densities where the strong near-field interaction cannot be neglected anymore. Finally, the synergy between full exact simulations and the RG effective approach could help to derive new fundamental bounds to the performance of quantum technological applications with cold atom ensembles, which constitutes an interesting direction to explore in the near future.

Finally, Ch. 4 starts with the realization that available optical materials in the visible range generically have an index of order one, with little research done to understand and overcome this limitation.

Ultrahigh index, low-loss optical materials at telecom or visible frequencies would have important implications for optical technologies and light-based applications due to better confinement and focusing of light. For example, a high n, associated with a reduction in the optical wavelength $\lambda = \lambda_0/n$ compared to the free-space value λ_0 could lead to better nanoscale resonators and waveguides to realize strong optical nonlinear interactions at the single-photon level, more compact metasurfaces for wavefront shaping or better resolution in microscopy and optical lithography, processes that are fundamentally limited by the diffraction limit.

For these reasons, in Ch.4, we introduced a minimal model that elucidates how large we *might expect* an index to become, under the ideal circumstances of a perfect 3D crystal, and anticipate the possible fundamental mechanisms that could limit its indefinite growth, leaving their exploration for future work.

The obtained central result is that in a dense, ordered configuration of point-like atoms, where multiple scattering and photon-mediated interactions are fully taken into account, quantum optics allows for the phase refractive index to be as big as $n_{\max} \sim \eta^{1/3}$, to be furthermore completely real. This confirms that, in contrast to the previous projects, the micro-

scopic correlations build-up and the constructive interference guaranteed by the perfect symmetry in an ideal crystal are not detrimental, but can be exploited to realize a more efficient light-matter interface.

We then argued that already the simplest model of an atom beyond the point-like approximation, i.e. a hydrogen atom can introduce complex dynamics of correlated electrons through tunneling. More studies will be therefore done soon to incorporate complex quantum chemistry and condensed matter effects into quantum optics in a simple effective way. Overall, this future work, besides trying to answer the fundamental question of why the refractive index of real-life material of order $n \sim 1$, should also both inspire new efforts to realize ultra-high index material but also discover new optical phenomena at the interplay between collective optical phenomena, multiple scattering, solid-state physics, and quantum chemistry.

If such a high index with low losses is indeed possible and once the regimes and the boundaries of the maximum achievable index will be clarified, an interesting path to take would be to explore its possible technological implications (quantum networks, quantum non-linear optics, quantum metrology...), as a high index at low losses necessarily implies an efficient light-matter interface. A concrete direction, for example, would be to study the engineering of photon-photon interaction with Rydberg atoms under EIT, a system that has been extensively studied in the context of MBE [233, 234].

Part III

Appendix

APPENDIX A

Numerical simulations: MBE vs. CDM

The analysis of Chapter 2 suggests the decay of spin-wave survival ratio follows $O_{\mathbf{k}}(t) \approx e^{-\Gamma_{\mathbf{k}} t}$ initially, with $\Gamma_{\mathbf{k}} = \Gamma_{\mathbf{k}}^{\text{coll}} + \gamma$ deviating from the standard MBE prediction by a local density-dependent rate $\gamma = \xi\eta\Gamma_0$. As seen, the additional term arises due to dephasing, and only appears by accounting for the effect of granularity in the dynamics of the dipole-dipole interactions, in particular, between close pairs of atoms.

This prediction with both MBE and CDM simulations can also be verified numerically. Indeed, a glimpse into the effect is provided by comparing CDM and MBE simulations of the spin-wave dynamics in Fig. 2.1 was also presented in Section 2.2. In particular, while the survival ratio $O_{\mathbf{k}}(t)$ is seen to be trivial within the MBE (dashed gray curve of Fig. 2.1(d)), the CDM predictions (dashed red curve) strongly deviate and decay faster. The important role of close-by pairs (having a distance less than $\lambda_0/2\pi$, about 3% percent of all atoms in the simulation) is illustrated by removing such pairs from the ensemble, which results in a survival ratio (dashed blue curve) that goes back to the MBE results at short times. In contrast, removing the same percentage of atoms randomly (dashed green) results in almost no difference, compared to CDM simulations of the original ensemble. Together, these simulations clearly show the dramatic effect that "freezing" macroscopic dynamics can have, in order to observe microscopic optical phenomena.

Here, for completeness and reproducibility, the practical implementation of these simulations will be discussed. For example, within the microscopic spin model, it will be shown how to evaluate quantities like the intensity of the emitted field or the spin-wave survival ratio. This will also allow us to concretely show how the smoothing approximation that MBE use to treat the field dynamics effectively washes out dipole-dipole interactions

and thus the microscopic correlations build up.

Because of its importance, the idea that physically, any dissipation of atomic excitations must be in the form of emitted photons, was repeated many times in the thesis. As argued, the specific properties of the emitted light are encoded in the quantum electric field operator (see the discussion around Eq. (1.8)), which reads:

$$\hat{\mathbf{E}}(\mathbf{r}) = \mu_0 d_{eg} \omega_0^2 \sum_i \mathbf{G}(\mathbf{r} - \mathbf{r}_i, \omega_0) \cdot \boldsymbol{\wp}\, \sigma_{ge}^i. \tag{A.1}$$

It can readily be verified that Eq. (A.1) is the solution to the Maxwell wave equation

$$\nabla \times \nabla \times \hat{\mathbf{E}} - \frac{\omega_0^2}{c^2} \hat{\mathbf{E}} = \frac{\omega_0^2}{\varepsilon_0 c^2} \hat{\mathbf{P}}(\mathbf{r}), \tag{A.2}$$

where the polarization density takes the form $\hat{\mathbf{P}}(\mathbf{r}) = \sum_j \delta(\mathbf{r} - \mathbf{r}_j) \boldsymbol{\wp}\, \sigma_{ge}^j$ for two-level atoms, which explicitly depends on the discrete atomic positions $\{\mathbf{r}_i\}_{i=1,\dots,N}$. As we are interested in linear dynamics, it suffices to consider the singly excited atomic state

$$|\psi(t)\rangle = \frac{1}{\sqrt{N}} \sum_j \beta_j(t) \sigma_{eg}^j |g_1, \cdots, g_N\rangle, \tag{A.3}$$

and define a single-photon wave function $\boldsymbol{\varepsilon}(\mathbf{r}, t) = \langle g_1, \cdots, g_N | \hat{\mathbf{E}} | \psi(t) \rangle$ and polarization fields $\hat{\mathbf{p}}(\mathbf{r}, t) = 1/\sqrt{N} \sum_j \boldsymbol{\wp}\, \beta_j \delta(\mathbf{r} - \mathbf{r}_j)$. These fields obey the same Maxwell equation (A.2), which is well known to be valid both in the classical as well as in the quantum regime. In other terms, in the single excitation sector, quantum and classical description coincides.

As discussed in the main text, we consider N two-level atoms with positions $\mathbf{r}_j$ (specified later), with resonant dipolar interaction specified by Eq. (2.1). To study spin-wave dynamics within the linear excitation regime, it suffices to initialize a spin-wave excitation with wavevector $\mathbf{k}$:

$$|\mathbf{k}\rangle = \frac{1}{\sqrt{N}} \sum_j e^{i\mathbf{k}\cdot\mathbf{r}_j} \sigma_{eg}^j |g_1, \cdots, g_N\rangle, \tag{A.4}$$

accordingly setting the initial phases on each atoms as $\beta_j(t = 0) = e^{i\mathbf{k}\cdot\mathbf{r}_j}$.

Because of the naturally occurring spontaneous emission and dipole-dipole interaction associated with the spin-model Hamiltonian of Eq. (1.12), the Schrödinger equation for the amplitudes $\beta_j(t)$ is readily found to be [119, 212]:

$$\dot{\beta}_j = -\frac{\Gamma_0}{2} \beta_j + i \frac{3}{2} \lambda_0 \Gamma_0 \sum_{l \neq j} \mathbf{G}_{xx}(\mathbf{r}_{jl}, \omega_0) \beta_l. \tag{A.5}$$

Notice that the dipole direction is fixed along the $\wp = \hat{\mathbf{x}}$ direction. Equivalently, the time evolved state is also captured by $|\mathbf{k}(t)\rangle = e^{-iHt}|\mathbf{k}\rangle$, i.e. by time-evolving under the effective Hamiltonian (1.12).

Once the time-evolved state is known, the relevant observables to the experiment can be constructed. For example, the spin-wave surviving ratio by Eq. (2.3) is evaluated as

$$O_{\mathbf{k}}(t) = |\langle \mathbf{k}|\mathbf{k}(t)\rangle|^2 = \left| \frac{1}{\sqrt{N}} \sum_j^N \beta_j(t) e^{-i\mathbf{k}\cdot\mathbf{r}_j} \right|^2 . \tag{A.6}$$

The expectation value of the electrical field $\varepsilon(\mathbf{r}, t) = \langle g_1, ..., g_N|\hat{\mathbf{E}}_s(\mathbf{r})|\psi(t)\rangle$ s instead given by

$$\boldsymbol{\varepsilon}(\mathbf{r}, t) = \frac{\omega_0^2}{\varepsilon_0 c^2} \sum_j^N \mathbf{G}(\mathbf{r} - \mathbf{r}_j, \omega_0) \cdot \wp \, \beta_j(t), \tag{A.7}$$

which can be completely evaluated both in space and time. Like this, for example, in Fig. 2.1 (a) and (b), the 3D field intensity $i_{\mathbf{k}} = |\boldsymbol{\varepsilon}(\mathbf{r}, 0)|^2$ at $t = 0$, is calculated on the plane $y = 0$, respectively for a matched ($|\mathbf{k}| = k_0$) and a mismacthed ($|\mathbf{k}| = 2.9k_0$) spin wave. For a phase-matched spin wave one can define the superradiance solid angle Ω_s as the solid angle around $\mathbf{k}$ over which a substantial fraction (*e.g.* 99%) of this coherent $\overline{\boldsymbol{\varepsilon}}(\mathbf{r}, t)$ emission is directed, and find that it is practically set by $\Omega_s = (k_0\sigma)^{-2}$ for the Gaussian distribution $\rho(\mathbf{r}) \sim e^{-r^2/2\sigma^2}$ [45, 188, 189]. The CDM approach can be used to predict observables and compare with experiments. Specifically, one can define $I_{\mathbf{k}}(t) \propto \int_{\Omega_s} |\boldsymbol{\varepsilon}(\mathbf{r}, t)|^2 d^2\Omega$ as the superradiant intensity, as represented in Fig. 2.1 (e).

One additional complexity that arises in disordered systems is that observables need to be averaged over many microscopic spatial configurations. Note that this averaging only retains the part of the field that has a coherent phase relationship with the spin wave, while eliminating the field that has a phase that randomly depends on the microscopic configuration. Performing an average over many microscopic spatial configurations $\{\mathbf{r}_j\}$ to obtain $\langle I_{\mathbf{k}}(t)\rangle$ and $\langle O_{\mathbf{k}}(t)\rangle$ as the final simulated observables to compare with the experimental data. In each sample atomic positions $\mathbf{r}_j$ are randomly and independently sampled according to the Gaussian distribution density distribution, $\rho(\mathbf{r}) = \rho_0 e^{-(x^2+y^2)/2\sigma^2 - z^2/2l_z^2}$ with $k_s\sigma, k_s l_z \gg 1$, with the specific values being fixed in Fig. 2.1.

Finally, while the initial amplitudes $\beta_j(t=0)$ have been fixed by hand in the method described above, the equations can readily be modified to

explicitly account for a weak probe pulse to initially excite the atomic amplitudes β_j. For the dilute sample with $\rho \ll k_0^3$ and with the nanosecond probe pulse in this work, we find that the difference in the simulated results is negligible.

A.1 MBE simulations

The Maxwell-Bloch equations (MBE) describe coherent coupling between continuous optical media (described by optical Bloch equations) and optical fields (described by Maxwell's equations), and is one of most common approaches to describe light-atom interactions [1, 2, 50–55] and performance of applications, e.g. quantum memories [3, 54].

These equations are generally derived from the standard approach in quantum optics and the goal is to derive the equation of motion for the field and the atomic degrees of freedom. Importantly, to simplify the description, it is assumed that the granularity of atoms is ignored, and the atomic medium treated as a smooth density distribution $\rho(\mathbf{r}) = \langle \sum_j \delta(\mathbf{r} - \mathbf{r}_j) \rangle$. The fields and polarizations can then be smoothed as well, $\overline{\boldsymbol{\varepsilon}}$ and $\overline{\mathbf{p}}$. In that case, the field (Maxwell) equation becomes

$$\nabla \times \nabla \times \overline{\boldsymbol{\varepsilon}} - \frac{\omega_0^2}{c^2} \overline{\boldsymbol{\varepsilon}} = \frac{\omega_0^2}{\varepsilon_0 c^2} \overline{\mathbf{p}}, \tag{A.8}$$

while the Bloch equation describing the evolution of the polarization in response to the field is

$$\dot{\overline{\mathbf{p}}} = -\frac{\Gamma_0}{2} \overline{\mathbf{p}} + \frac{\Gamma_0}{2} \varepsilon_0 \chi_0(\mathbf{r}) \overline{\boldsymbol{\varepsilon}}(\mathbf{r}), \tag{A.9}$$

where the linear susceptibility is $\chi_0(\mathbf{r}) = \rho(\mathbf{r})\alpha_0/\varepsilon_0$ with $\alpha_0 = 2i|\wp|^2/\hbar\Gamma_0$. It has to be noticed that Eq. (A.9) constitutes the "smoothed-out" version of Eq. (A.5) for the polarization field.

Finally, Eq. (A.9) is the generalization of the MBE that we presented in the introductory chapter of the thesis (Eq. (1.1)) for non-uniform distribution of emitters and in the resonant case ($\Delta = 0$).

As before, our goal now is to solve the Maxwell-Bloch equations (A.8) and (A.9), starting from a phase-matched spin wave as the initial excitation $\overline{\mathbf{p}}(\mathbf{r}, t = 0) = (\wp/\sqrt{N})\rho(\mathbf{r})e^{i\mathbf{k}_s \cdot \mathbf{r}}$. For a smooth density distribution

$$\rho(\mathbf{r}) = \rho_0 e^{-(x^2+y^2)/2\sigma^2 - z^2/2l_z^2}, \tag{A.10}$$

with $k_s\sigma, k_s l_z \gg 1$, we can assume that the field and polarization have slowly-varying envelope $\tilde{\boldsymbol{\varepsilon}}$ and $\tilde{\mathbf{p}}$, related to the original quantities by $\overline{\boldsymbol{\varepsilon}} = \tilde{\boldsymbol{\varepsilon}} e^{i\mathbf{k}_s\cdot\mathbf{r}}$ and $\overline{\mathbf{p}} = \tilde{\mathbf{p}} e^{i\mathbf{k}_s\cdot\mathbf{r}}$. In that case, the wave equation significantly simplifies,

$$2ik_s\partial_Z\tilde{\boldsymbol{\varepsilon}} = -\nabla_\perp^2\tilde{\boldsymbol{\varepsilon}} - \frac{\omega_0^2}{\varepsilon_0 c^2}\tilde{\mathbf{p}}. \tag{A.11}$$

For convenience, a Z-direction to align with that of the spin wave direction $\mathbf{k}_s$ has been defined, while $\nabla_\perp$ denotes the divergence operator in the XY-plane. The boundary condition for the field is given by $\tilde{\boldsymbol{\varepsilon}} \to 0$ as $Z \to -\infty$. To simulate the coupled equations (A.9) and (A.11), we discretize a simulation space with $L_X = L_Y = 10\sigma, L_Z = 10l_z$ into $N_X \times N_Y \times N_Z$ 3D grids. The grid size is chosen to support the slowly varying $\tilde{\boldsymbol{\varepsilon}}$, $\tilde{\mathbf{p}}$ only, and do not need to be very fine. Practically, we find $N_{X,Y,Z} = 400$ allows for convergence for both type "A" and "B" samples in this work. One can therefore directly solve Eqs. (A.9) and (A.11) in the time domain and use this to construct the superradiant field emission $\tilde{\boldsymbol{\varepsilon}}(x, y, z, t)$ and the superradiant intensity, $I_{\mathbf{k}}(t) = \int_{\Omega_s} d\Omega |\tilde{\boldsymbol{\varepsilon}}(\mathbf{r}, t)|^2$, integrated over the solid angle of emission. Equivalently, one can also define the smooth MBE version of the survival ratio, $O_{\mathbf{k}} = |\int d\mathbf{r}^3 \tilde{\mathbf{p}}^*(\mathbf{r}, 0) \cdot \tilde{\mathbf{p}}(\mathbf{r}, t)|^2$, of the initialized spin wave order. In Fig. 2.1(c) and 2.1(d), the MBE simulations are performed assuming a smooth atomic cloud of the same Gaussian density distribution from from which the samples of atomic positions were extracted before in the CDM simulations.

APPENDIX B

Effect of atomic motion

All the discussions so far in this work assume that the dipole spin waves are excited in a motionless gas of atoms. Here, we estimate the errors associated with this assumption. We first analyze the impact of atomic motion to the near-field interaction associated with Eq. (2.4). For a thermal ensemble, the relative motion of an atomic pair leads to a position change of $\delta r_1 = v_{\mathrm{T}}\delta t$ during the spin-wave evolution time δt. Furthermore, considering the energy shift of an interacting pair at close distances, $\omega_{\pm}(\mathbf{r}) = \pm 3\Gamma_0(3\cos^2\theta - 1)/4k_0^3r^3$, one sees that they create a van der Waals force that accelerates the relative motion, leading to a velocity change $\delta v \sim 3v_r \times |\omega_{\pm}\delta t|/k_0 r$ and an associated relative displacement $\delta r_2 \sim 3v_r\delta t \times |\omega_{\pm}\delta t|/2k_0 r$. Here $v_r = \hbar k_0/m \sim 6$ mm/s is the recoil velocity of the $D2$ excitation, and $v_{\mathrm{T}} \approx 50$ mm/s is the thermal velocity of our $T \sim 30$ μK ^{87}Rb sample. The validity of the $P(\omega) \sim 1/\omega^2$ scaling analysis of the frequency distribution of nearby pairs, calculated in Sec. 2.4, requires a positional change $\delta r_{1,2} \ll r$, which sets an upper bound to $|\omega_{\pm}|$, and thus to the density, during the observation time δt. This bound is given by $|\omega| \ll \min(\Gamma_0(\Gamma_0 k_0 v_r \delta t^2)^{-3/5}, \Gamma_0(k_0 v_{\mathrm{T}}\delta t)^{-3})$. For example, for $\delta t = T_{\mathrm{i}} = 30$ ns, we find $|\omega_{\pm}| \ll 100\Gamma_0$. Since the frequency distribution broaden with the density, i.e. it width is roughly given by $\Delta\omega \sim \eta\Gamma_0$, breaking thin bound would require densities on the orders of $\eta \sim 100$, here, not explored. Equivalently, the atomic motion also sets a characteristic Doppler dephasing time $\tau_{\mathrm{D}} = 1/k_0 v_{\mathrm{T}}$ [211], which is at the microsecond level in this experiment and is expected to affect negligibly the spin-wave decay [188].

APPENDIX C

Band Structure Calculations

In this appendix, we review the systematic approach to performing the calculation of the band structures and the decay rates of the atomic excitation that naturally arise when the atoms are organized in regular lattices.

As already introduced, for an infinite periodic Bravais lattice (single atom per unit cell) the single excitation eigenstates are, due to Bloch theorem, spin waves with definite momentum (Bloch modes)

$$|\mathbf{k}\rangle = \sum_j e^{i\mathbf{k}\cdot\mathbf{r}_j}\sigma_{eg}^j|g\rangle \tag{C.1}$$

where $\mathbf{k}$ is the associated Bloch vector, chosen to be in the first Brillouin zone $[-\pi/d, \pi/d]^3$ and where d is the lattice constant. As discussed in the main text, given the eigenfunction it is immediate to find the eigenvalues of the dipole-dipole Hamiltonian (Eq.(2.1)) for such a spin wave, $H|\mathbf{k}\rangle = (J_\mathbf{k} - i\Gamma_\mathbf{k}/2)\,|\mathbf{k}\rangle$, where the real and the imaginary part, respectively describing the dispersive and dissipative behavior are given by:

$$J_\mathbf{k} = \omega_0 + \mathrm{Re}(\chi_\mathbf{k}) \tag{C.2}$$

$$\Gamma_\mathbf{k} = \Gamma_0 - 2\mathrm{Im}(\chi_\mathbf{k}), \tag{C.3}$$

having defined the sum

$$\chi_\mathbf{k} = -\frac{3\pi\Gamma_0}{k_0}\sum_{\mathbf{r}\neq 0} e^{i\mathbf{k}\cdot\mathbf{r}}\wp^*\cdot\mathbf{G}_0(\mathbf{r},\omega_0)\cdot\wp. \tag{C.4}$$

The important result to be discussed in this appendix is that it is found that in 3D lattices is that their propagation can be described solely in terms of a real band structure since the decay rate is $\Gamma_\mathbf{k} = 0$ for every $\mathbf{k}$.

A numerical approach to evaluate the sum Eq. (C.4) can be always used in principle, however, in this way, already the presence of long-range interaction makes the summation of the Green's tensor over all the lattice sites converge slowly, making an accurate computation difficult. We will review the procedure to perform this summation in momentum space instead, where convergence is in principle faster than in position space and in free space where the analytical expression of the Green's tensor in momentum space can be used to push the analytical calculations further. For example, the decay rates and the energy shifts for the 1D chain are evaluated analytically [90]. In the 2D case, for a simple square lattice, only the decay rates are obtained analytically. Numerically instead, the band structure of a topologically non-trivial 2D lattice is derived in [171]. Here, the focus will be on reviewing the results obtained on 3D arrays, where the band structure of a 3D simple cubic and of a diamond lattice are respectively calculated in Ref. [229] and Ref. [231].

C.1 Sums in momentum space

The summation over an infinite lattice can be converted in a sum over momentum space by using the Poisson identity

$$\sum_{\mathbf{r}\in L} e^{i(\mathbf{p}+\mathbf{k})\cdot\mathbf{r}} = \frac{1}{\mathcal{V}} \sum_{\mathbf{Q}\in RL} (2\pi)^{d_L} \delta^{(d_L)}(\mathbf{Q}-\mathbf{p}-\mathbf{k}) \tag{C.5}$$

where d_L is the lattice dimension, $\mathcal{V}$ is the volume of the unit cell and the $\mathbf{Q} \in RL$ are the vectors in the reciprocal lattice, related to $\{\mathbf{r}_i\}_{i=1,\dots,N} \in L$ by the relationship $\mathbf{r}\cdot\mathbf{Q} = 2\pi m$ with $m \in \mathbb{N}$. In order to apply Eq. (C.5) we make use of the representation of the Green's tensor in momentum space [229]:

$$\begin{aligned} \mathbf{G}_0(\mathbf{r}) &= \int \frac{d^3p}{(2\pi)^3} e^{i\mathbf{p}\cdot\mathbf{r}} \tilde{\mathbf{G}}_0(\mathbf{p}) \\ \tilde{\mathbf{G}}_0(\mathbf{p}) &= \frac{1}{k_0^2} \frac{k_0^2 \mathbb{1} - \mathbf{p}\otimes\mathbf{p}}{k_0^2 - p^2}. \end{aligned} \tag{C.6}$$

While it will become more important later, it is important to notice that such quantity it is purely real. The sum over the lattice thus reads:

$$\sum_{\mathbf{r}\in L} e^{i\mathbf{k}\cdot\mathbf{r}}\mathbf{G}_0(\mathbf{r}) = \int \frac{d^3p}{(2\pi)^3}\sum_{\mathbf{r}\in L} e^{i(\mathbf{p}+\mathbf{k})\cdot\mathbf{r}}\tilde{\mathbf{G}}_0(\mathbf{p}) = \\ = \frac{1}{\mathcal{V}}\int \frac{d^3p}{(2\pi)^3}\sum_{\mathbf{Q}\in RL}(2\pi)^3\delta^{(3)}(\mathbf{p}+\mathbf{k}-\mathbf{Q})\tilde{\mathbf{G}}_0(\mathbf{p}) = \frac{1}{\mathcal{V}}\sum_{\mathbf{Q}\in RL}\tilde{\mathbf{G}}_0(\mathbf{Q}-\mathbf{k}). \tag{C.7}$$

After adding and subtracting the zero term of the Green's tensor, the sum can be therefore fully rewritten in momentum space:

$$\sum_{\mathbf{r}\neq 0} e^{i\mathbf{k}\cdot\mathbf{r}}\mathbf{G}_0(\mathbf{r}) = \sum_{\mathbf{r}\in L} e^{i\mathbf{k}\cdot\mathbf{r}}\mathbf{G}_0(\mathbf{r}) - \mathbf{G}_0(0) = \frac{1}{\mathcal{V}}\sum_{\mathbf{Q}\in RL}\tilde{\mathbf{G}}_0(\mathbf{Q}-\mathbf{k}) - \mathbf{G}_0(0). \tag{C.8}$$

It is therefore possible to write down a general procedure to evaluate the energy shift and the decay rates for an infinite lattice in 3D, in an efficient way in momentum space.

$$\chi_{\mathbf{k}} = -\frac{3\pi\Gamma_0}{k_0}\wp^*\cdot\left[\frac{1}{\mathcal{V}}\sum_{\mathbf{Q}\in RL}\tilde{\mathbf{G}}_0(\mathbf{Q}-\mathbf{k}) - \mathbf{G}_0(0)\right]\cdot\wp. \tag{C.9}$$

However, both terms are now divergent, only their difference being finite. The behavior is caused by the well-known divergence of the Green's function at the origin, roughly $G_0(r) \sim_0 1/r^3$, which comes from treating atoms as point-like dipoles. An established regularization technique to control the difference between these two diverging quantities is to smear the position of each atom over a smooth distribution [171, 229] and is discussed in the next section.

C.2 Green's tensor regularization

The regularization scheme to capture the difference between two divergent quantities is based on integrating the Green's tensor over some particular smooth distribution $\mathcal{R}$, smearing out over a finite volume the divergent part at $\mathbf{r} = 0$ [229]:

$$\mathbf{G}_0^*(\mathbf{r}) := \int d^3\mathbf{x}\ \mathbf{G}_0(\mathbf{r}-\mathbf{x})\mathcal{R}(a,\mathbf{x}) \\ \mathcal{R}(a,\mathbf{x}) = \frac{1}{(\sqrt{2\pi}a)^3}e^{-x^2/2a^2} \tag{C.10}$$

where a acts as a regulation parameter. A natural choice is to take a Gaussian distribution but in principle all the choices of the $\mathcal{R}$ function that makes the zero-fluctuations limit ($a \to 0$) of the regularized Green's tensor

$$\lim_{a\to 0} \mathbf{G}_0^*(a, \mathbf{r}) = \mathbf{G}_0(\mathbf{r}) \tag{C.11}$$

to tend to the original one. By doing so all the calculations in which the divergence at the origin cause problems can be performed safely, taking the limit only at the end.

Looking at equation (C.9) and substituting for the newly introduced regularized quantities one needs to evaluate this new regularized Green's tensor at position $\mathbf{r} = 0$. Carefully calculating such quantity (see Refs. [171, 229]) gives:

$$\mathbf{G}_0^*(0) = \mathbb{1}\frac{k_0}{6\pi}\left(-\frac{(-1/2) + (k_0 a)^2}{\sqrt{\frac{\pi}{2}}(k_0 a)^3} - \frac{\operatorname{erfi}\frac{k_0 a}{\sqrt{2}} - i}{e^{(k_0 a)^2}}.\right) \tag{C.12}$$

The result is consistent with what is well known about the imaginary part of Green's function in free space, encoding the rate at which atoms dissipate into free space modes. In concrete, in the limit of a point-like atom:

$$-\frac{3\pi\Gamma_0}{k_0}\wp^* \cdot \mathrm{Im}\mathbf{G}_0^*(0) \cdot \wp = \frac{\Gamma_0}{2}e^{-a^2k_0^2/2} \underset{a\to 0}{=\!\!\longrightarrow} \frac{\Gamma_0}{2}. \tag{C.13}$$

Moving forward one can also derive the regularized tensor in momentum space. Following equation (C.10) and exploiting the convolution theorem it is easy to show that the regularized Green's tensor in momentum space is simply the original one but scaled by a Gaussian factor

$$\tilde{\mathbf{G}}_0^*(\mathbf{p}) = \frac{1}{k_0^2}\frac{k_0^2\mathbb{1} - \mathbf{p}\otimes\mathbf{p}}{k_0^2 - p^2}e^{-a^2p^2/2} \tag{C.14}$$

Under the regularization scheme the sum of (C.4), evaluated for an infinite 3D lattice is given by

$$\chi_{\mathbf{k}} = -\frac{3\pi\Gamma_0}{k_0}\wp^* \cdot \left[\frac{1}{\mathcal{V}}\sum_{\mathbf{Q}\in RL}\tilde{\mathbf{G}}_0^*(\mathbf{Q}-\mathbf{k}) - \mathbf{G}_0^*(0)\right] \cdot \wp. \tag{C.15}$$

This last expression is thus equivalent to Eq. (C.9) but with the substitution in favor of regularized quantities. Finally, in the last section below, we discuss the decay rates and the band structure in the important point-like limit ($a \to 0$) of interest.

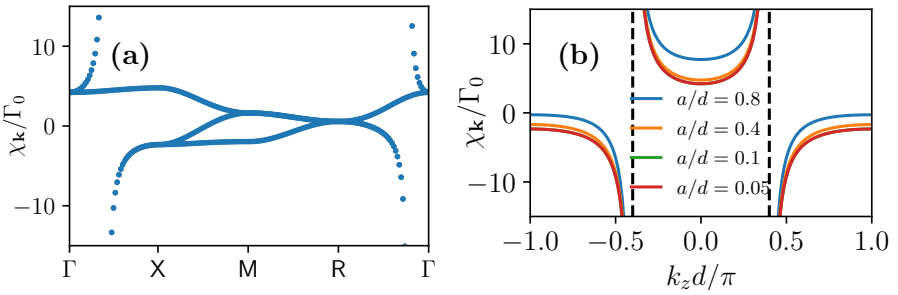

Figure C.1: (a) Photonic band structure of a 3D infinite array of atoms in a simple cubic lattice, along the standard irreducible path. Lattice constant is chosen to be $d/\lambda_0 = 0.2$. (b) Convergence of the momentum sum to the exact band structure (unidirectional) for a 3D chain of atoms in free space. Summing on few lattice sites, $\sim 25^3$ in these simulations, the sum Eq. (C.9) is numerically implemented for different values of the regularization parameter a/d. Convergence is achieved already for values of $a/d = 0.1$.

C.3 Band structure and convergence

Importantly, also the regularized Green's tensor in momentum space is purely real such that some imaginary components, describing dissipation, can only come from the regularized self-energy of Eq. (C.12). As a result, for every 3D geometry, every decay contains a vanishing term like

$$\Gamma_{\mathbf{k}} = \Gamma_0 - 2\mathrm{Im}\chi_{\mathbf{k}} \sim \Gamma_0(1 - e^{-a^2 k_0^2/2}) \underset{a\to 0}{\longrightarrow} 0, \tag{C.16}$$

This simply corresponds to the fact that excitations can never escape from an infinite 3D lattice that covers the whole space. The system is therefore only characterized by the dispersion relation:

$$J_{\mathbf{k}} = \omega_0 + \chi_{\mathbf{k}} \tag{C.17}$$

This quantity can be now easily implemented numerically with the procedure described above. For a simple cubic lattice for example, and a specific lattice constant, the band structure is plotted in Fig. C.1(a) for momenta along the standard irreducible path in 3D. For every spin-wave momentum, three propagating modes, with their respective polarization and energy shift exist. Moreover, the system does not possess a full band gap, i.e. for every frequency, there are multiple propagating modes associated with the same eigenenergy $J_{\mathbf{k}}$. As argued in the main text, however, for a sub-wavelength lattice we want to focus on the propagation of spin waves along a single

direction and for a single polarization, as plotted in Fig. 4.2, for example along with $\hat{\mathbf{z}}$. This corresponds to the path $-X \to \Gamma \to X$ in Fig. C.1(a).

Finally, as expected and represented in Fig. C.1(b), convergence to exact band structure (for example the unidirectional one) can be achieved with modest computational resources [171, 229]

Bibliography

[1]K. Hammerer, A. S. Sørensen, and E. S. Polzik, "Quantum interface between light and atomic ensembles", Reviews of Modern Physics **82**, 1041 (2010).

[2]M. Fleischhauer and M. D. Lukin, "Quantum memory for photons: Dark-state polaritons", Physical Review A **65**, 022314 (2002).

[3]P. Vernaz-Gris, K. Huang, M. Cao, A. S. Sheremet, and J. Laurat, "Highly-efficient quantum memory for polarization qubits in a spatially-multiplexed cold atomic ensemble", Nature Communications **9**, 363 (2018).

[4]Y. F. Hsiao, P. J. Tsai, H. S. Chen, S. X. Lin, C. C. Hung, C. H. Lee, Y. H. Chen, Y. F. Chen, I. A. Yu, and Y. C. Chen, "Highly Efficient Coherent Optical Memory Based on Electromagnetically Induced Transparency", Physical Review Letters **120**, 183602 (2018).

[5]Y. Wang, J. Li, S. Zhang, K. Su, Y. Zhou, K. Liao, S. Du, H. Yan, and S. L. Zhu, "Efficient quantum memory for single-photon polarization qubits", Nature Photonics **13**, 346 (2019).

[6]W. Wasilewski, K. Jensen, H. Krauter, J. J. Renema, M. V. Balabas, and E. S. Polzik, "Quantum noise limited and entanglement-assisted magnetometry", Physical Review Letters **104**, 133601 (2010).

[7]I. D. Leroux, M. H. Schleier-Smith, and V. Vuletić, "Implementation of cavity squeezing of a collective atomic Spin", Physical Review Letters **104**, 73602 (2010).

[8]R. J. Sewell, M. Koschorreck, M. Napolitano, B. Dubost, N. Behbood, and M. W. Mitchell, "Magnetic sensitivity beyond the projection noise limit by spin squeezing", Physical Review Letters **109**, 253605 (2012).

[9]O. Hosten, N. J. Engelsen, R. Krishnakumar, and M. A. Kasevich, "Measurement noise 100 times lower than the quantum-projection limit using entangled atoms", Nature **529**, 505 (2016).

[10]Z. Chen, J. G. Bohnet, J. M. Weiner, K. C. Cox, and J. K. Thompson, "Cavity-aided nondemolition measurements for atom counting and spin squeezing", Physical Review A **89**, 043837 (2014).

[11]K. C. Cox, G. P. Greve, J. M. Weiner, and J. K. Thompson, "Deterministic Squeezed States with Collective Measurements and Feedback", Physical Review Letters **116**, 093602 (2016).

[12]R. J. Lewis-Swan, M. A. Norcia, J. R. Cline, J. K. Thompson, and A. M. Rey, "Robust Spin Squeezing via Photon-Mediated Interactions on an Optical Clock Transition", Physical Review Letters **121**, 070403 (2018).

[13]B. Julsgaard, A. Kozhekin, and E. S. Polzik, "Experimental long-lived entanglement of two macroscopic objects", Nature **413**, 400 (2001).

[14]H. Gorniaczyk, C. Tresp, J. Schmidt, H. Fedder, and S. Hofferberth, "Single-photon transistor mediated by interstate Rydberg interactions", Physical Review Letters **113**, 053601 (2014).

[15]D. Tiarks, S. Baur, K. Schneider, S. Dürr, and G. Rempe, "Single-photon transistor using a Förster resonance", Physical Review Letters **113**, 053602 (2014).

[16]D. Tiarks, S. Schmidt-Eberle, T. Stolz, G. Rempe, and S. Dürr, "A photon–photon quantum gate based on Rydberg interactions", Nature Physics **15**, 124 (2019).

[17]Y. O. Dudin and A. Kuzmich, "Strongly interacting Rydberg excitations of a cold atomic gas", Science **336**, 887 (2012).

[18]T. Peyronel, O. Firstenberg, Q. Y. Liang, S. Hofferberth, A. V. Gorshkov, T. Pohl, M. D. Lukin, and V. Vuletić, "Quantum nonlinear optics with single photons enabled by strongly interacting atoms", Nature **488**, 57 (2012).

[19]I. Bloch, J. Dalibard, and W. Zwerger, "Many-body physics with ultracold gases", Reviews of Modern Physics **80**, 885 (2008).

[20]M. A. Norcia, R. J. Lewis-Swan, J. R. Cline, B. Zhu, A. M. Rey, and J. K. Thompson, "Cavity-mediated collective spin-exchange interactions in a strontium superradiant laser", Science **361**, 259 (2018).

[21]H. Bernien, S. Schwartz, A. Keesling, H. Levine, A. Omran, H. Pichler, S. Choi, A. S. Zibrov, M. Endres, M. Greiner, V. Vuletic, and M. D. Lukin, "Probing many-body dynamics on a 51-atom quantum simulator", Nature **551**, 579 (2017).

[22]P. Scholl, M. Schuler, H. J. Williams, A. A. Eberharter, D. Barredo, K.-N. Schymik, V. Lienhard, L.-P. Henry, T. C. Lang, T. Lahaye, A. M. Läuchli, and A. Browaeys, "Quantum simulation of 2D antiferromagnets with hundreds of Rydberg atoms", Nature **595**, 233 (2021).

[23]P. De Vries, D. V. Van Coevorden, and A. Lagendijk, "Point scatterers for classical waves", Reviews of Modern Physics **70**, 447 (1998).

[24]Y.-S. Chin, M. Steiner, and C. Kurtsiefer, "Nonlinear photon-atom coupling with 4Pi microscopy", Nature Communications **8**, 1200 (2017).

[25]S. J. van Enk and H. J. Kimble, "Single atom in free space as a quantum aperture", Physical Review A **61**, 051802 (2000).

[26]S. J. van Enk and H. J. Kimble, "Strongly focused light beams interacting with single atoms in free space", Physical Review A **63**, 023809 (2001).

[27]B. Darquié, M. P. A. Jones, J. Dingjan, J. Beugnon, S. Bergamini, Y. Sortais, G. Messin, A. Browaeys, and P. Grangier, "Controlled Single-Photon Emission from a Single Trapped Two-Level Atom", Science **309**, 454 (2005).

[28]G. Hétet, L. Slodička, M. Hennrich, and R. Blatt, "Single Atom as a Mirror of an Optical Cavity", Physical Review Letters **107**, 133002 (2011).

[29]M. K. Tey, Z. Chen, S. A. Aljunid, B. Chng, F. Huber, G. Maslennikov, and C. Kurtsiefer, "Strong interaction between light and a single trapped atom without the need for a cavity", Nature Physics **4**, 924 (2008).

[30]M. K. Tey, G. Maslennikov, T. C. Liew, S. A. Aljunid, F. Huber, B. Chng, Z. Chen, V. Scarani, and C. Kurtsiefer, "Interfacing light and single atoms with a lens", New Journal of Physics **11**, 43011 (2009).

[31]G. Wrigge, I. Gerhardt, J. Hwang, G. Zumofen, and V. Sandoghdar, "Efficient coupling of photons to a single molecule and the observation of its resonance fluorescence", Nature Physics **4**, 60 (2008).

[32]S. Haroche and J.-M. Raimond, *Exploring the Quantum* (Oxford University Press, Aug. 2006), pp. 1–616.

[33]H. Walther, B. T. Varcoe, B. G. Englert, and T. Becker, "Cavity quantum electrodynamics", Reports on Progress in Physics **69**, 1325 (2006).

[34]A. Reiserer and G. Rempe, "Cavity-based quantum networks with single atoms and optical photons", Reviews of Modern Physics **87**, 1379 (2015).

[35]A. D. Boozer, A. Boca, R. Miller, T. E. Northup, and H. J. Kimble, "Reversible state transfer between light and a single trapped atom", Physical Review Letters **98**, 193601 (2007).

[36]M. Hijlkema, B. Weber, H. P. Specht, S. C. Webster, A. Kuhn, and G. Rempe, "A single-photon server with just one atom", Nature Physics **3**, 253 (2007).

[37]K. M. Birnbaum, A. Boca, R. Miller, A. D. Boozer, T. E. Northup, and H. J. Kimble, "Photon blockade in an optical cavity with one trapped atom", Nature **436**, 87 (2005).

[38]T. Wilk, S. C. Webster, A. Kuhn, and G. Rempe, "Single-atom single-photon quantum interface", Science **317**, 488 (2007).

[39]D. Tiarks, S. Schmidt, G. Rempe, and S. Dürr, "Optical π phase shift created with a single-photon pulse.", Science advances **2**, e1600036 (2016).

[40]B. Hacker, S. Welte, G. Rempe, and S. Ritter, "A photon-photon quantum gate based on a single atom in an optical resonator", Nature **536**, 193 (2016).

[41]H. J. Kimble, "The quantum internet", Nature **453**, 1023 (2008).

[42]E. T. Jaynes and F. W. Cummings, "Comparison of Quantum and Semiclassical Radiation Theories with Application to the Beam Maser", Proceedings of the IEEE **51**, 89 (1963).

[43]S. Fan, Ş. E. Kocabaş, and J.-T. Shen, "Input-output formalism for few-photon transport in one-dimensional nanophotonic waveguides coupled to a qubit", Physical Review A **82**, 063821 (2010).

[44]P. McManamon, T. Dorschner, D. Corkum, L. Friedman, D. Hobbs, M. Holz, S. Liberman, H. Nguyen, D. Resler, R. Sharp, and E. Watson, "Optical phased array technology", Proceedings of the IEEE **84**, 268 (1996).

[45]M. O. Scully, E. S. Fry, C. H. Ooi, and K. Wódkiewicz, "Directed spontaneous emission from an extended ensemble of N atoms: Timing is everything", Physical Review Letters **96**, 010501 (2006).

[46]P. Sebbah, *Waves and Imaging through Complex Media* (Kluwer Academic Publishers, 2001).

[47]I. M. Vellekoop and A. P. Mosk, "Focusing coherent light through opaque strongly scattering media", Optics Letters **32**, 2309 (2007).

[48]F. Arecchi and R. Bonifacio, "Theory of optical maser amplifiers", IEEE Journal of Quantum Electronics **1**, 169 (1965).

[49]S. L. McCall and E. L. Hahn, "Self-induced transparency by pulsed coherent light", Physical Review Letters **18**, 908 (1967).

[50]Y. R. Shen, *The Principles of Nonlinear Optics*, Wiley classics library (Wiley, 2003).

[51]C. M. Bowden and J. P. Dowling, "Near-dipole-dipole effects in dense media: Generalized Maxwell-Bloch equations", Physical Review A **47**, 1247 (1993).

[52]Y. Castin and K. Molmer, "Maxwell-Bloch equations: A unified view of nonlinear optics and nonlinear atom optics", Physical Review A **51**, R3426 (1995).

[53]M. Fleischhauer and S. F. Yelin, "Radiative atom-atom interactions in optically dense media: Quantum corrections to the Lorentz-Lorenz formula", Physical Review A **59**, 2427 (1999).

[54]A. V. Gorshkov, A. André, M. Fleischhauer, A. S. Sørensen, and M. D. Lukin, "Universal approach to optimal photon storage in atomic media", Physical Review Letters **98**, 123601 (2007).

[55]A. A. Svidzinsky, X. Zhang, and M. O. Scully, "Quantum versus semiclassical description of light interaction with atomic ensembles: Revision of the Maxwell-Bloch equations and single-photon superradiance", Physical Review A **92**, 013801 (2015).

[56]M. Fleischhauer, A. Imamoglu, and P. J. Marangos, "Electromagnetically induced transparency", Reviews of Modern Physics **77**, 633 (2005).

[57]L. Vestergaard Hau, S. E. Harris, Z. Dutton, and C. H. Behroozi, "Light speed reduction to 17 metres per second in an ultracold atomic gas", Nature **397**, 594 (1999).

[58]N. Sangouard, C. Simon, H. de Riedmatten, and N. Gisin, "Quantum repeaters based on atomic ensembles and linear optics", Reviews of Modern Physics **83**, 33 (2011).

[59]P. Kok, W. J. Munro, K. Nemoto, T. C. Ralph, J. P. Dowling, and G. J. Milburn, "Linear optical quantum computing with photonic qubits", Reviews of Modern Physics **79**, 135 (2007).

[60]M. D. Lukin, "Colloquium : Trapping and manipulating photon states in atomic ensembles", Reviews of Modern Physics **75**, 457 (2003).

[61]C. Liu, Z. Dutton, C. H. Behroozi, and L. V. Hau, "Observation of coherent optical information storage in an atomic medium using halted light pulses", Nature **409**, 490 (2001).

[62]D. F. Phillips, A. Fleischhauer, A. Mair, R. L. Walsworth, and M. D. Lukin, "Storage of light in atomic vapor", Physical Review Letters **86**, 783 (2001).

[63]M. D. Eisaman, A. André, F. Massou, M. Fleischhauer, A. S. Zibrov, and M. D. Lukin, "Electromagnetically induced transparency with tunable single-photon pulses", Nature **438**, 837 (2005).

[64]T. Chanelière, D. N. Matsukevich, S. D. Jenkins, S. Y. Lan, T. A. Kennedy, and A. Kuzmich, "Storage and retrieval of single photons transmitted between remote quantum memories", Nature **438**, 833 (2005).

[65]P. R. Hemmer, A. V. Turukhin, M. S. Shahriar, and J. A. Musser, "Raman-excited spin coherences in nitrogen-vacancy color centers in diamond", Optics Letters **26**, 361 (2001).

[66]J. J. Longdell, E. Fraval, M. J. Sellars, and N. B. Manson, "Stopped light with storage times greater than one second using electromagnetically induced transparency in a solid", Physical Review Letters **95**, 063601 (2005).

[67]A. E. Kozhekin, K. Mølmer, and E. Polzik, "Quantum memory for light", Physical Review A **62**, 033809 (2000).

[68]J. Nunn, I. A. Walmsley, M. G. Raymer, K. Surmacz, F. C. Waldermann, Z. Wang, and D. Jaksch, "Mapping broadband single-photon wave packets into an atomic memory", Physical Review A **75**, 011401 (2007).

[69]S. A. Moiseev and S. Kröll, "Complete reconstruction of the quantum state of a single-photon wave packet absorbed by a doppler-broadened transition", Physical Review Letters **87**, 173601 (2001).

[70]B. Kraus, W. Tittel, N. Gisin, M. Nilsson, S. Kröll, and J. I. Cirac, "Quantum memory for nonstationary light fields based on controlled reversible inhomogeneous broadening", Physical Review A **73**, 020302 (2006).

[71]G. Hétet, J. J. Longdell, M. J. Sellars, P. K. Lam, and B. C. Buchler, "Multimodal properties and dynamics of gradient echo quantum memory", Physical Review Letters **101**, 203601 (2008).

[72]G. Hétet, J. J. Longdell, A. L. Alexander, P. K. Lam, and M. J. Sellars, "Electro-Optic Quantum Memory for Light Using Two-Level Atoms", Physical Review Letters **100**, 023601 (2008).

[73]M. P. Hedges, J. J. Longdell, Y. Li, and M. J. Sellars, "Efficient quantum memory for light", Nature **465**, 1052 (2010).

[74]I. Iakoupov and A. S. Sørensen, "An efficient quantum memory based on two-level atoms", New Journal of Physics **15**, 085012 (2013).

[75]Y.-W. Cho, G. T. Campbell, J. L. Everett, J. Bernu, D. B. Higginbottom, M. T. Cao, J. Geng, N. P. Robins, P. K. Lam, and B. C. Buchler, "Highly efficient optical quantum memory with long coherence time in cold atoms", Optica **3**, 100 (2016).

[76]J. L. Everett, P. Vernaz-Gris, G. T. Campbell, A. D. Tranter, K. V. Paul, A. C. Leung, P. K. Lam, and B. C. Buchler, "Time-reversed and coherently enhanced memory: A single-mode quantum atom-optic memory without a cavity", Physical Review A **98**, 063846 (2018).

[77]G. T. Campbell, K. R. Ferguson, M. J. Sellars, B. C. Buchler, and P. K. Lam, "Echo-Based Quantum Memory", in *Quantum information* (Wiley, Apr. 2016), pp. 723–740.

[78]G. T. Campbell, K. R. Ferguson, M. J. Sellars, B. C. Buchler, and P. K. Lam, "Echo-Based Quantum Memory", arXiv:1902.04313v1 (2019).

[79]E. L. Hahn, "Spin echoes", Physical Review **80**, 580 (1950).

[80]L. Novotny and B. Hecht, *Principles of nano-optics* (Cambridge University Press, 2006), pp. 1–539.

[81]F. J. De Abajo, "Colloquium: Light scattering by particle and hole arrays", Reviews of Modern Physics **79**, 1267 (2007).

[82]R. J. Bettles, S. A. Gardiner, and C. S. Adams, "Enhanced Optical Cross Section via Collective Coupling of Atomic Dipoles in a 2D Array", Physical Review Letters **116**, 103602 (2016).

[83]G. Facchinetti, S. D. Jenkins, and J. Ruostekoski, "Storing Light with Subradiant Correlations in Arrays of Atoms", Physical Review Letters **117**, 243601 (2016).

[84]E. Shahmoon, D. S. Wild, M. D. Lukin, and S. F. Yelin, "Cooperative Resonances in Light Scattering from Two-Dimensional Atomic Arrays", Physical Review Letters **118**, 113601 (2017).

[85]S.-M. Yoo and S. M. Paik, "Cooperative optical response of 2D dense lattices with strongly correlated dipoles", Optics Express **24**, 2156 (2016).

[86]R. H. Dicke, "Coherence in Spontaneous Radiation Processes", Physical Review **93**, 99 (1954).

[87]H. T. Dung, L. Knöll, and D.-G. Welsch, "Resonant dipole-dipole interaction in the presence of dispersing and absorbing surroundings", Physical Review A **66**, 063810 (2002).

[88]S. Y. Buhmann, *Dispersion Forces I* (Springer-Verlag, 2012).

[89]T. Caneva, M. T. Manzoni, T. Shi, J. S. Douglas, J. I. Cirac, and D. E. Chang, "Quantum dynamics ofropagatinghotons with strong interactions: A generalized input-output formalism", New Journal of Physics **17**, 113001 (2015).

[90]A. Asenjo-Garcia, J. D. Hood, D. E. Chang, and H. J. Kimble, "Atom-light interactions in quasi-one-dimensional nanostructures: A Green's-function perspective", Physical Review A **95**, 33818 (2017).

[91]A. Asenjo-Garcia, M. Moreno-Cardoner, A. Albrecht, H. J. Kimble, and D. E. Chang, "Exponential improvement in photon storage fidelities using subradiance & "selective radiance" in atomic arrays", Physical Review X **7**, 31024 (2017).

[92]R. Dum, P. Zoller, and H. Ritsch, "Monte Carlo simulation of the atomic master equation for spontaneous emission", Physical Review A **45**, 4879 (1992).

[93]K. Mølmer, Y. Castin, and J. Dalibard, "Monte Carlo wave-function method in quantum optics", Journal of the Optical Society of America B **10**, 524 (1993).

[94]A. J. Daley, "Quantum trajectories and open many-body quantum systems", Advances in Physics **63**, 77 (2014).

[95]D. A. Stech, *Quantum and Atom Optics*, 2022.

[96]J. Eisert, M. Friesdorf, and C. Gogolin, "Quantum many-body systems out of equilibrium", Nature Physics **11**, 124 (2015).

[97]W. Guerin, M. O. Araújo, and R. Kaiser, "Subradiance in a Large Cloud of Cold Atoms", Physical Review Letters **116**, 083601 (2016).

[98]M. O. Araújo, I. Krešić, R. Kaiser, and W. Guerin, "Superradiance in a Large and Dilute Cloud of Cold Atoms in the Linear-Optics Regime", Physical Review Letters **117**, 073002 (2016).

[99]P. Weiss, M. O. Araújo, R. Kaiser, and W. Guerin, "Subradiance and radiation trapping in cold atoms", New Journal of Physics **20**, 063024 (2018).

[100]T. S. Do Espirito Santo, P. Weiss, A. Cipris, R. Kaiser, W. Guerin, R. Bachelard, and J. Schachenmayer, "Collective excitation dynamics of a cold atom cloud", Physical Review A **101**, 013617 (2020).

[101]Y. A. Fofanov, I. M. Sokolov, R. Kaiser, and W. Guerin, "Subradiance in dilute atomic ensembles: Role of pairs and multiple scattering", Physical Review A **104**, 023705 (2021).

[102]A. Cipris, R. Bachelard, R. Kaiser, and W. Guerin, "van der Waals dephasing for Dicke subradiance in cold atomic clouds", Physical Review A **103**, 033714 (2021).

[103]G. Ferioli, A. Glicenstein, L. Henriet, I. Ferrier-Barbut, and A. Browaeys, "Storage and Release of Subradiant Excitations in a Dense Atomic Cloud", PRX **11**, 021031 (2021).

[104]O. Morice, Y. Castin, and J. Dalibard, "Refractive index of a dilute Bose gas", Physical Review A **51**, 3896 (1995).

[105]J. Ruostekoski and J. Javanainen, "Optical linewidth of a low density fermi-dirac gas", Physical Review Letters **82**, 4741 (1999).

[106]S. Jennewein, M. Besbes, N. J. Schilder, S. D. Jenkins, C. Sauvan, J. Ruostekoski, J. J. Greffet, Y. R. Sortais, and A. Browaeys, "Coherent Scattering of Near-Resonant Light by a Dense Microscopic Cold Atomic Cloud", Physical Review Letters **116**, 233601 (2016).

[107]S. Jennewein, L. Brossard, Y. R. Sortais, A. Browaeys, P. Cheinet, J. Robert, and P. Pillet, "Coherent scattering of near-resonant light by a dense, microscopic cloud of cold two-level atoms: Experiment versus theory", Physical Review A **97**, 053816 (2018).

[108]S. D. Jenkins, J. Ruostekoski, J. Javanainen, S. Jennewein, R. Bourgain, J. Pellegrino, Y. R. Sortais, and A. Browaeys, "Collective resonance fluorescence in small and dense atom clouds: Comparison between theory and experiment", Physical Review A **94**, 023842 (2016).

[109]P. C. Bons, R. de Haas, D. de Jong, A. Groot, and P. van der Straten, "Quantum Enhancement of the Index of Refraction in a Bose-Einstein Condensate", Physical Review Letters **116**, 173602 (2016).

[110]N. J. Schilder, C. Sauvan, Y. R. Sortais, A. Browaeys, and J. J. Greffet, "Near-Resonant Light Scattering by a Subwavelength Ensemble of Identical Atoms", Physical Review Letters **124**, 073403 (2020).

[111]G. Labeyrie, F. De Tomasi, J. C. Bernard, C. A. Müller, C. Miniatura, and R. Kaiser, "Coherent backscattering of light by cold atoms", Physical Review Letters **83**, 5266 (1999).

[112]Y. Bidel, B. Klappauf, J. C. Bernard, D. Delande, G. Labeyrie, C. Miniatura, D. Wilkowski, and R. Kaiser, "Coherent light transport in a cold strontium cloud", Physical Review Letters **88**, 2039021 (2002).

[113]C. M. Aegerter and G. Maret, "Coherent Backscattering and Anderson Localization of Light", Progress in Optics **52**, 1 (2009).

[114]S. E. Skipetrov and I. M. Sokolov, "Absence of anderson localization of light in a random ensemble of point scatterers", Physical Review Letters **112**, 023905 (2014).

[115]T. Sperling, L. Schertel, M. Ackermann, G. J. Aubry, C. M. Aegerter, and G. Maret, "Can 3D light localization be reached in 'white paint'?", New Journal of Physics **18**, 013039 (2016).

[116]S. E. Skipetrov, "Localization Transition for Light Scattering by Cold Atoms in an External Magnetic Field", Physical Review Letters **121**, 093601 (2018).

[117]F. Cottier, A. Cipris, R. Bachelard, and R. Kaiser, "Microscopic and Macroscopic Signatures of 3D Anderson Localization of Light", Physical Review Letters **123**, 083401 (2019).

[118]I. M. Vellekoop, A. Lagendijk, and A. P. Mosk, "Exploiting disorder for perfect focusing", Nature Photonics **4**, 320 (2010).

[119]F. Andreoli, M. J. Gullans, A. A. High, A. Browaeys, and D. E. Chang, "Maximum Refractive Index of an Atomic Medium", PRX **11**, 11026 (2021).

[120]S. Fölling, A. Widera, T. Müller, F. Gerbier, and I. Bloch, "Formation of spatial shell structure in the superfluid to mott insulator transition", Physical Review Letters **97**, 60403 (2006).

[121]D. Barredo, V. Lienhard, S. de Léséleuc, T. Lahaye, and A. Browaeys, "Synthetic three-dimensional atomic structures assembled atom by atom.", Nature **561**, 79 (2018).

[122]F. Le Kien, S. Dutta Gupta, V. I. Balykin, and K. Hakuta, "Spontaneous emission of a cesium atom near a nanofiber: Efficient coupling of light to guided modes", Physical Review A **72**, 032509 (2005).

[123]E. Vetsch, D. Reitz, G. Sagué, R. Schmidt, S. T. Dawkins, and A. Rauschenbeutel, "Optical interface created by laser-cooled atoms trapped in the evanescent field surrounding an optical nanofiber", Physical Review Letters **104**, 203603 (2010).

[124]A. Goban, K. S. Choi, D. J. Alton, D. Ding, C. Lacroûte, M. Pototschnig, T. Thiele, N. P. Stern, and H. J. Kimble, "Demonstration of a state-insensitive, compensated nanofiber trap", Physical Review Letters **109**, 033603 (2012).

[125]P. Lodahl, S. Mahmoodian, and S. Stobbe, "Interfacing single photons and single quantum dots with photonic nanostructures", Reviews of Modern Physics **87**, 347 (2015).

[126]X. Gu, A. F. Kockum, A. Miranowicz, Y.-x. Liu, and F. Nori, "Microwave photonics with superconducting quantum circuits", Physics Reports **718-719**, 1 (2017).

[127]J. T. Shen and S. Fan, "Strongly correlated two-photon transport in a one-dimensional waveguide coupled to a two-level system", Physical Review Letters **98**, 153003 (2007).

[128]D. E. Chang, L. Jiang, A. V. Gorshkov, and H. J. Kimble, "Cavity QED with atomic mirrors", New Journal of Physics **14**, 63003 (2012).

[129]M. Mirhosseini, E. Kim, X. Zhang, A. Sipahigil, P. B. Dieterle, A. J. Keller, A. Asenjo-Garcia, D. E. Chang, and O. Painter, "Cavity quantum electrodynamics with atom-like mirrors", Nature **569**, 692 (2019).

[130]A. Albrecht, L. Henriet, A. Asenjo-Garcia, P. B. Dieterle, O. Painter, and D. E. Chang, "Subradiant states of quantum bits coupled to a one-dimensional waveguide", New Journal of Physics **21**, 025003 (2019).

[131]K. Stannigel, P. Rabl, and P. Zoller, "Driven-dissipative preparation of entangled states in cascaded quantum-optical networks", New Journal of Physics **14**, 063014 (2012).

[132]H. Pichler, T. Ramos, A. J. Daley, and P. Zoller, "Quantum optics of chiral spin networks", Physical Review A **91**, 042116 (2015).

[133]T. Ramos, H. Pichler, A. J. Daley, and P. Zoller, "Quantum Spin Dimers from Chiral Dissipation in Cold-Atom Chains", Physical Review Letters **113**, 237203 (2014).

[134]S. Mahmoodian, M. Čepulkovskis, S. Das, P. Lodahl, K. Hammerer, and A. S. Sørensen, "Strongly Correlated Photon Transport in Waveguide Quantum Electrodynamics with Weakly Coupled Emitters", Physical Review Letters **121**, 143601 (2018).

[135]A. González-Tudela, C. L. Hung, D. E. Chang, J. I. Cirac, and H. J. Kimble, "Subwavelength vacuum lattices and atom-atom interactions in two-dimensional photonic crystals", Nature Photonics **9**, 320 (2015).

[136]A. González-Tudela, V. Paulisch, H. J. Kimble, and J. I. Cirac, "Efficient Multiphoton Generation in Waveguide Quantum Electrodynamics", Physical Review Letters **118**, 213601 (2017).

[137]M. T. Manzoni, L. Mathey, and D. E. Chang, "Designing exotic many-body states of atomic spin and motion in photonic crystals", Nature Communications **8**, 1 (2017).

[138]S. Mahmoodian, G. Calajó, D. E. Chang, K. Hammerer, and A. S. Sørensen, "Dynamics of Many-Body Photon Bound States in Chiral Waveguide QED", Physical Review X **10**, 031011 (2020).

[139]V. Paulisch, H. J. Kimble, and A. González-Tudela, "Universal quantum computation in waveguide QED using decoherence free subspaces", New Journal of Physics **18**, 043041 (2016).

[140]R. J. Bettles, S. A. Gardiner, and C. S. Adams, "Cooperative eigenmodes and scattering in one-dimensional atomic arrays", Physical Review A **94**, 043844 (2016).

[141]J. Ruostekoski and J. Javanainen, "Arrays of strongly coupled atoms in a one-dimensional waveguide", Physical Review A **96**, 033857 (2017).

[142]Y. X. Zhang and K. Mølmer, "Theory of Subradiant States of a One-Dimensional Two-Level Atom Chain", Physical Review Letters **122**, 203605 (2019).

[143]Y. X. Zhang, C. Yu, and K. Mølmer, "Subradiant bound dimer excited states of emitter chains coupled to a one dimensional waveguide", Physical Review Research **2**, 013173 (2020).

[144]E. Munro, A. Asenjo-Garcia, Y. Lin, L. C. Kwek, C. A. Regal, and D. E. Chang, "Population mixing due to dipole-dipole interactions in a one-dimensional array of multilevel atoms", Physical Review A **98**, 33815 (2018).

[145]J. D. Joannopoulos, S. G. Johnson, J. N. Winn, and R. D. Meade, *Photonic crystals: Molding the flow of light* (Princeton University Press, 2011).

[146]S. John and T. Quang, "Spontaneous emission near the edge of a photonic band gap", Physical Review A **50**, 1764 (1994).

[147]T. Lund-Hansen, S. Stobbe, B. Julsgaard, H. Thyrrestrup, T. Sünner, M. Kamp, A. Forchel, and P. Lodahl, "Experimental realization of highly efficient broadband coupling of single quantum dots to a photonic crystal waveguide", Physical Review Letters **101**, 113903 (2008).

[148]A. Goban, C. L. Hung, S. P. Yu, J. D. Hood, J. A. Muniz, J. H. Lee, M. J. Martin, A. C. McClung, K. S. Choi, D. E. Chang, O. Painter, and H. J. Kimble, "Atom-light interactions in photonic crystals", Nature Communications **5**, 3808 (2014).

[149]A. Goban, C. L. Hung, J. D. Hood, S. P. Yu, J. A. Muniz, O. Painter, and H. J. Kimble, "Superradiance for Atoms Trapped along a Photonic Crystal Waveguide", Physical Review Letters **115**, 063601 (2015).

[150]S. P. Yu, J. D. Hood, J. A. Muniz, M. J. Martin, R. Norte, C. L. Hung, S. M. Meenehan, J. D. Cohen, O. Painter, and H. J. Kimble, "Nanowire photonic crystal waveguides for single-atom trapping and strong light-matter interactions", Applied Physics Letters **104**, 111103 (2014).

[151]T. G. Tiecke, J. D. Thompson, N. P. De Leon, L. R. Liu, V. Vuletić, and M. D. Lukin, "Nanophotonic quantum phase switch with a single atom", Nature **508**, 241 (2014).

[152]S. John and J. Wang, "Quantum electrodynamics near a photonic band gap: Photon bound states and dressed atoms", Physical Review Letters **64**, 2418 (1990).

[153]S. John and J. Wang, "Quantum optics of localized light in a photonic band gap", Physical Review B **43**, 12772 (1991).

[154]G. Kurizki, "Two-atom resonant radiative coupling in photonic band structures", Physical Review A **42**, 2915 (1990).

[155]J. S. Douglas, H. Habibian, C.-L. Hung, A. V. Gorshkov, H. J. Kimble, and D. E. Chang, "Quantum many-body models with cold atoms coupled to photonic crystals", Nature Photonics **9**, 326 (2015).

[156]V. S. Ferreira, J. Banker, A. Sipahigil, M. H. Matheny, A. J. Keller, E. Kim, M. Mirhosseini, and O. Painter, "Collapse and Revival of an Artificial Atom Coupled to a Structured Photonic Reservoir", Physical Review X **11**, 041043 (2021).

[157]D. E. Chang, J. S. Douglas, A. González-Tudela, C.-L. Hung, and H. J. Kimble, "Colloquium : Quantum matter built from nanoscopic lattices of atoms and photons", Reviews of Modern Physics **90**, 031002 (2018).

[158]M. T. Manzoni, D. E. Chang, and J. S. Douglas, "Simulating quantum light propagation through atomic ensembles using matrix product states", Nature Communications **8**, 1743 (2017).

[159]H. Zoubi and H. Ritsch, "Lifetime and emission characteristics of collective electronic excitations in two-dimensional optical lattices", Physical Review A **83**, 063831 (2011).

[160]S. D. Jenkins and J. Ruostekoski, "Controlled manipulation of light by cooperative response of atoms in an optical lattice", Physical Review A **86**, 031602 (2012).

[161]R. J. Bettles, S. A. Gardiner, and C. S. Adams, "Cooperative ordering in lattices of interacting two-level dipoles", Physical Review A **92**, 063822 (2015).

[162]R. T. Sutherland and F. Robicheaux, "Collective dipole-dipole interactions in an atomic array", Physical Review A **94**, 013847 (2016).

[163]J. Rui, D. Wei, A. Rubio-Abadal, S. Hollerith, J. Zeiher, D. M. Stamper-Kurn, C. Gross, and I. Bloch, "A subradiant optical mirror formed by a single structured atomic layer", Nature **583**, 369 (2020).

[164]M. T. Manzoni, M. Moreno-Cardoner, A. Asenjo-Garcia, J. V. Porto, A. V. Gorshkov, and D. E. Chang, "Optimization of photon storage fidelity in ordered atomic arrays", New Journal of Physics **20**, 83048 (2018).

[165]R. J. Bettles, M. D. Lee, S. A. Gardiner, and J. Ruostekoski, "Quantum and nonlinear effects in light transmitted through planar atomic arrays", Communications Physics **3**, 1 (2020).

[166]A. Cidrim, T. S. Do Espirito Santo, J. Schachenmayer, R. Kaiser, and R. Bachelard, "Photon Blockade with Ground-State Neutral Atoms", Physical Review Letters **125**, 073601 (2020).

[167]L. A. Williamson, M. O. Borgh, and J. Ruostekoski, "Superatom Picture of Collective Nonclassical Light Emission and Dipole Blockade in Atom Arrays", Physical Review Letters **125**, 073602 (2020).

[168]R. Bekenstein, I. Pikovski, H. Pichler, E. Shahmoon, S. F. Yelin, and M. D. Lukin, "Quantum metasurfaces with atom arrays", Nature Physics **16**, 676 (2020).

[169]Z. Y. Wei, D. Malz, A. González-Tudela, and J. I. Cirac, "Generation of photonic matrix product states with Rydberg atomic arrays", Physical Review Research **3**, 23021 (2021).

[170]M. Moreno-Cardoner, D. Goncalves, and D. E. Chang, "Quantum Nonlinear Optics Based on Two-Dimensional Rydberg Atom Arrays", Physical Review Letters **127**, 263602 (2021).

[171]J. Perczel, J. Borregaard, D. E. Chang, H. Pichler, S. F. Yelin, P. Zoller, and M. D. Lukin, "Topological Quantum Optics in Two-Dimensional Atomic Arrays", Physical Review Letters **119**, 023603 (2017).

[172]R. J. Bettles, J. Minář, C. S. Adams, I. Lesanovsky, and B. Olmos, "Topological properties of a dense atomic lattice gas", Physical Review A **96**, 041603 (2017).

[173]J. Perczel, J. Borregaard, D. E. Chang, S. F. Yelin, and M. D. Lukin, "Topological Quantum Optics Using Atomlike Emitter Arrays Coupled to Photonic Crystals", Physical Review Letters **124**, 083603 (2020).

[174]J. Javanainen and J. Ruostekoski, "Light propagation beyond the mean-field theory of standard optics", Optics Express **24**, 993 (2016).

[175]W. Yang and R.-B. Liu, "Quantum many-body theory of qubit decoherence in a finite-size spin bath", Physical Review B **78**, 085315 (2008).

[176]K. W. Stone, K. Gundogdu, D. B. Turner, X. Li, S. T. Cundiff, and K. A. Nelson, "Two-Quantum 2D FT Electronic Spectroscopy of Biexcitons in GaAs Quantum Wells", Science **324**, 1169 (2009).

[177]X. Dai, M. Richter, H. Li, A. D. Bristow, C. Falvo, S. Mukamel, and S. T. Cundiff, "Two-dimensional double-quantum spectra reveal collective resonances in an atomic vapor", Physical Review Letters **108**, 193201 (2012).

[178]H. Li, A. D. Bristow, M. E. Siemens, G. Moody, and S. T. Cundiff, "Unraveling quantum pathways using optical 3D Fourier-transform spectroscopy", Nature Communications **4**, 1390 (2013).

[179]G. Nardin, G. Moody, R. Singh, T. M. Autry, H. Li, F. Morier-Genoud, and S. T. Cundiff, "Coherent excitonic coupling in an asymmetric double InGaAs quantum well arises from many-body effects", Physical Review Letters **112**, 046402 (2014).

[180]B. Lomsadze and S. T. Cundiff, "Frequency-Comb Based Double-Quantum Two-Dimensional Spectrum Identifies Collective Hyperfine Resonances in Atomic Vapor Induced by Dipole-Dipole Interactions", Physical Review Letters **120**, 233401 (2018).

[181]S. Yu, M. Titze, Y. Zhu, X. Liu, and H. Li, "Long range dipole-dipole interaction in low-density atomic vapors probed by double-quantum two-dimensional coherent spectroscopy", Optics Express **27**, 28891 (2019).

[182]N. Bloembergen, E. M. Purcell, and R. V. Pound, "Relaxation effects in nuclear magnetic resonance absorption", Physical Review **73**, 679 (1948).

[183]W. Derbyshire, M. van den Bosch, D. van Dusschoten, W. MacNaughtan, I. Farhat, M. Hemminga, and J. Mitchell, "Fitting of the beat pattern observed in NMR free-induction decay signals of concentrated carbohydrate–water solutions", Journal of Magnetic Resonance **168**, 278 (2004).

[184]P. R. Zangara and H. M. Pastawski, "Loschmidt echo in many-spin systems: a quest for intrinsic decoherence and emergent irreversibility", Physica Scripta **92**, 033001 (2017).

[185]J. Li, R. Fan, H. Wang, B. Ye, B. Zeng, H. Zhai, X. Peng, and J. Du, "Measuring Out-of-Time-Order Correlators on a Nuclear Magnetic Resonance Quantum Simulator", Physical Review X **7**, 031011 (2017).

[186]G. A. Starkov and B. V. Fine, "Free induction decays in nuclear spin-12 lattices with a small number of interacting neighbors: The cases of silicon and fluorapatite", Physical Review B **101**, 024428 (2020).

[187]J. H. Eberly, "Emission of one photon in an electric dipole transition of one among N atoms", Journal of Physics B: Atomic, Molecular and Optical Physics **39**, S599 (2006).

[188]Y. He, L. Ji, Y. Wang, L. Qiu, J. Zhao, Y. Ma, X. Huang, S. Wu, and D. E. Chang, "Atomic spin-wave control and spin-dependent kicks with shaped subnanosecond pulses", Physical Review Research **2**, 043418 (2020).

[189]Y. He, L. Ji, Y. Wang, L. Qiu, J. Zhao, Y. Ma, X. Huang, S. Wu, and D. E. Chang, "Geometric Control of Collective Spontaneous Emission", Physical Review Letters **125**, 213602 (2020).

[190]Y. He, Q. Cai, L. Ji, Z. Fang, Y. Wang, L. Qiu, L. Zhou, S. Wu, S. Grava, and D. E. Chang, "Unraveling disorder-induced optical dephasing in an atomic ensemble", arXiv:2101.10779v1 (2021).

[191]M. Gross and S. Haroche, "Superradiance: An essay on the theory of collective spontaneous emission", Physics Reports **93**, 301 (1982).

[192]L. S. Levitov, "Delocalization of vibrational modes caused by electric dipole interaction", Physical Review Letters **64**, 547 (1990).

[193]D. S. Fisher, "Random antiferromagnetic quantum spin chains", Physical Review B **50**, 3799 (1994).

[194]K. Damle, O. Motrunich, and D. A. Huse, "Dynamics and transport in random antiferromagnetic spin chains", Physical Review Letters **84**, 3434 (2000).

[195]O. Motrunich, S.-C. Mau, D. A. Huse, and D. S. Fisher, "Infinite-randomness quantum Ising critical fixed points", Physical Review B **61**, 1160 (2000).

[196]G. Refael and J. E. Moore, "Entanglement entropy of random quantum critical points in one dimension", Physical Review Letters **93**, 260602 (2004).

[197]F. Iglói and C. Monthus, "Strong disorder RG approach of random systems", Physics Reports **412**, 277 (2005).

[198]R. Vosk and E. Altman, "Many-body localization in one dimension as a dynamical renormalization group fixed point", Physical Review Letters **110**, 067204 (2013).

[199]G. Refael and E. Altman, "Strong disorder renormalization group primer and the superfluid–insulator transition", Comptes Rendus Physique **14**, 725 (2013).

[200]S. Grava, Y. He, S. Wu, and D. E. Chang, "Renormalization group analysis of near-field induced dephasing of optical spin waves in an atomic medium", New Journal of Physics **24**, 013031 (2022).

[201]H. Shim, Z. Kuang, and O. D. Miller, "Optical materials for maximal nanophotonic response [Invited]", Optical Materials Express **10**, 1561 (2020).

[202]H. Shim, F. Monticone, and O. D. Miller, "Fundamental Limits to the Refractive Index of Transparent Optical Materials", Advanced Materials **33**, 2103946 (2021).

[203]J. B. Khurgin, "Expanding the Photonic Palette: Exploring High Index Materials", ACS Photonics **9**, 743 (2022).

[204]L. Henriet, J. S. Douglas, D. E. Chang, and A. Albrecht, "Critical open-system dynamics in a one-dimensional optical-lattice clock", Physical Review A **99**, 023802 (2019).

[205]L. A. Williamson and J. Ruostekoski, "Optical response of atom chains beyond the limit of low light intensity: The validity of the linear classical oscillator model", Physical Review Research **2**, 023273 (2020).

[206]S. J. Masson, I. Ferrier-Barbut, L. A. Orozco, A. Browaeys, and A. Asenjo-Garcia, "Many-Body Signatures of Collective Decay in Atomic Chains", Physical Review Letters **125**, 263601 (2020).

[207]C. Brif, R. Chakrabarti, and H. Rabitz, "Control of quantum phenomena: Past, present and future", New Journal of Physics **12**, 075008 (2010).

[208]J. A. Jones, "Quantum computing with NMR", Progress in Nuclear Magnetic Resonance Spectroscopy **59**, 91 (2011).

[209]J. H. Van Vleck, "The dipolar broadening of magnetic resonance lines in crystals", Physical Review **74**, 1168 (1948).

[210]S. J. Roof, K. J. Kemp, M. D. Havey, and I. M. Sokolov, "Observation of Single-Photon Superradiance and the Cooperative Lamb Shift in an Extended Sample of Cold Atoms", Physical Review Letters **117**, 073003 (2016).

[211]S. L. Bromley, B. Zhu, M. Bishof, X. Zhang, T. Bothwell, J. Schachenmayer, T. L. Nicholson, R. Kaiser, S. F. Yelin, M. D. Lukin, A. M. Rey, and J. Ye, "Collective atomic scattering and motional effects in a dense coherent medium", Nature Communications **7**, 1 (2016).

[212]B. Zhu, J. Cooper, J. Ye, and A. M. Rey, "Light scattering from dense cold atomic media", Physical Review A **94**, 023612 (2016).

[213]F. Cottier, R. Kaiser, and R. Bachelard, "Role of disorder in super- and subradiance of cold atomic clouds", Physical Review A **98**, 013622 (2018).

[214]M. O. Scully, "Single Photon Subradiance: Quantum Control of Spontaneous Emission and Ultrafast Readout", Physical Review Letters **115**, 243602 (2015).

[215]S. Prasad and R. J. Glauber, "Coherent radiation by a spherical medium of resonant atoms", Physical Review A **82**, 063805 (2010).

[216]C. C. Kwong, T. Yang, M. S. Pramod, K. Pandey, D. Delande, R. Pierrat, and D. Wilkowski, "Cooperative emission of a coherent superflash of light", Physical Review Letters **113**, 223601 (2014).

[217]S. Zhang, C. Liu, S. Zhou, C. S. Chuu, M. M. Loy, and S. Du, "Coherent control of single-photon absorption and reemission in a two-level atomic ensemble", Physical Review Letters **109**, 263601 (2012).

[218]L. Bellando, A. Gero, E. Akkermans, and R. Kaiser, "Cooperative effects and disorder: A scaling analysis of the spectrum of the effective atomic Hamiltonian", Physical Review A **90**, 063822 (2014).

[219]A. F. Karr, D. J. Daley, and D. Vere-Jones, "An Introduction to the Theory of Point Processes.", Journal of the American Statistical Association **85**, 262 (1990).

[220]S. V. Syzranov, M. L. Wall, B. Zhu, V. Gurarie, and A. M. Rey, "Emergent Weyl excitations in systems of polar particles", Nature Communications **7**, 13543 (2016).

[221]S. Y. Buhmann, L. Knöll, D.-G. Welsch, and H. T. Dung, "Casimir-Polder forces: A nonperturbative approach", Physical Review A **70**, 052117 (2004).

[222]M. O. Scully and A. A. Svidzinsky, "The Super of Superradiance", Science **325**, 1510 (2009).

[223]R. Friedberg and J. T. Manassah, "Analytic expressions for the initial Cooperative Decay Rate and Cooperative Lamb Shift for a spherical sample of two-level atoms", Physics Letters A **374**, 1648 (2010).

[224]T. Bienaimé, M. Petruzzo, D. Bigerni, N. Piovella, and R. Kaiser, "Atom and photon measurement in cooperative scattering by cold atoms", Journal of Modern Optics **58**, 1942 (2011).

[225]W. Guerin, M. T. Rouabah, and R. Kaiser, "Light interacting with atomic ensembles: collective, cooperative and mesoscopic effects", Journal of Modern Optics **64**, 895 (2017).

[226]H. De Riedmatten, M. Afzelius, M. U. Staudt, C. Simon, and N. Gisin, "A solid-state light-matter interface at the single-photon level", Nature **456**, 773 (2008).

[227]T. Zhong, J. M. Kindem, E. Miyazono, and A. Faraon, "Nanophotonic coherent light-matter interfaces based on rare-earth-doped crystals", Nature Communications **6**, 8206 (2015).

[228]M. Zhong, M. P. Hedges, R. L. Ahlefeldt, J. G. Bartholomew, S. E. Beavan, S. M. Wittig, J. J. Longdell, and M. J. Sellars, "Optically addressable nuclear spins in a solid with a six-hour coherence time", Nature **517**, 177 (2015).

[229]M. Antezza and Y. Castin, "Fano-Hopfield model and photonic band gaps for an arbitrary atomic lattice", Physical Review A **80**, 013816 (2009).

[230]M. Antezza and Y. Castin, "Spectrum of Light in a Quantum Fluctuating Periodic Structure", Physical Review Letters **103**, 123903 (2009).

[231]M. Antezza and Y. Castin, "Photonic band gap in an imperfect atomic diamond lattice: Penetration depth and effects of finite size and vacancies", Physical Review A **88**, 033844 (2013).

[232]H. H. Jen, G.-D. Lin, and Y.-C. Chen, "Resonant dipole-dipole interactions in electromagnetically induced transparency", Physical Review A **105**, 063711 (2022).

[233]A. V. Gorshkov, J. Otterbach, M. Fleischhauer, T. Pohl, and M. D. Lukin, "Photon-photon interactions via Rydberg blockade", Physical Review Letters **107**, 133602 (2011).

[234]E. Zeuthen, M. J. Gullans, M. F. Maghrebi, and A. V. Gorshkov, "Correlated Photon Dynamics in Dissipative Rydberg Media", Physical Review Letters **119**, 43602 (2017).